MODIFICATION OF INJECTION MOULDING MACHINE AND COMPARATIVE ANALYSIS OF CARBON NANOTUBE/ HIGH DENSITY POLYETHYLENE NANOCOMPOSITE

BY

SYLVESTER GADIMOH, B.Sc. (ABU, 2000), M.Sc (ABU 2006)

Ph.D/SCIEN/17413/2007-2008

A DISSERTATION SUBMITTED TO THE SCHOOL OF POSTGRADUATE STUDIES, AHMADU BELLO UNIVERSITY, ZARIA IN PARTIAL FULFILLMENT OF THE REQUIREMENTS FOR THE AWARD OF THE DEGREE OF DOCTOR OF PHILOSOPHY IN FIBRE SCIENCE AND POLYMER TECHNOLOGY

DEPARTMENT OF TEXTILE SCIENCE AND TECHNOLOGY,

AHMADU BELLO UNIVERSITY, ZARIA

NIGERIA

MAY, 2013

DEDICATION

This thesis work is dedicated to my family.

DECLARATION

I declare that the work in this dissertation entitled Modification of Injection Moulding Machine and Comparative Analysis of Carbon nanotube/High Density Polyethylene Nanocomposite has been carried out by me in the department of Textile Science and Technology. The information derived from the literature has been duly acknowledged in the text and a list of references provided. No part of this dissertation was previously presented for another degree at this or any other institution.

Sylvester Gadimoh _____ MAY, 2013

CERTIFICATION

This dissertation entitled Modification of Injection Moulding Machine and Comparative Analysis of Carbon nanotube/ High Density Polyethylene Nanocomposite by SYLVESTER GADIMOH meets the regulations governing the award of the degree of doctor of philosophy in Fibre Science and Polymer Technology of Ahmadu Bello University, and is approved for its contribution to knowledge and literary presentation.

Prof. E. G. Kolawole _____ May, 2013
Chairman, Supervisory Committee

Prof. P.O. Nkeonye _____ May, 2013
Member, Supervisory Committee

Late Prof. D. S. Madakson _____ May, 2013
Member, Supervisory Committee

Dr. Abdullahi Danladi _____ May, 2013
Head of Department

Prof. Adebayo A. Joshua _____ May, 2013
Dean, School of Postgraduate Studies

ACKNOWLEDGEMENT

It is not often that you are forced to sit down and think about who you want to thank when work such as this is completed. It was only when I started that I realized just how many people have influenced and supported me, both professionally and personally. This is my humble attempt at recording my gratitude to those people.

First and foremost, I would like to thank the Almighty God, through my Lord Jesus Christ the author and finisher of our faith, for the opportunity He has given me to undertake this work.

I wish to immensely thank my major supervisor, and advisor Prof. E.G. Kolawole. He has an enviable ability to find the important results in a sea of data and always leads me in the right direction. I will also be eternally grateful to him for his fatherly care, unalloyed support and encouragement at all times.

Similarly, I sincerely thank the other members of my supervisory team in persons of Prof. P.O. Nkeonye and late Prof. Madakson of the Department of Mechanical Engineering, A.B.U., Zaria.

I particularly wish to thank Prof. P.O. Nkeonye and Prof. M.K. Yakubu for their availability and unwavering support and encouragement throughout the period of this research work and in my educational endeavours. It means a great deal to have two people I admire so much on my side. Thanks also to Prof. U.S. Ishiaku for his valuable contribution to this work.

To all the other members of the department, to mention just a few: Prof. K.A. Bello, the H.O.D. Dr. Abdullahi Danladi, Dr. A.S. Lawal, Dr. Benjamin Dauda, Dr. Kogo, etc., I say thank you all for your contribution to this work especially during seminar presentations.

I will also like to use this opportunity to thank Mr. Allan Wrong Wu of Guangzhou, China for his immerse support for the search for the university where the test and analysis was conducted. He finally linked me up with Prof. Jing Cheng of the Chinese Medical University, who is a renowned scholar in the area of nanotechnology.

I was very ably assisted by Prof. Jing Cheng who made sure all my samples were properly analysed; in fact he personally moved with me from one department to another at Zhejiang University in Hangzhou, China. The final round of testing and the job of preparing this thesis were made a whole lot more pleasant and efficient, thanks to Prof. Jin Chen for the help in sourcing for up to date literature in the area of nanocomposites. My ulmost gratitude goes to all those that were instrumental to my tests and analyses in Zhejiang University, China whose names are too numerous to mention.

My thanks go to the National Research Institute for Chemical Technology (NARICT), Zaria, for releasing me for this study and to the staff of the textile division for their encouragement. I will not fail to thank Lekan Lawal in particular for his assistance in conducting water absorption test in NARICT, Zaria.

At this point in time, I want to thank the management and staff of Sharptech Engineering Limited Kano, for their patience and support during the fabrication and modification of the injection moulding machine. I particularly want to thank Mr. Stephen Alabi, Jonathan O. Asibi (manager), Engr. Abdul Lawal, Saka Lawal, and all others who in one way or the

other contributed to the success fabrication and modification of the injection moulding machine.

Finally, I want to thank my family, ‘Engr.’ Caleb Gadimoh, Bernice Kelly Gadimoh and my lovely wife Precious Dupe Gadimoh, for their unwavering patience, support and encouragement during the course of this work.

ABSTRACT

An injection moulding machine has been modified for the direct compounding of nanocomposites; the technique involves incorporating automated hopper feeders extruder onto conventional injection moulding machine which automatically feed carbon nanotube (CNT) into a molten stream of matrix in a nano-scale manner so that it is thoroughly dispersed by the action of the shear mixing of the extruder screw directly attached to the feeder and passing the material into the injection barrel where it is further mixed and dispersed before injecting into the mould. Single-walled carbon nanotube /high density polyethylene (SWCNT/HDPE) nanocomposites with several concentrations (0.2, 0.4, 0.6, 0.8, 1 wt %) were compounded using both conventional and the modified injection moulding machine for the purpose of comparative analysis of both compounding systems. A good dispersion of the CNT in the matrix and a good CNT–polymer interfacial adhesion were verified by scanning electron microscopy (SEM) and atomic force microscopy (AFM). The Raman spectral measurements of the characteristic bands of the SWNTs in the sample of the modified injection moulding machine indicate an effective interaction between SWCNTs and HDPE matrix. The rheological percolation threshold of the nanocomposites was between 0.2 and 1 wt% for the nanocomposite from the modified system while 0.8 and 1 wt % was obtained for nanocomposite from the conventional injection moulding (CIM) system. The electrical properties test showed that by using the modified system, a very low percolation threshold was obtained (~0.20-0.4%). In contrast, a higher percolation threshold was obtained for the nanocomposite produced with the CIM (~0.8-1wt %). From the mechanical property analysis, on the overall, there was a good interfacial bond between CNT and HDPE which manifested as appreciable increment of storage modulus and decreasing tendency of loss modulus; this implied good dispersion.

TABLE OF CONTENT

TITLE PAGE ……...ii

DEDICATION……..iii

DECLARATION……..iv

CERTIFICATION……v

ACKNOWLEDGEMENT……vi

ABSTRACT……ix

TABLE OF CONTENT……...x

LIST OF FIGURES……xv

LIST OF TABLES……...xx

LIST OF PLATES……...xxi

ABBREVIATIONS, DEFINITIONS, GLOSSARY AND SYMBOLS…….xxii

CHAPTER ONE: INTRODUCTION

1.1 Introduction……1

1.2 Statement of the Research…..……6

1.3 Objective of the Research……..7

1.4 Significance of the Research ……7

CHAPTER TWO: LITERATURE REVIEW

2.1 Introduction……8

2.2 Carbon Nanotube-reinforced Systems…….10

2.2.1 Structure and properties of CNTs……10

2.2.2 Carbon nanotube synthesis……..14

2.3 Classification of nanocomposites……...15

2.4 Polymer matrix nanocomposite……...16

2.4.1 Treatment of carbon nanotubes for nanocomposites production..……...20

2.4.2 High Density Polyethylene (HDPE) ……..20

2.4.2.1 Physical properties HDPE……...21

2.4.3 Properties of PCNT Nanocomposite……21

2.4.3.1 Mechanical properties…….25

2.4.3.2 Electrical and optical properties…….27

2.5 Characterization Techniques for Nanocomposites……28

2.5.1 Scanning Electron Microscopy (SEM) and Atomic Force Microscopy (AFM)...29

2.5.2 Transmission Electron Microscopy……....31

2.5.3 X-Ray Diffraction (XRD) technique……...32

2.5.4 Differential Scanning Calorimetry: DSC…….33

2.6 Application of CNT Nanocomposites..……...……..33

2.6.1 Flame retardant nanocomposites..……...33

2.6.2 Nanocomposites with high mechanical stability, stiffness, strength, toughness...33

2.6.3 Nanocomposite solar cells……...34

2.6.4 Nanocomposite membrane for gas separation and gas permeability……....34

2.7 Manufacturing of CNT Nanocomposites……34

2.7.1 Recent advance in CNTs processing: dispersion and orientation…….38

2.8 Future Outlook……...41

2.9 Adapted Manufacturing method for the Project……..……...43

2.9.1 Plastic injection moulding machines……....43

2.9.2 History of plastic injection moulding machine……44

2.9.3 The plastic injection moulding process……45

2.10 Design Theory……..……46

2.10.1 Design considerations……46

2.10.2 Design of components……...48

2.10.2.1 The hopper……48

2.10.2.2 The flow theory……..49

2.10.2.3 The heat flow theory……..52

2.10.2.4 The barrel……...53

2.10.2.5 The circumferential (hoop) stress……..54

2.10.2.6 The longitudinal stress……54

2.10.2.7 Barrel heat flow……..55

2.10.2.8 The screw……55

2.10.2.9 The feed section……..56

2.10.2.10 The compression or transition section……...56

2.10.2.11 The metering zone……..56

2.10.2.12 Shaft design……56

2.10.2.13 Bearing selection……....58

2.10.2.14 Motor selection……..….59

2.10.2.15 The pelletising die……...60

CHAPTER THREE:MATERIALS, DESIGN AND METHODS

3.1 Materials ……61

3.1.1 Experimental materials and equipment ……61

3.1.2 Fabrication materials and equipment ……62

3.2 Machine design……..…63

3.2.1 Design Calculations……..….64

3.2.1.1 Capacity of hopper…….....64

3.2.1.2 Maximum pressure at feed…….65

3.2.1.3 Volume flow rate…….……65

3.2.1.4 Heat requirement…….66

3.2.1.5 Determination of minimum safe diameter of shaft……...67

3.2.1.6 Bearing selection…….69

3.2.1.7 Motor selection……...70

3.3 Construction, Assembly and Operation….……71

3.3.1 Material selection……....71

3.3.2 Fabrication of parts……..71

3.3.3 The hopper……...71

3.3.4 The barrel……71

3.3.5 The die…….72

3.3.6 The frame……72

3.3.7 The screw……72

3.3.8 Purchased parts……72

3.3.9 Assembly and Inspection ……...73

3.3.10 Working principles of the plastic injection moulding machine……74

3.3.11 Machine maintenance/safety precaution……...76

3.4 Experimental Methods……..……..76

3.4.1 Compounding process A……..……76

3.4.2 Compounding process B……..……77

3.5 Characterization Procedures……78

3.5.1 Morphological analysis and dispersion evaluation of CNTs in the samples….78

3.5.2 Crystalline characteristics (DSC and XRD)…….78

3.5.3 Orientation determination (Raman Spectroscopy)……..79

3.5.4 Electrical conductivity……..79

3.5.5 Mechanical properties……..80

3.5.6 Melt rheology……...80

3.5.6 Oxidation temperature (TGA)……..81

CHAPTER FOUR: RESULTS AND DISCUSSIONS

4.1 Design results……..…….82

4.1.1 Developed feeding and dispersion system……...83

4.1.2 Production parameters……..……83

4.1.3 Production challenges……..….84

4.2 Results of the Comparative Analysis of Samples…….....84

4.2.1 Morphological analysis of samples of both compounding methods……..85

4.2.2 Dispersion evaluation of the nanocomposite samples…….88

4.2.3 Crystalline characteristics (DSC and XRD)……...91

4.2.4 Orientation determination (Raman Spectroscopy)……93

4.2.5 Electrical conductivity……95

4.2.6 Mechanical properties…….96

4.2.7 Melt rheology…….102

4.2.8 Oxidation temperature (TGA)……103

CHAPTER FIVE: CONCLUSION AND RECOMMENDATION

5.1 Conclusion……108

5.2 Recommendation…….109

REFERENCES……..110

APPENDICES …….132

LIST OF FIGURES

Figure 1.1: Schematic of nanoscale fillers (Courtesy of Nanocomposite Science and Technology, (2003)…….....2

Figure 1.2: (a) Surface area per unit volume vs. particle size for spherical particles that are ideally dispersed, and (b) interparticle distance for spherical particles that are ideally dispersed……..3

Figure 2.1: Schematic of the nature of roll up of nanotube……....11

Figure 2.2: Schematic of a: (a) single-wall and (b) multiwall nanotube…….…….....11

Figure 2.3: Schematic of nanotube morphologies. (a) Armchair, (b) zig-zag, and (c) chiral…….……...……...12

Figure 2.4: Tensile strength comparison of common engineering materials…..…….....14

Figure 2.5: Procedures for preparing MWCNT/HDPE composite firm…….…….....19

Figure 2.6: Modification of carbon nanotube with organic agents…….…….....20

Figure 2.7: SEM images of a) SnS nanoflowers b) ABS/SnS c) Bi_2S_3 nanorods d) ABS/Bi_2S_3……...…….....30

Figure 2.8: AFM images of a) pure ABS b) ABS/SnS nanocomposite…….…….....30

Figure 2.9: TEM images of a) PMMA/TiO_2 nanocomposite b) ABS/OMMT nanocomposite…….…….....31

Figure 2.10: XRD patterns of a) pristine sodium montmorillonite b) modified montmorillonite (OMT) c) ABS/OMT nanocomposite…….....32

Figure 2.11: Schematic representation of convergent Hopper…….....48

Figure 2.12: single start screw…….…….....50

Figure 2.13: Analysis of stresses induced in a thin walled cylinder…….....54

Figure 2.14: Basic elements of a single-stage extruder screw …….…….....55

Figure 2.15: Line diagram of the shaft……..…….....56

Figure 2.16: Die Section…….....60

Figure 3.1: Sketch diagram of the proposed modification…….....64

Figure 3.2: Line diagram of feeder hopper……...…….....64

Figure 3.3: (a) Subassembly and (b) Assembly drawing of the modified injection moulding machine…….....73

Figure 3.4: ASTM D638 Standard Tensile bar specimen…….....77

Figure 3.5: Schematic illustrations of the test specimens employed in the test…….....79

Figure 4.1: Principle of operation of the developed automated feeder hopper…...83

Figure 4.2: SEM images of the three specimens randomly selected from Sample A1 = 0.2 wt% SWCNT……....85

Figure 4.3: SEM images of the three specimens randomly selected from Sample A2 = 0.4 wt% SWCNT……..85

Figure 4.4: SEM images of the three specimens randomly selected from Sample A3 = 0.6 wt% SWCNT……..85

Figure 4.5: SEM images of the three specimens randomly selected from Sample A4 = 0.8 wt% SWCNT……..86

Figure 4.6: SEM images of the three specimens randomly selected from Sample A5 = 1.0 wt% SWCNT……..86

Figure 4.7: SEM images of the three specimens randomly selected from Sample B1 = 0.2 wt% SWCNT……..86

Figure 4.8: SEM images of the three specimens randomly selected from Sample B2 = 0.4 wt% SWCNT……..86

Figure 4.9: SEM images of the three specimens randomly selected from Sample B3 = 0.6 wt% SWCNT……..87

Figure 4.10: SEM images of the three specimens randomly selected from Sample B4 = 0.8 wt% SWCNT……..87

Figure 4.11: SEM images of the three specimens randomly selected from Sample B5 = 1.0 wt% SWCNT……..87

Figure 4.12: SEM image of 2wt% SWCNT/HDPE nanocomposite of Sample A…88

Figure 4.13: SEM image of 0.2wt% SWCNT/HDPE nanocomposite of Sample B..88

Figure 4:14: TEM image of 0.2wt% SWCNT/HDPE Nanocomposite of sample B…..89

Figure 4.15: AFM image of the 0.2wt% of SWCNT/HDPE nanocomposite sample A and B respectively……..90

Figure 4.16: AFM image of the 0.6% SWCNT/HDPE nanocomposite sample A and B respectively……..90

Figure 4.17: AFM image of the 1wt% SWCNT/HDPE nanocomposite sample A and B respectively……....90

Figure 4:18. Variation of DSC curves of 2wt% SWCNT nanocomposite ……...91

Figure 4.19: XRD patterns showing the Intensity vs 2Ɵ for the pure HDPE and for the nanocomposites indicated on the plot……....92

Figure 4.20: Comparison of the Raman spectra of pure HDPE (lower trace), pure CNTs (upper trace), and 1wt% CNT/HDPE composite (middle trace)……...…....94

Figure 4.21: Electrical conductivity vs. CNT loading for uniformly dispersed sample B and agglomerated sample A……...96

Figure 4.22: Comparison of the flexural strength vs CNT wt% loading of Sample A and B…….....97

Figure 4.23: Young's modulus vs time for HDPE and 1 wt% CNT for sample B …....98

Figure 4.24: Storage modulus vs frequency for HDPE and 1 wt% CNT for sample B..99

Figure 4.25: Loss modulus vs frequency for HDPE and 1 wt% CNT for sample B.....100

Figure 4.26: Damping factor (Tan δ vs frequency) of HDPE and 1wt% CNT sample B..101

Figure 4.27: (a) Complex viscosity (Z_) vs. frequency (ω) and (b) storage modulus (G0) vs. frequency (ω) for the SWCNT/HDPE nanocomposites and the pure HDPE (T ¼ 200 ^{0}C)…….....103

Figure 4.28: Variation of d(weight loss)/dT of HDPE…….....104

Figure 4.29: Variation of d(weight loss)/dT of Sample A5…….....104

Figure 4.30: Variation of d(weight loss)/dT of Sample B5…….....105

LIST OF TABLES

Table 4.1: Design parameters……82

Table 4.2: Production parameters…….83

LIST OF PLATES

Plate 1: Picture of the Tensile Bar Nanocomposite produced by the machine…….84

Plate 2: Small Scale Conventional Injection Moulding Machine ……133

Plate 3: Fabrication work on the Modification of the Injection Moulding Machine……132

Plate 4: Assembly of the Modified Injection Moulding machine…….133

Plate 5: Assembled machine …….133

Plate 6: XRD Test in progress Zhejing University, China……134

Plate 7: SEM Test in progress at Zhejing University, China……135

Plate 8: Professor Cheng Jing of Chinese Medical University…….135

ABBREVIATIONS, DEFINITIONS, GLOSSARY AND SYMBOLS

Percolation: A concept that describes the formation of an interconnected path that will give rise to a flow of current.

Nanocomposite: These are nanoscale filled composites; in which the filler is <100 nm in at least one dimension.

SWCNT: Single walled Carbon nanotube

Carbon nanotubes: Graphitic sheets rolled into seamless tubes

CVD: Chemical vapour deposition

PECVD: Plasma enhanced chemical vapour deposition

Functionalization: The refluxing of a suspension of oxidized CNTs with the amine

HDPE: High density polyethylene defined by a density greater or equal to 0.941 g/cm^3. It has a low degree of branching and thus stronger intermolecular forces and tensile strength.

TEM: Transmission electron microscopy,

SEM: Scanning electron microscopy

AFM: Atomic force microscopy,

XRD: X-ray diffraction.

DSC: Differential scanning calorimetry.

D **:**	The hopper diameter,
f **:**	The static coefficient of friction on the wall,
ρb :	The bulk density of the material
K **:**	The ratio of principal stresses at all points.
δ :	The effective angle of friction
P **:**	Pressure in barrel
A **:**	Area of screw
ASTM D638:	Standard tensile bar specimen
TGA:	An experimental technique in which the weight of a sample is measured as a function of sample temperature or time

CHAPTER ONE

INTRODUCTION

1.1 Introduction

Polymer composites are important commercial materials with applications that include filled elastomers for damping, electrical insulators, thermal conductors, and high-performance composites for use in aircraft, and materials with synergistic properties are chosen to create composites with tailored properties; for example, high-modulus but brittle carbon fibres are added to low-modulus polymers to create a stiff, lightweight composite with some degree of toughness. In recent years, however, the limit of optimizing composite properties of traditional micrometer-scale composite fillers has been reached, because the properties achieved usually involve compromises. Stiffness is traded for toughness, or toughness is obtained at the cost of optical clarity. In addition, macroscopic defects due to regions of high or low volume fraction of filler often lead to breakdown or failure (RTO Lecture Series, 2005).

Recently, a large window of opportunity has opened to overcome the limitations of traditional micrometer-scale polymer composites with the advent of nanoscale filled polymer composites (called nanocomposites); in which the filler is <100 nm in at least one dimension (Figure 1.1); A polymer nanocomposite is chiefly made by adding nanofillers into polymer matrix. Carbon nanotubes (CNTs) are the most exploited filler, because of their incredible strength and efficient conducting ability. Although some nanofilled composites such as carbon black (Bueche, 1957) and fumed silica (Kuriakose, et al., 1986) filled polymers have been used for more than a century; research and development of nanofilled polymers has greatly increased in recent years, for several reasons. First,

unprecedented combinations of properties have been observed in some polymer nanocomposites.

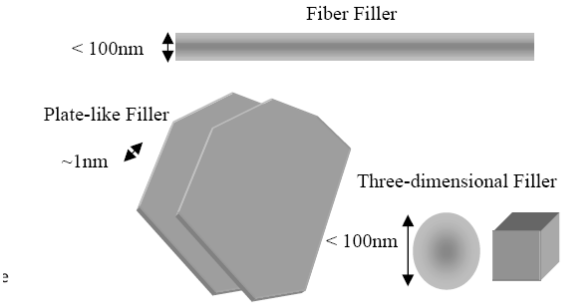


Figure 1.1: Schematic of nanoscale fillers (Courtesy of Ajayan, et al., 2003).

For example, the inclusion of equi-axed nanoparticles in thermoplastics, and particularly in semi-crystalline thermoplastics, increases the yield stress, the tensile strength, and Young's modulus (Sumita, et al., 1983) compared to pure polymer. A volume fraction of only 0.04 mica-type silicates (MTS) in epoxy increases the modulus below the glass transition temperature by 58% and the modulus in the rubbery region by 450% (Giannelis, 1996).

A second reason for the large increase in research and development efforts was the 'discovery' of carbon nanotubes in the early 1990s (Iijima, 1991). Although more careful review has shown that nanotubes have been observed since the 1960s (Colbert and Smalley, 2001), it was only in the mid-1990s that they were made in the quantities required for property evaluation of composites. The properties of these carbon nanotubes, particularly strength and electrical properties are significantly different from those of graphite and offer exciting possibilities for new composite materials.

Third, significant development in the chemical processing of nanoparticles and in the in situ processing of nanocomposites has led to unprecedented control over the morphology of such composites. It has also created an almost unlimited ability to control the interface between the matrix and the filler.

Nano-fillers have obvious advantages of small size, which enable them not to scatter light significantly, and thus it is possible to make composites with altered electrical or mechanical properties that retain their optical clarity. In addition, the small size means that the particles do not create large stress concentrations and thus do not compromise the ductility of the polymer. A similar concept applies for electrical breakdown strength. The small size of nanofillers can also lead to unique properties of the particles themselves. For example, single-walled nanotubes are essentially molecules, free from defects, and have a modulus as high as 1 TPa and strengths that may be as high as 500 GPa.

Figures 1.2 (a) and (b) show surface area per unit volume vs. particle size for spherical particles that are ideally dispersed, and the interparticle distance for spherical particles that are ideally dispersed respectively.

(a)

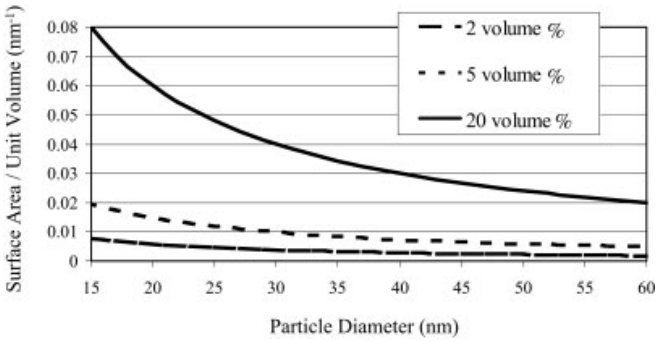
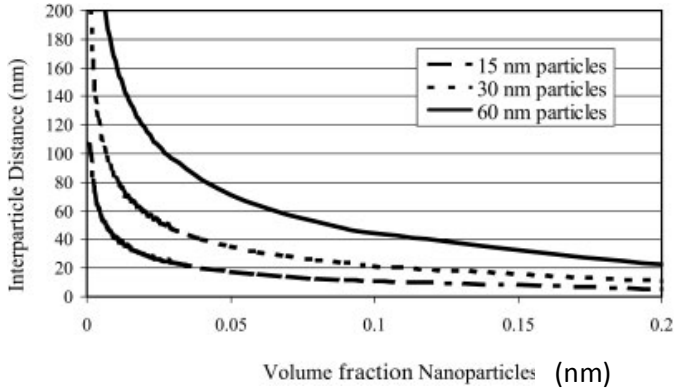


Figure 1.2: (a) Surface area per unit volume vs. particle size for spherical particles that are ideally dispersed.

(b)



(nm)

Figure 1.2 (b) interparticle distance for spherical particles that are ideally dispersed.

In addition to the effect of size on particle properties, the small size of the fillers leads to an exceptionally large interfacial area in the composites. In Figure 1.2(a): shows the surface area per unit volume as a function of particle size for spherical particles that are ideally dispersed, the increase in surface area below 100 nm is dramatic. The interface controls the degree of interaction between the filler and the polymer and thus controls the properties. Therefore, the greatest challenge in developing polymer nanocomposites may be learning to control the interface.

Polymer composites are manufactured commercially for many diverse applications such as sporting goods, aerospace components, automobiles, etc. In the last 20 years, there has been a strong emphasis on the development of polymeric nanocomposites, where at least one of the dimensions of the filler material is of the order of a nanometer (see figure 1.1), the final product does not have to be in nanoscale, but can be micro- or macroscopic in size (RTO Lecture Series, 2005). This surge in the field of nanotechnology has been greatly facilitated by the advent of scanning tunneling microscopy and scanning probe microscopy in the early 1980s. With these powerful tools, scientists are able to see the nature of the surface structure with atomic resolution (Ajayan, et al., 2003). Simultaneously, the rapid growth of computer technology has made it easier to characterize and predict the properties at the nanoscale via modeling and simulation (RTO Lecture Series, 2005).

In general, the unique combination of the nanomaterial's characteristics, such as size, mechanical properties, and low concentrations necessary to effect change in a polymer matrix, coupled with the advanced characterization and simulation techniques now available, have generated much interest in the field of nanocomposites. In addition, many polymer nanocomposites can be fabricated and processed in ways similar to that of

conventional polymer composites, making them particularly attractive from a manufacturing point of view.

Nature has mastered the use of nanocomposites, and researchers, as usual, are learning from their natural surroundings. In 1998, Chemistry in Britain published an article titled 'Nano sandwiches' (Oriakhi, 1998), stating, 'Nature is a master chemist with incredible talent'. Using natural reagents and polymers such as carbohydrates, lipids, and proteins, nature makes strong composites such as bones, shells, and wood. These are examples of nanocomposites, made by mixing two or more phases such as particles, layers or fibres, where at least one of the phases is in the nanometre size range. Nanoscale science and technology research is progressing with the use of a combination of atomic scale characterization and detailed modeling (RTO Lecture Series, 2005).

'The properties of nanocomposite materials depend not only on the properties of their individual parents but also on their morphology and interfacial characteristics' (Oriakhi, 1998).

In the US, due to the potential promise that nanotechnology holds, federal funding for nanotechnology R&D has increased substantially since inception of the National Nanotechnology Initiative (NNI), from $464 million in 2001 to an estimated $982 million in 2005. The 2006 budget request that President Bush sent to Congress calls for a total NNI budget of $1.052 billion (http://www.nano.gov/). These tremendous funding opportunities in nanotechnology are geared toward new and improved products and more efficient manufacturing processes for a wide range of applications. But unfortunately, the opposite is

the case in Nigeria where the Government is yet to acknowledge the advent and opportunities of nanotechnology.

Although research in the field of CNT/polymer composites has been conducted on thermoplastics such as ABS, PC, PMMA, PP and PS, to our knowledge, no mechanical properties of SWCNT/HDPE have been reported. On the other hand, HDPE provides excellent chemical resistance, high impact strength, good fatigue and abrasive wear resistance, low coefficient of friction, and moderate stiffness and rigidity. It has a very wide range of applications including orthopaedic implants, distribution pipes and auto parts. To utilize and enhance these properties of HDPE, especially to improve its stiffness and rigidity, CNTs can be used to make CNT/HDPE composites.

In this work, High Density Polyethylene (HDPE) will be compounded with carbon nanotube such that the filler single-walled carbon nanotubes (SWNTs) form a 3D-interconnected network of nanowires that give percolation curves at very low volume percentages of filler. The samples will be analyzed to determine the smallest amount of SWCNTs needed to optimize conductivity; in other words, the percolation threshold will be determined for the HDPE/SWCNT nanocomposite. Two different techniques would be implemented to fabricate these materials: 1) Mechanical mixing and moulding with conventional injection moulding machine and 2) Moulding directly with the developed modified injection moulding technique.

1.2 Statement of the Research

Production of nanocomposites with well dispersed nanotubes and low percolation threshold using existing/traditional compounding techniques is very difficult due to the strong

tendency of the nanotubes to agglomerate, and where it is achieved, more often than not at high weight%, there is possibility of splitting of agglomerate nanotubes in the nanocomposite when subjected to force. Therefore, premature failure takes place in the final product and electrical conductivity is often not attainable. To improve dispersion, percolation and compatibility in polymer matrices, nanotubes are being functionalized (pitalskya, *et al.* 2010; Salavati and Bazarganipour, 2007). But the processes of functionalizing the nanotube more often than not affects the properties of the nanotubes and hence that of the final product.

1.3 Objectives of the Research

a. To modify an existing injection moulding machine for compounding of well dispersed carbon nanotube/HDPE nanocomposites.
b. To optimize the modified injection moulding machine for the production of well dispersed and low percolation threshold nanocomposite.
c. To carry out comparative analysis of the samples from the conventional injection machine and the modified injection moulding machine, so as to ascertain the performance of the modified injection moulding machine in the production of well dispersed nanocomposite.

1.4 Significance of the Research

The significance of this work is to present to the public the present challenges in the development of carbon nanotube nanocomposite and introduce new way of tackling the challenges of dispersion and percolation in nanocomposite.

CHAPTER TWO

LITERATURE REVIEW

2.1 Introduction

The transition from microparticles to nanoparticles yields dramatic changes in physical properties. Nanoscale materials have a large surface area for a given volume (Luo and Daniel, 2003). Since many important chemical and physical interactions are governed by surfaces and surface properties (RTO Lecture Series, 2005), a nanostructured material can have substantially different properties from a larger-dimensional material of the same composition. In the case of particles and fibres, the surface area per unit volume is inversely proportional to the material's diameter, thus, the smaller the diameter, the greater the surface area per unit volume (Luo and Daniel, 2003). Common particle geometries and their respective surface area-to-volume ratios are shown in Figure 1.2(a). Typical nanomaterials currently under investigation include nanoparticles, nanotubes, nanofibres, fullerenes, and nanowires. In general, these materials are classified by their geometries (Schmidt, *et al., 2002*); broadly the three classes are particle, layered, and fibrous materials (Thostenson, *et al.*, 2005; Schmidt, *et al., 2002*). Carbon black, silica nanoparticle, polyhedral oligomeric sislesquioxanes (POSS) can be classified as nanoparticle reinforcing agents while nanofibres and carbon nanotubes are examples of fibrous materials (Schmidt, D., *et. al. 2002*). When the filler has a nanometer thickness and a high aspect ratio (30–1000) plate-like structure, it is classified as a layered nanomaterial (such as an organosilicate) (Alexandre and Dubois, 2000). In general, nanomaterials provide reinforcing efficiency because of their high aspect ratios (Luo and Daniel, 2003). The

properties of a nanocomposite are greatly influenced by the size scale of its component phases and the degree of mixing between the two phases. Depending on the nature of the components used (layered silicate or nanofibre, cation exchange capacity, and polymer matrix) and the method of preparation, significant differences in composite properties may be obtained (Park *et al.,* 2001).

Analogously, in fibrous or particle-reinforced polymer nanocomposites (PNCs), dispersion of the nanoparticle and adhesion at the particle–matrix interface play crucial roles in determining the mechanical properties of the nanocomposite. Without proper dispersion, the nanomaterial will not offer improved mechanical properties over that of conventional composites, in fact, a poorly dispersed nanomaterial may degrade the mechanical properties (Gorga and Cohen, 2004). Additionally, optimizing the interfacial bond between the particle and the matrix, one can tailor the properties of the overall composite, similar to what is done in macrocomposites. For example, good adhesion at the interface will improve properties such as interlaminar shear strength, delamination resistance, fatigue, and corrosion resistance.

Finally, it is important to recognize that nanocomposites research is extremely broad, encompassing areas such as electronics and computing, data storage, communications, aerospace and sporting materials, health and medicine, energy, environmental, transportation, and national defense applications (RTO Lecture Series, 2005). The focus of this review is to highlight the state of knowledge in processing, manufacturing, characterization, material properties, challenges, and potential applications for the most common polymer nanocomposites.

2.2 Carbon Nanotube-reinforced Systems

Carbon nanotubes are graphitic sheets rolled into seamless tubes (i.e., arrangements of carbon hexagons into tube-like fullerenes) and have diameters ranging from about a nanometre to tens of nanometres with lengths up to centimetres. Nanotubes have received much attention due to their interesting properties (high modulus and electrical/thermal conductivity) since their discovery by Iijima in 1991, (Iijima, 1991; Iijima and Ichihashi, 1993). Since then, significant effort has been made to incorporate nanotubes into conventional materials (such as polymers) for improved strength and conductivity (Bower, *et al.*, 1999; Haggenmueller, *et al.*, 2000). Moreover, many potential applications have been proposed for carbon nanotubes, including conductive and high-strength composites; energy storage and energy conversion devices; sensors; field emission displays and radiation sources; hydrogen storage media and nanometer-sized semiconductor devices; probes and interconnects (Lau and Hui, 2002).

2.2.1 Structure and Properties of CNTs

Nanotubes can be synthesized in two structural forms, single-wall and multiwall (as shown in Figure 2.1). The first tubules Iijima discovered exhibited the multiwall structure of concentric nanotubes forming one tube defining a multiwall nanotube (MWNT) (with a constant interlayer separation of $0.34A^{\circ}$), (Iijima, 1991).

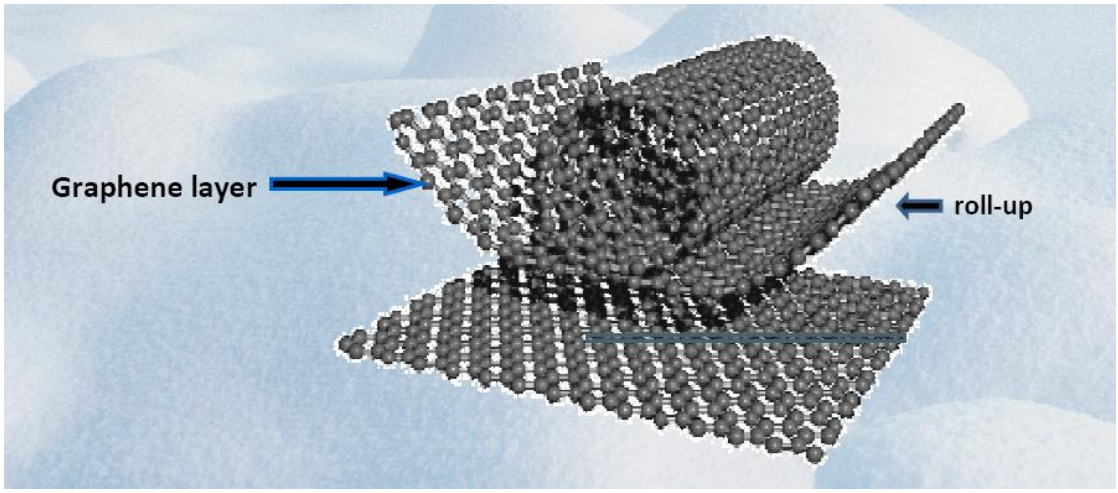


Figure 2.1: Schematic of the nature of roll up of nanotube.
(Courtesy; http://www.cnanotech.com and http://www.fibrils.com)

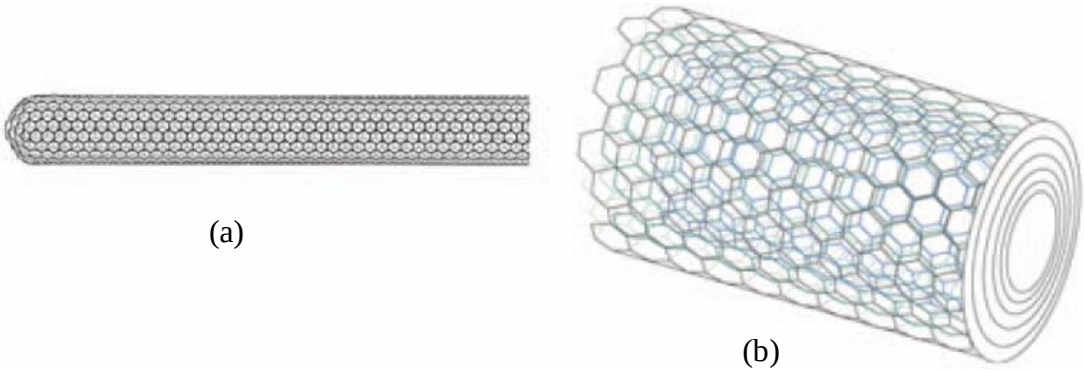


Figure 2.2: Schematic of a: (a) single-wall and (b) multiwall nanotube.
(Courtesy; http://www.cnanotech.com and http://www.fibrils.com)

Two years later, Iijima observed a single-shell structure believed to be the precursor to the MWNTs (Iijima and Ichihashi, 1993). This single graphitic sheet, rolled into a tube with a cap at both ends, and a diameter of around 1 nm, is defined as a single-wall nanotube (SWNT) (Iijima and Ichihashi, 1993; Bethune, *et al.*, 1993). Additionally, nanotubes are described using one of three different morphologies: armchair, zigzag, and chiral (as shown in Figure 2.3) (Lau and Hui, 2002; Dresselhaus, *et al.*, 1996).

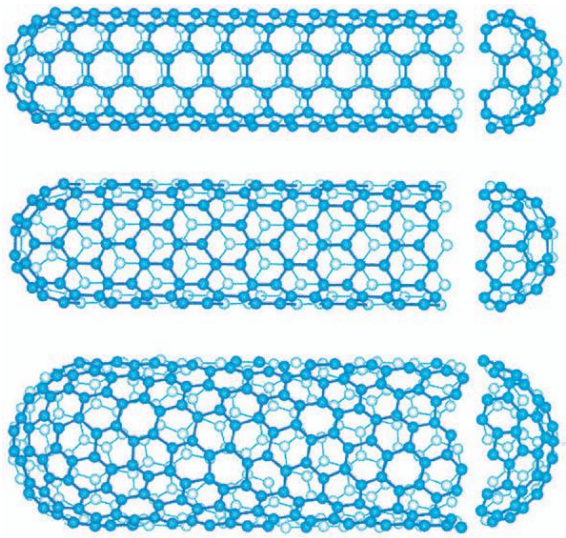


Figure 2.3: Schematic of nanotube morphologies. (a) Armchair, (b) zig-zag, and (c) chiral. (Courtesy; Elsevier, 2005)

Lau and Hui (Lau and Hui, 2002) gave a comprehensive review on the structures of nanotubes and three types of nanotube structures: zigzag (n, 0), armchair (n, n), and chiral (n, m where n 6¼m). The behaviour is determined based on a mathematical model developed using the chiral vector indices (Iijima and Ichihashi, 1993). All arm-chair and one-third of zig-zag nanotubes are metallic having a continuous conduction band. The remaining two-thirds of the zig-zag nanotubes are semiconductors, having an energy gap in the conduction band (Harris, 1999). Based on their very high aspect ratio (>1000), carbon nanotubes possess an interesting combination of physical properties. Attempts to determine the physical properties of the carbon nanotubes have been conducted both experimentally and theoretically. Originally, researchers used the vibration of the nanotubes as a function of temperature to calculate a Young's modulus of 1 TPa (Treacy, *et al.*, 1996). Such high strength as compared to other materials, as shown in Figure 2.4 below, led to a pronounced interest in carbon nanotube enabled materials. Common methods to measure the elastic properties of individual nanotubes include micro-Raman spectroscopy (Lourie, *et al.*,

1998), thermal oscillations by TEM (Treacy, *et al.*, 1996; Krishnan, *et. al.* 1998), and the application of a force to a nanotube rope suspended across a pit using an atomic forcemicroscope cantilever (Salvetat, *et al.*, 1999; Walters, *et al.* 1999). Other groups measured the properties of a rope and obtained an average value for each tube based on the number of nanotubes in the rope (Li, *et al.*, 2000; Pan, *et. al.* 1999). The experimental values measured ranged from significantly below theoretical values to values in agreement with the theory. These methods have produced tensile modulus and strength values for single- and multiwall nanotubes ranging from 270 GPa to 1 TPa and 11 GPa to 200 GPa respectively (Lau and Hui, 2002).

Modeling techniques such as molecular dynamics, empirical potentials, and first principles total-energy, continuum shell, and empirical lattice model have been used to describe the elastic properties of the nanotubes (Lu, 1997; Yakobson, *et al.*, 1996). The empirical lattice models, previously used to calculate the elastic properties of graphite, led to tensile modulus values in the range of 1 TPa for multi- and single-wall nanotubes (Lu, 1997). These values compared well with the diamond structure and outperform conventional carbon fibres. In addition to the mechanical properties, researchers have investigated the electrical and thermal conductivities of nanotubes. In a similar fashion, modeling has been used to determine the conductivity via the structure of the nanotubes as compared with graphite. Much of the theoretical work found that conductivity is greatly dependent on the small structural variations in the nanotubes (Ebbesen, *et. al.*, 1996). For example Berber et al. (2000) found unusually high thermal conductance of 6600W/m K at room temperature for a particular nanotube structure using nonequilibrium and equilibrium molecular dynamics. In addition, the static electrical conductive and superconductive natures of

nanotubes were modeled based on the conductivity of the graphite sheet structure (Benedict, *et. al.,* 1995).

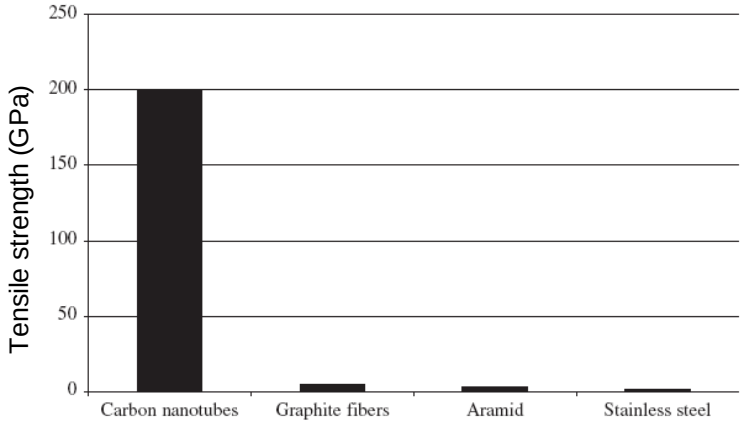


Figure 2.4: Tensile strength comparison of common engineering materials. (Courtesy, Elsevier, 2005)

Experimentally, Hone et al. (1999), reported slightly lower values in the range of 1750–5800W/m K for the room temperature of a single nanotube rope by comparing the temperature drop across a constantan rod of known thermal conductance to a nanotube mat sample in series with the rod. For electrical conductivity, experimental four-probe measurements of individual nanotubes showed resistivities in the range of 5.1Ω, 10Ω, 6–5.8Ωcm (or conductivities ranging from 0.17 to 196,078 S/cm) (Ebbesen, *et. al.,* 1996).

2.2.2 Carbon Nanotube Synthesis

The three main methods of manufacturing nanotubes include direct-current arc discharge, laser ablation, and chemical vapor deposition (CVD). A thorough discussion on each of these production methods can be found in the April 2004 MRS Bulletin (Liu, *et. al.,* 2004). Direct-arc discharge and laser ablation were the first techniques used to produce gram quantities of CNTs. In both methods, the evaporation of solid carbon is used to condense carbon gas. The products of such methods are normally tangled and poorly oriented. The CVD produces nanotubes from the decomposition of a continuously supplied carbon

containing gas onto a substrate. Due to the continuous supply of the gas, high-purity nanotubes can be produced on a larger (or industrial) volume scale. Producing the nanotubes in an ordered array with controlled length and diameter can also be achieved via CVD methods. Furthermore, plasma enhanced chemical vapor deposition (PECVD) results in further nanotube uniformity within the array (Thostenson, *et. al.*, 2001). In 2001, a team led by Schlittler developed a self-assembly method for making an ordered array of nanotubes with identical geometry and high purity (Schlittler, *et. al.*, 2001). More recently, the McGill university researchers in Canada developed a new method and apparatus to produce CNTs with the possibility of a scale up to large industrial levels that is based on thermal plasma technology (having temperatures between 4000 and 25,000^{0}C, which is created by electric arcs or magnetic induction discharges) to overcome the current low-volume production methods and high production costs (Meunier, 2005; McGill, 2004).

2.3 Classification of nanocomposites

Nanocomposites can be classified in many ways, but the popular among them is based on the nano-filler dimensional morphology of the nanocomposite. This classification is as shown below;

1. Zero dimensional nanomaterial such as nanoparticle (Salavati-Niasari , *et al.* 2009).
2. One dimensional nanomaterial such as nanowire and nanotube
3. Two dimensional nanomaterial such as silicate layers
4. Three dimensional nanomaterial such as zeolites (Salavati-Niasari M. 2009)

2.4 Polymer matrix nanocomposites

Scientists have long been investigating how to improve the properties of composite materials with lower and lower filler sizes, the recent trend in composite research is nanocomposites. Nanocomposites refer to composites in which one phase has nanoscale morphology such as nanoparticles, nanotubes or lamellar nanostructure (Mouritz and Gibson, 2006; Hull and Kandola, 2009)

The improvement of the properties by the addition of particles can be achieved when there is: a. Adequately good interaction between the nanoparticles and the matrix

b. Good dispersion of particles within the matrix.

Depending on the methods of dispersion of the nanoparticles in the nanocomposites, covalent bonds, ionic bonds, Van der Waals forces, or hydrogen bonding could exist between the matrix and filler components (Ratna, 2005).

Currently there are four commonly used methods for incorporating carbon nanotubes into a polymer matrix (Jin et. al., 2002; Pótschke et. al., 2002): direct mixing, in situ polymerization, solution method, and melt processing. While direct mixing generally applies only to thermosetting polymers, all the other methods can be used for thermoplastic polymers. In the direct mixing method, carbon nanotubes are dispersed, by mechanical mixing or by sonication, into a low-viscosity thermosetting resin such as epoxy (Gojny et al., 2003). Then the resin in the mixture is cured in a non-reversible exothermic polymerization reaction, resulting in a CNT/polymer composite.

During the process or in situ polymerization (Park et. al., 2002; Jia et al., 1999), carbon nanotubes are added to un-polymerized solution containing the polymer monomer. The nanotubes are mechanically dispersed into the solution. In some cases, they become chemically attached to the polymer chains (Jia et. al., 1999). The insitu polymerization seems to be a promising method to fabricate C NT / polymer composites. However, before this method can be used in industrial scale processes, the problem of dispersing carbon nanotubes uniformly into a large amount of solution remains. Direct mixing is used to disperse CNTs in thermosetting polymers and in situ polymerization is used to disperse CNTs in thermoplastic polymers. The approach followed is quite similar. In both methods, carbon nanotubes are initially added into a low molecular weight, low-viscosity liquid and a stable solution with well-dispersed nanotubes is obtained by mixing. Finally the nanotubes are locked into the polymer matrix by curing or polymerization.

In the solution approach, a solvent is used to dissolve a solid thermoplastic polymer and CNTs are added to the resulting solution. The solvent is then evaporated, the thermoplastic re-solidifies and a CNT/polymer composite is formed (Safadi et. al., 2002)**.** The evaporation of a large amount of solvent currently makes this method impractical for mass production. For a chemically resistant polymer such as HDPE, only a few toxic solvents (toluene and xylene) can dissolve it at elevated temperatures with low solubility. Thus, in such cases, the solution method should be the last resort.

In melt processing, carbon nanotubes are mechanically dispersed into a polymer melt (prepared by heating) using a mixer or a compounder (Andrews et al., 2002)**.** The central idea is to use fluid shear forces to break nanotube aggregates or prevent their formation. This approach is simple and compatible with existing polymer processing techniques such

as extrusion, injection and compression moulding. Therefore it holds promise for use in large-scale industrial applications.

Although research in the field of CNT/polymer composites has been conducted on thermoplastics such as ABS, PC, PMMA, PP and PS, to our knowledge, no mechanical properties of CNT/HDPE have been reported. On the other hand, HDPE provides excellent chemical resistance, high impact strength, good fatigue and abrasive wear resistance, low coefficient of friction, and moderate stiffness and rigidity. It has a very wide range of applications including orthopaedic implants, distribution pipes and auto parts. To utilize and enhance these properties of HDPE, especially to improve its stiffness and rigidity, CNTs can be used to make CNT/HDPE composites.

Most of the researchers have incorporated nanotubes into thermoplastic polymers due to their ease of processibility. This allows fibres or films to be made and other objects to be easily melt processed into molded parts. Research has been performed using both amorphous and semicyrstalline polymers with varying degrees of success. The nanotubes have been shown to toughen and stiffen amorphous brittle materials such as polymethyl methacrylate (PMMA) (Jin, *et. al.*, 2001; Zeng, *et. al.*, 2004) as well as in semicrystalline polymers such as PP (McCullen, *et. al.*, 2006).

In addition to the toughening and stiffening effects, morphological changes are the subject of discussion for semicrystalline polymers such as PP. Research literature has suggested that nanotubes act as nucleating agents in these materials leading to new crystallographic morphologies and ultimately increased strength (Assouline, *et. al.*, 2003; Sandler, *et. al.* 2003).

A typical example is the study conducted by Wenzhong (2003), in which the melt processing method was used to make MWCNT/HDPE composite films as shown below.

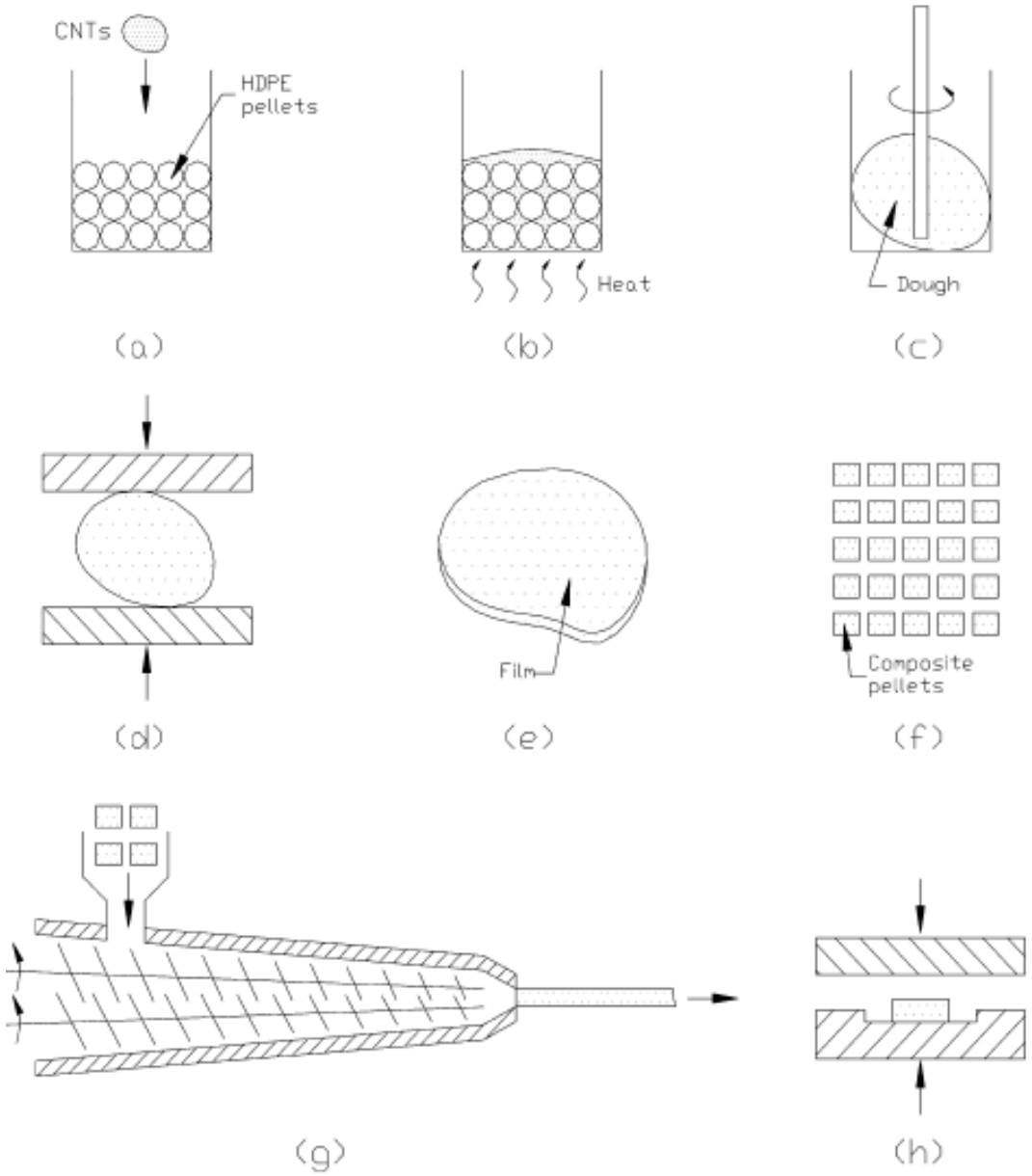


Figure 2.5: Procedures for preparing MWCNT/HDPE composite film, (Courtesy; Wenzhong, 2003)

2.4.1 Treatment of carbon nanotubes for nanocomposites production

Functionalization of carbon nanotubes is an effective way to improve interaction between CNTs and polymer matrix. Treatment has been performed by oxidation using a mixture of sulfuric and nitric acids. The oxidized carbon nanotubes were then functionalized with different types of agents such as amines or $SOCl_2$ (Fig 2.6).The functionalization has been performed by refluxing a suspension of oxidized CNTs with the amine to ensure a quantitative conversion (pitalskya, *et al.* 2010; Salavati and Bazarganipour, 2007).

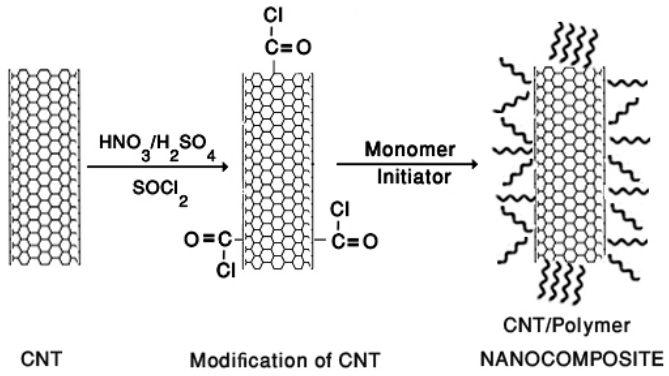


Figure 2.6: Modification of carbon nanotube with organic agents

However, there are still concerns as to whether this treatment adversely affects the properties of the functionized nanotube.

2.4.2 High density polyethylene (HDPE)

Most manufacturers decide upon polyethylene as the polymer of choice for the plastic moulding process because of its availability, ease of use, and suitable properties. According to recent reports 80% - 90% of all polymers used in the plastic moulding industry are polyethylene compounds (HDPE, LDPE and LLDPE), although PVC, nylon and

polypropylene are also used. Polyethylene is created through the polymerization of ethylene.

Chemical Composition; the ethylene molecule is C_2H_4 ($CH_2=CH_2$)

A.K.A. Polyethene, HDPE (High Density Polyethylene) is defined by a density of greater or equal to 0.941 g/cm^3. HDPE has a low degree of branching and thus stronger intermolecular forces and tensile strength. HDPE can be produced by chromium/silica catalysts, Ziegler-Natta catalysts or metallocene catalysts. The lack of branching is ensured by an appropriate choice of catalyst.

2.4.2.1 Physical Properties HDPE:

	Value:
Tensile Strength:	0.20 - 0.40 N/mm^2
Notched Impact Strength:	no break
Thermal Coefficient of Expansion:	100 - 220 x 10^{-6}
Max. Continued Use Temperature:	65 ^{o}C (149 ^{o}F)
Melting Point:	126 ^{o}C (259 ^{o}F)
Density:	0.941 - 0.965 g/cm^3

2.4.3 Properties of PCNT Nanocomposite

Research has been carried out to study mechanical (Allaoui, *et. al.* 2002), thermal (Lau, *et. al.* 2005), and electrical (Valentini, *et. al.*, 2004; Sandler, *et. al.*, 1999; Martin, *et. al.* 2004), properties of thermosetting polymer/nanotube composites with various results. Of the various thermosetting polymers that have been reported in the literature, epoxies have been the most commonly used. Recent research has shown that the tensile toughness of 1wt% MWNTs in PMMA exhibited the same tensile properties as composites fabricated with

1wt% SWNTs in PMMA (Gorga and Tsabba, 2006) using the dispersion process outlined by Sabba and Thomas (2004). Both samples were drawn to a 12 : 1 draw ratio. In each case, the dispersion of nanotubes was excellent (as shown by electron microscopy); however, no special dispersion treatment (other than melt mixing) was needed for the MWNT composite, therefore making the MWNTs the favourable toughening particle for PMMA. Research has shown mechanical property improvements with the addition of both SWNTs and MWNTs to PP. As discussed earlier, dispersion of the nanotubes plays a large role in property improvements. One study showed that the addition of 1wt% SWNTs via melt blending did not significantly improve the mechanical properties (Bhattacharyya, *et. al.,* 2003). In the study, SEM images showed micrometer scale aggregates and nanotube ropes within the sample. Some research has suggested that the aggregates could act as stress concentrators inhibiting the property improvement. However, from the slight increases, the aggregates were either not big enough to create stress concentrations, or the strength of the ropes was greater than the losses from the stress concentrations. The research concluded that better nanotube dispersion would lead to more rope, less aggregates, and ultimately significant mechanical property improvements.

In another study, significant property improvements were observed when adding SWNTs to PP (Kearns and Shambaugh, 2002). The nanotubes were first dispersed in the polymer using solution processing. After removing the solvent, the fibres were melt spun and post drawn for improved dispersion and orientation. The addition of 0.5 and 1wt% demonstrated an increase in tensile strength and modulus values. At 1 wt%, the tensile strength and modulus were 40 and 55% higher than neat PP fibres. However, additions of 1.5 and 2wt% made spinning of the fibres difficult and led to lower mechanical properties. A similar

maximum in mechanical properties as a function of nanotube loading was also noted in another study in both conventional tensile experiments and dynamic mechanical analysis (Moore, *et. al.,* 2004). The study looked at the properties of both as-spun fibre and postdrawn PP/SWNT fibres. Additionally, the studies investigated many differences in low melt flow rate and high melt flow rate PP. The basic tensile qualitative behaviour of neat PP (high initial modulus, sharp yield, and stretching to very long elongations) was observed in the as-spun nanocomposites. However, the nanocomposites exhibited lower elongation to break values. Increased tensile strength was noted for the low melt flow rate samples and the opposite for the high melt flow rate samples. Furthermore, the post-drawn low flow rate samples increased in tensile strength up to 1% and then decreased. The higher concentrations caused the fibres to become brittle and difficult to draw. All of the high melt flow rate samples exhibited a decrease in ultimate tensile strength. The dynamic mechanical analysis produced results similar to conventional tensile tests. Within the temperature limits, the storage modulus, E0, increased with increasing nanotube additions. At higher temperatures, E0 of post-drawn samples started to decrease. The concentration of 1% was found to be the optimal value for E0. Moreover, as evidenced by the tensile test, the post-drawing process created a far stiffer material. In contrast, the loss modulus, E00, shows little to no discernible trend as related to molecular weight of PP or nanotube concentration.

Research of PP/MWNTs has been performed to a lesser extent than SWNTs. In one study, functionalized nanotubes were added to chlorinated PP to create composite films (Coleman, *et. al.* 2004). The study noted an upward shift in the yield point on the stress–strain curve and consequently increased yield strength. Additionally, the Young's modulus, ultimate

tensile strength, and toughness increased with increasing nanotube volume fraction by a factor of 3.1, 3.9, and 4.4, respectively. From the data and previously derived composite models, mathematical models based on volume fraction were developed for the Young's modulus and composite strength. In another study, PP/multi-wall nanotube powder was created using a pan milling process (Xia, *et. al.* 2004). The pan milling of the neat PP reduced the elongation at break significantly. However, the addition of nanotubes increased the elongation at break (over pan-milled PP) through crystal structure changes and induced PP orientation. Again an optimal 1% nanotube loading exhibited increased Young's modulus and yield strength. The pan milling allows for better dispersion, reduces the number of defects, curvature, and entanglements, and enhances the polymer/nanotube adhesion.

Recently, Dondero and Gorga (McCullen, *et. al.* 2006) showed that 0.25wt% MWNTs in drawn PP (with a 12 : 1 draw ratio) increased tensile toughness by 32% and modulus by 138% over drawn PP. The DSC supported the conclusion of modulus increases via load transfer rather than increased crystallinity.

Johnson et al. (2004) manufactured CNT/polyethylene composites using extrusion to determine mechanical properties such as stiffness, work to failure, wear resistance, etc. Ren, *et al.* (2003) investigated the fatigue behaviour (under repeated mechanical loads) of unidirectional, aligned SWNT reinforced epoxy composite, which is demonstrated in long-term structural applications as well as in aerospace application. O'Donnell and Sprong (2004) investigated the potential impact of carbon nanotube reinforced polymer (CNRP) composites on commercial aircraft. The CNRP composite structured airframes are modeled through the utilization of Euro Control's Base of Aircraft Data and from traditional flight

dynamics theory. They considered notional Boeing 747-400 and 757-200; Airbus A320 and Embraer E145 with CNRP and replaced the entire volume of structural aluminium with CNRP composites, without including any modifications to the geometry or design of the airframe. In their model, weight reduction affects aircraft performance in terms of fuel saving and efficiency. Hsiao et al. (2003) showed the potential of CNT to reinforce the adhesives. They joined two composite laminates with toughened epoxy adhesives and MWNT for bonding graphite fibre/epoxy composite laminates with improved shear strength (O'Donnell and Sprong, 2004). Jihua and Liang and other coworkers proposed a bucky paper/resin infiltration (wetted in epoxy) approach for fabricating nanocomposite (Gou, *et. al.,* 2002). They suggested that bucky paper can provide a number of advantages for controlling dispersion, alignment, and high tube loading and is also easy for composite processing. Through a filtration process, SWNTs were fabricated into thin membranes called bucky papers to form networks of SWNT ropes. The heavy curvature of the composite sample is an example of tube alignment (Liang, *et al.* 2003). This is the effective approach for bulk polymeric composites with control in plane SWNT alignment and high nanotube content (Liang, *et al.* 2003).

2.4.3.1 Mechanical Properties

One of the primary reasons for adding fillers to polymers is to improve their mechanical performance. For example, the addition of high-modulus fillers increases the modulus and the strength of a polymer. In traditional composites, unfortunately, this often comes at the cost of a substantial reduction in ductility, and sometimes in impact strength, because of stress concentrations caused by the fillers. Well-dispersed nanofillers, on the other hand, can improve the modulus and strength and maintain or even improve ductility because their

small size does not create large stress concentrations. In addition, the large interfacial area of nanocomposites provides an opportunity for altering the matrix properties in unique ways.

In traditional composites, the modulus can be predicted, within bounds, and the mechanism that leads to a change in modulus is load transfer. For example, if a high modulus filler is added to a lower-modulus polymer, then load transfers from the matrix to the filler, leading to an increase in modulus. One important issue in nanocomposites is how load is transferred from the matrix to the filler. This is a complicated question, because in some nanocomposites the polymer chain and filler are almost the same size, and in others, the fillers are atomically smooth, with few functional groups to which the polymer can bond.

To fully understand the modulus of nanocomposites, a second mechanism in addition to load transfer must be considered. For example, the filler can constrain the mobility of the polymer chains as well as their relaxation spectra (Baschnagel and Binder, 1999), which can change the glass transition temperature (Kendall and Sherliker, 1980) and modulus of the matrix.

The modulus of nanotubes may be significantly higher than that of any graphite fibre, and therefore, they have the potential to yield higher composite moduli at the same filler volume fraction than a graphite fibre composite. In addition, because of their small size, if properly dispersed, nanotubes may not decrease the strain-to-failure. But, how is load transferred to a nanotube? Qian et. al., (2000) and Yu et. al., (2000) have shown, as first described by Wagner (1998), that MWNTs fail via a sword-and-sheath mechanism (see section 2.2.1). This implies that, even if load is transferred to the outermost nanotube in a

MWNT, the inner tubes slide within the concentric cylinder and do not carry much load. This situation limits the efficiency of MWNT/polymer composites, because only a small portion of the volume fraction of the MWNT carries load. Evidence for this was shown for MWNT/polystyrene composites, in which the effective modulus of the MWNT in the composite was only 500 GPa (Wagner, 1998), but the measured modulus of the MWNT is close to 1TPa. Therefore, to minimize the number of layers not carrying load, 2–3 layers are preferable.

For SWNT composites, the SWNT are in a bundle and, as was suggested earlier, individual SWNTs may slip within the bundle. Work by Yu et al. (2000) showed that, if only the nanotubes on the outer edge of a SWNT in a bundle are used to calculate the modulus, it is close to the predicted 1 TPa. However, if the whole area of the bundle is used, the calculated modulus is considerably lower. This suggests that, until the SWNT are isolated from the bundles or the bundles are crosslinked, the modulus of composites made from these materials will be limited. Fortunately, progress is being made in obtaining significant volume fractions of exfoliated nanotubes (Chen, et al. 1998).

2.4.3.2 Electrical and Optical Properties

The electrical and optical properties of nanofilled polymers are exciting areas of research. This is particularly true because of the possibility of creating composites with unique combinations of functionalities, such as electrically conducting composites with good wear properties that are optically clear. Such properties can result because nanoparticles, with diameters distinctly below the Rayleigh scattering limit, still display their solid-state physical properties when embedded in transparent matrices.

Optical composites have been defined as composites consisting of optically active nanoparticles embedded in a transparent host material, often a polymer (Barber, et. al., 1997). Optical composites take advantage of the optical properties of materials that are hard to grow in single-crystal form or that require protection from the environment and give them the ease of processing afforded many polymers. In addition, sometimes the material must be used at the nanoscale to achieve specific optical properties, and the matrix is used just to hold the particles together and provide processability. For example, high-grade optical composites, with properties otherwise obtainable only in optical glasses, become accessible through the use of polymer moulding techniques.

Electrical properties are expected to be different when the fillers get to the nanoscale for several reasons. First, quantum effects begin to become important, because the electrical properties of nanoparticles can change compared to the bulk. Second, as the particle size decreases, the interparticle spacing decreases for the same volume fraction. Therefore, percolation can occur at lower volume fractions. For example, the high aspect ratio of carbon nanotubes or exfoliated graphite leads to percolation at a lower volume fraction and thus increases in electrical conductivity of polymers at a lower volume fraction than in nonexfoliated graphite (Xiao, et. al., 2001).

2.5 Characterization Techniques for Nanocomposites

As the nanocomposite properties dramatically depend on the good dispersion of the filler in the matrix, it is necessary to develop technical methods to characterise the nanodispersion.

For determination of morphology, polymer matrix nanocomposite were characterized by some techniques such as Transmission Electron Microscopy, TEM, Scanning Electron Microscopy, SEM, Atomic Force Microscopy, AFM and X-ray Diffraction, XRD.

Characterization tools are crucial to comprehend the basic physical and chemical properties of PNCs. For structural applications, it facilitates the study of emerging materials by giving information on some intrinsic properties (Meyyappan, 2004). Various techniques for characterization are discussed below:

2.5.1 Scanning Electron Microscopy (SEM) and Atomic Force Microscopy (AFM)

SEM is used to determine the morphology and shape of particles on the surface of material. In polymer matrix nanocomposite especially when low amount of nanoparticles is added to polymer, polymeric chains cover the nanoparticles, such that the surface image of the SEM cannot be used to determine the morphology of the nanoparticles in matrix**.** One way for determination of nanoparticles in polymeric matrix is by using cross sectional SEM image, which is prepared by cutting a small cross section of the polymeric nanocomposite sample and then immersing it in liquid nitrogen for nearly some minute to ensure it is completely frozen. It is then removed from the liquid nitrogen and immediately broken or fractured. AFM is also used to determine the morphology of particles at the surface of thin film sample, and high loading nanoparticle (fillers) can be detected in polymeric matrix. For example SEM images of tin and bismuth sulphide nanostructure and polymer matrix nanocomposite of those with acrylonitrile butadiene styrene (ABS) copolymer are shown in Fig 2.7, which confirm that SEM images cannot perfectly determine nanoparticles in polymer matrix (Salavati-Niasari, *et al.* 2009; Salavati-Niasari, *et. al.*, 2010). AFM images

of pure copolymer and ABS/tin sulfide are also given in Fig 2.8, which shows the same results.

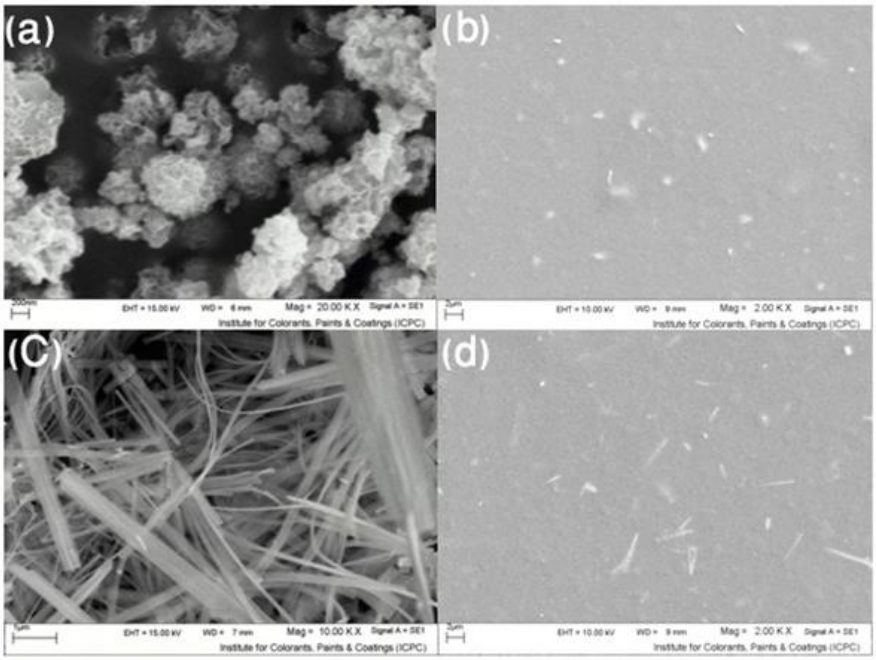


Figure 2.7: SEM images of a) SnS nanoflowers b) ABS/SnS c) Bi_2S_3 nanorods d) ABS/Bi_2S_3 Courtesy: (Salavati-Niasari, *et al.* 2009; Salavati-Niasari, *et al.* 2010).

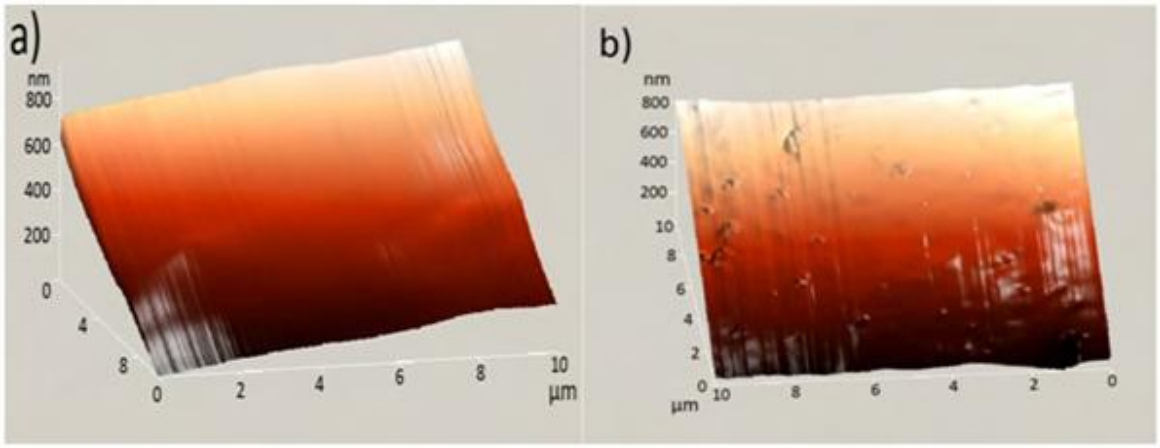


Figure 2.8: AFM images of a) pure ABS b) ABS/SnS nanocomposite

2.5.2 Transmission Electron Microscopy

Transmission Electron Microscopy (TEM) is widely employed, in its simplest bright-field mode, as a tool for direct visualization of the nanocomposite structure of polymer nanocomposites. This is possible because there exists sufficient contrast for the transmitted electrons between the polymer matrix and most filler (inorganic material such as metal oxides). In the extreme case, high-resolution TEM can even provide a qualitative picture of the inorganic filler crystal structure (Morgan and Wilkie, 2007). One must remember that to obtain one TEM requires only a miniscule piece of material and one cannot be certain that this is representative of the whole. The morphology can only be clearly determined by sampling enough of the material (Bras, *et al.* 2005). Fig. 2.9 a) shows TEM image of PMMA/TiO_2 and TEM image of ABS/clay is shown in Fig. 2.9 b) (Wang, *et al.* 2004; Laachachi, *et al.* 2005).

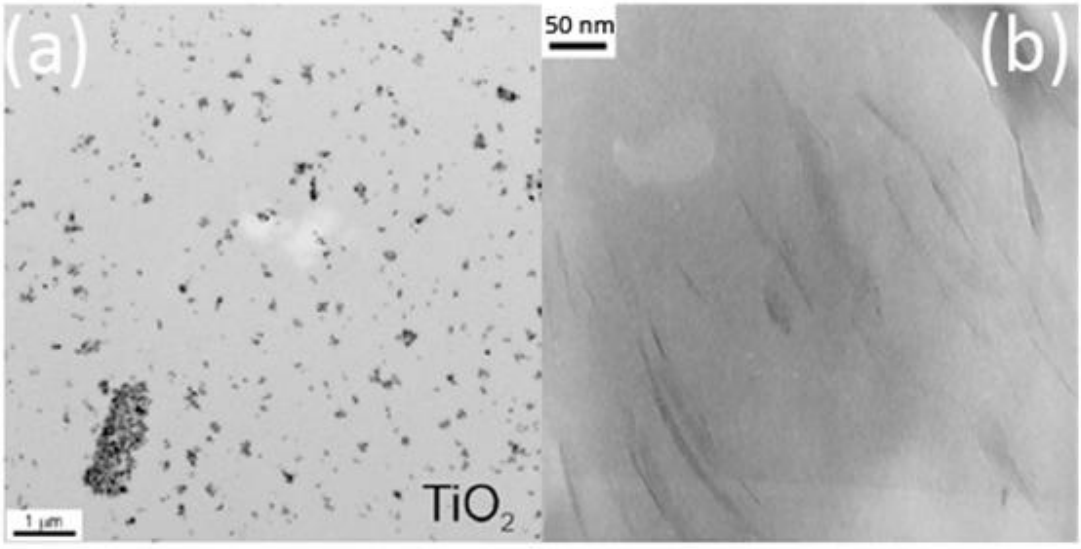


Figure 2.9: TEM images of a) PMMA/TiO_2 nanocomposite b) ABS/OMMT nanocomposite, (Courtesy; Wang, *et al.* 2004; Laachachi, *et al.* 2005)

2.5.3 X-Ray Diffraction (XRD) technique

XRD enables the determination of the *d*-spacing of the clay. An immiscible system is obtained if the *d*-spacing in the presence of the polymer is unchanged from that of the pristine clay. If the *d*-spacing increases, this indicates that intercalation has occurred. Since the registry between the clay layers is lost in an exfoliated system, no peak is expected.

Unfortunately, this same situation will occur if the clay is extensively disordered, so XRD information alone is not enough to identify the morphology. For these reasons, in general, XRD analysis is not used alone in studies to deduce the nanocomposite morphology (Bras, *et al.* 2005).

XRD pattern ABS–clay hybrid nanocomposites are shown in Fig 2.10. With exchange of Na+ by alkyl ammonium, distance between layers increase and XRD peak shift to lower angle. XRD patterns of ABS-OMMT because of intercalation of single chains of ABS in the galleries of the host shows an increasing interlayer distance and peak shift to lower angle (Wang, *et al.* 2004).

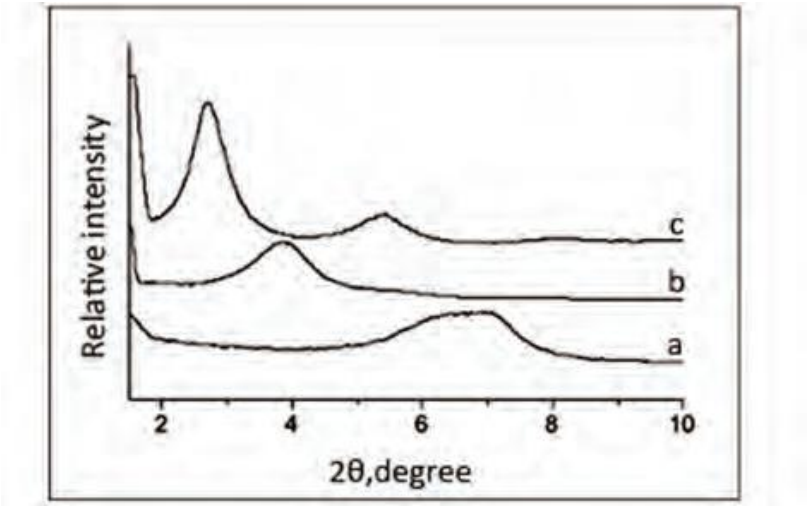


Figure 2.10: XRD patterns of a) pristine sodium montmorillonite b) modified montmorillonite (OMT) c) ABS/OMT nanocomposite. (Courtesy; Wang S, *et al.* 2004)

2.5.4 Differential scanning calorimetry: DSC

DSC is the most widely used of the thermal techniques available to the analyst and provides a fast and simple method for obtaining beneficial information about a material. A DSC analyzer measures the energy changes that occur as a sample is heated, cooled or held isothermally. The energy changes enable the user to find and measure the transitions that occur in the sample quantitatively such as measurement of glass transitions (Gabbott, 2008).

2.6 Application of CNT Nanocomposites

2.6.1 Flame retardant nanocomposites

Together with numerous advantages that synthetic polymeric materials provide to society in everyday life, there is one obvious disadvantage related to the high flammability of many synthetic polymers**.** Consequently, improving the fire retardant behaviour of polymers is a major challenge for extending their use to most applications. Nanocomposites are very attractive due to the fact that small amount of nanostructure can lead to great improvement in fire resistant property of nanocomposites, (Ajayan, et al., 2003).

2.6.2 Nanocomposites with high mechanical stability, stiffness, strength, toughness

By using minimal addition levels, excellent mechanical properties can be achieved. For example polyamide-6clay nanocomposite, containing 5% clay, shows an increase of 40% in tensile strength, 68% in tensile modulus, 60% in flexural strength and 126% in flexural modulus (Bras, *et al.* 2005).

2.6.3 Nanocomposite solar cells

Polymer-based solar cells have the capability of being used to make cheap large flexible panels. The only downside is substantially low efficiency compared to commercial solar cells (Kothurkar, 2004). Cadmium chalcogenides such as CdS nanoparticles in polymers have been used to make solar cells. Numerous efforts are being taken to improve the efficiency of the cells. In general a higher density of the nanoparticles is advantageous. Control of the band edge of the particles is also very important factor controlling the efficiency of the solar cell. Polymer semiconductor nanocomposites offer the promise of a new generation of hybrid materials with numerous possibilities of applications such as in optical displays, catalysis, photovoltaics, gas sensors, electrical devices, mechanics, photo-conductors and superconductor devices (Kothurkar, 2004).

2.6.4 Nanocomposite membrane for gas separation and gas permeability

Many inorganic types of filler are dispersed in polymer matrices to improve pure polymeric membrane properties and constituted mixed-matrix membranes (MMMs). Result of such mixed matrix membrane is the superior transport properties. With addition of low amount of nanoparticles to polymeric membrane, we achieve great increase in permeability of membrane. There are many reports of improved penetrate permeability (Kim and Marand, 2008).

2.7 Manufacturing of CNT Nanocomposites

In some of these areas, fundamental studies of mechanical, electrical, thermal, optical, and chemical properties are required along with related research for real applications. For manufacturing of nano-phased structural polymer composite material, the first step will be

choice of a fabrication method. Some of the widely used methods for manufacturing conventional composite parts are wet lay-up, pultrusion, resin transfer molding (RTM), vacuum assisted resin transfer molding (VARTM), autoclave processing, resin film infusion (RFI), prepreg method, filament winding, fibre placement technology, etc. (Mazumder, 2002).

Wet lay-up is a simple method compared to other composite manufacturing methods; it allows the resin to be applied only in the mold, but the mechanical properties of the product are poor due to voids and the final product is nonuniform. Pultrusion is a low cost continuous process with a high production rate. But near the die assembly, the prepreg or materials accumulate and can create a jam. Voids can be also created if the dies run with too much opening for the fibre volume input. Moreover, a constant cross section is a limitation of this process (Mazumder, 2002). But the fibres in pultruded material are generally well aligned (Roy, *et. al.*, 2005); it helps to reduce fibre misalignment in the composite through optimization of manufacturing process variables, such as pull-speed, preformer temperature, nanoparticle alignment and/or dispersion. The RTM is a closed mold operation (Mazumder, 2002). In this process, resin flow and fibre wet-out are critical issues; resin flows in the plane as well as in the transverse directions of the preform. Fibre wet-out depends on the fibre architecture and permeability of the preform. Recent developments in textile and resin technology have allowed the designer and manufacturer to use RTM for the fabrication of parts for the primary and secondary structures (Octeau, *et. al.*, 2004). Advanced textile technology has helped to increase the wetability of the preforms. A fibre volume fraction of 55–60% can be achieved. Higher toughness can be achieved by using three-dimensional weaving and stitching technology. The VARTM is an

adaptation of the RTM; a widely used single-sided tooling process such as open molds are used to make the parts using vacuum (Mazumder, 2002). This process has certain advantages like a relatively low cost for high volume production, very large and complex parts are possible with improved surface finish, higher fibre volume fraction than hand lay-up and as it is a closed system, it reduces environmental concerns more than hand layup. Both in RTM and VARTM, if the resin viscosity is high it restricts the flow of resin. The effect of nanoconstituents on the matrix resins creates a problem in the altered resin viscosity and cure kinetics (Fielding, *et. al.*, 2004), and there is a possibility of dry spots or uneven distribution of resin over the entire volume of the reinforcement (Hussain, *et. al.* 2005).

Autoclave processing is a promising technique to process and manufacture different complex shapes of high-quality composite structures (Mazumder, 2002). It has the ability to process both thermoset and thermoplastic composites with uniform thickness and minimum porosity. However, the major difficulty in this process is the higher capitalization cost. But with the increasing requirement for high-performance composite materials for new generation aircrafts, autoclave application remains one of the most widely used techniques in the aerospace industry (Chen and Tanguay, 2004).

Resin film infusion (RFI) is similar to RTM where a thin film or sheet of solid resin is laid into the mold and preform is laid on top of the resin film under heat and pressure. Resin impregnated unidirectional or woven fabric (partially cured) is used in the prepreg method with vacuum bagging and autoclave processing. Although the method is labour intensive, resin distribution in preform is usually uniform.

In filament winding, resin impregnated fibres are wrapped over a mandrel at the same or different winding angles to form a part. Complicated cylindrical parts, pressure vessels, fuel and water tanks for storage and transportation, and pipes can be manufactured by this method. The viscosity-related problems of the resin systems can be eliminated in this technique (Mahfuz, *et. al.*, 2005). But the critical task is programming the wet winding in this technique.

Filament winding is a cost-effective alternative for fabricating spherical and cylindrical parts (even those with varying diameters and surface contours). However, it cannot lay tow on a concave surface. Fibre placement is one of the technologies developed for automation and affordability of composite manufacturing. Fibre placement developed as a logical combination of filament winding and automated tape placement technique to overcome many of the limitations of each manufacturing method. Although tape laying systems generally are more efficient than fibre placement in making large flat panels and components with simple curvatures, fibre placement can accommodate much more severe curvature as well as complex contours. Fibre placement eliminates the crossover points produced in filament winding, can crimp fibres, and reduce mechanical properties.

For advanced structural applications, it is required to incorporate nano-reinforcements into macroscopic functions and validate them at the nanometric level. Recently, nanocomposites have been introduced in structural applications, such as automotive parts, gas barrier films, scratch-resistant coating, flame-retardant cables, etc. Also RTM, VARTM, RFI, and filament winding techniques can be used to manufacture nanocomposite parts for various applications including commercial aircraft structures for Boeing, Airbus, as well as many products in the industrial markets. Routine use of nanocomposites in automotive and

aerospace industries is a long-term prospect as these are risk-averse sectors and extensive testing and characterization alone takes significant time (RTO Lecture Series, 2005). But more emphasis should be given to technology development and for this issue participation from engineering communities are urgently needed. Hence, it will be easier to develop a product and bring out a product from the lab (RTO Lecture Series, 2005).

2.7.1 Recent Advances in CNTs Processing: Dispersion and Orientation

Two essential components for optimal reinforcement in particle-reinforced composite systems are filler dispersion and orientation. Dispersion of single-wall carbon nanotubes (SWCNTs) and higher concentrations of multi-wall carbon nanotubes (MWNTs) into a polymer matrix has been one of the largest challenges to date (Haggenmueller, *et. al.* 2000), due to the aggregation of the nanotubes as a result of the van der Waals interactions between individual tubes. Consistent dispersion of reinforcing material throughout the matrix leads to consistent load transfer from matrix to particle. Moreover, it can assist with the realization of a network for conductivity of electrical and thermal energy. Many composite researchers believe that SWNTs will be the ultimate reinforcements for the next generation high performance structural and multifunctional composite materials. Thostenson et. al. (2001) stated some critical issues in the processing of CNT polymer composites in their review; uniform dispersion (Shaffer and Windle, 1999; Gong, et. al., 2000), wetting and alignment of the carbon nanotubes (Jin and Bower, 1998; Ajayan, *et. al.,* 1994) in the polymer matrix and functionalization of CNT for the nanotube/matrix interfacial bonding (Thostenson, *et. al.* 2001). The SWCNTs agglomerate more easily than MWNTs due to their size differences (i.e., greater surface area) and can form ropes or aligned bundles of SWNTs. The SWNTs often require more specialization to produce than

MWNTs. Therefore, the cost of purified SWNTs tends to be greater than that for MWNTs. The MWNTs, on the other hand, have been found to demonstrate lower mechanical, electrical, and thermal properties due to the ability of the concentric nanotubes to slide past each other. Due to the inherent tube within a tube structure, the MWNTs tend to have a larger diameter (10 nm) as compared with SWNTs (1 nm). However, improvements in nanotube fabrication have led to MWNTs with more precise, smaller diameters. This may lead to the nanotubes with improved properties over larger diameter MWNTs with less agglomeration than SWNTs.

Similarly, orientation in the direction of applied forces allows for greater load transfer. If the particle is oriented in a direction other than the direction of the applied force, the full potential of the particle cannot be realized. In addition, having all the particles oriented in the same direction allows for easier transfer of energy (electrical or thermal). Achieving consistent dispersion and orientation will allow optimal property improvements. Researchers have used many different techniques in an attempt to disperse nanotubes in polymer matrices including solution chemistry to functionalize the nanotube surface (Chen, J., *et. al.* 1998; Mitchell, *et. al.,* 2002; Bubert, *et. al.,* 2003; Eitan, *et. al.,* 2003; Jang, *et. al.* 2003), the use of polymers to coat the nanotube surface (Star, *et. al.,* 2001) in situ polymerization of the nanocomposite (Jia, *et. al.* 1999; Deng, *et. al.* 2002), ultrasonic dispersion in solution (Safadi, *et. al.,* 2002; Qian, *et. al.* 2000), melt processing (Gorga and Cohen, 2004; Bhattacharyya, *et. al.,* 2003), the use of surfactants (Gong, *et. al.* 2000; Shaffer, *et. Al.,* 1998), electrospinning (Dror, *et. al.,* 2003), electrode chemistry (Chen, *et. al.,* 2000) and gelation/crystallization (Bin, *et. al.,* 2003). In gelation/crystallization experiments, the nanotubes were dissolved in a solvent, polymer solution was added, a gel

was formed, the gel was formed into a film, and finally the solvent was evaporated (Bin, *et. al.* 2003). Nanotube surface modifications used plasma treatment or chemical oxidation to attach the functional groups. These groups allowed the nanotubes to bond better to the matrix and overcome the van der Waals interactions between nanotubes (Jang, *et. al.* 2003). Melt compounding involves creating a preblend by dry mixing polymer powder with nanotube powder. The preblend is fed into an extruder allowing for control of shear, temperature, and residence time. After the residence time, the material is extruded in the film or fibre form (Gorga and Cohen, 2004). Good dispersion alone has shown moderate property improvements, but nanotube alignment, or orientation, has led to further improvements. Using melt compounding followed by melt drawing, has shown a significant increase in mechanical properties (Potschke, *et. al.*, 2002; McCullen, *et. al.*, 2006). Transmission and scanning electron microscopy have shown good dispersion and orientation using such methodology (Gorga, and Cohen, 2004). These improvements have been shown to increase until an optimal loading level and then decrease above this concentration (Gorga and Cohen, 2004; Wilbrink, *et. al.* 2001). In addition to mechanical drawing, the inherent conductive nature of carbon nanotubes has been utilized to induce alignment. For example, the application of a magnetic field to a nanocomposite sample during or after processing has shown nanotube alignment (Choi, *et. al.*, 2003). To bring out the anisotropic nature of nanotubes, Walters et al. (2001) prepared a freestanding aligned SWCNT film by filtering the nanotube dispersion under a high magnetic field up to 19 T. Kimura and Ago (2002) applied this technique to MWNT–polymer composites and obtained anisotropic composites, with a better percolation path and higher elastic modulus and glass transition temperature. Fan and Advani (2005) subjected the vinylester resin system to shear flow for MWNT orientation and used a second-order orientation tensor to

describe the orientation in 2D plane. Again, the optimal properties, as predicted by such models as Halpin–Tsai, have not been achieved due to poor interfacial bonding, variations in nanotube structure, and variations in properties.

2.8 Future Outlook

The potential of nanocomposites in various sectors of research and application is promising and attracting increasing investment from Governments and business in many parts of the world (Nanoscience and Nanotechnologies, 2004). While there are some niche applications where nanotechnology has penetrated the market, the major impact will be at least a decade away. Currently, there are a few cosmetic products made by incorporating nanoparticles on the market. To create such macroscale materials, many issues surrounding the incorporation of nanotubes into a matrix, strategies for property improvement, and the mechanisms responsible for those property improvements still remain critical. Since only a moderate success has been made over the last 20 years, researchers must continue to investigate strategies to optimize the fabrication of nanotube-enabled materials to achieve both improved mechanical and transport properties (Lau, *et al.* 2006).

Biodegradable polymer-based nanocomposites have a great deal of future promise for potential applications as high-performance biodegradable materials. These are entirely new types of materials based on plant and nature materials (organoclay). When disposed of in compost, these are safely decomposed into CO_2, water, and humus through the activity of microorganisms. The CO_2 and water will become corn or sugarcane again through plant photosynthesis. Undoubtedly, their unique properties originating from the controlled nanostructure paves the way for a much broader range of applications (already

commercially available through Unitika Ltd., Japan), and opens a new dimension for plastics and composites.

According to several sources (Chemical Business Newsbase, Plastic News), a significant increase in turnover of about 100%/year, leading to a value of about 1500 million Euro (ca. 500,000 ton/year of polymer nanocomposites) in 2009 is expected (Ebenau, 2002). Even if these numbers are overly optimistic, they highlight the tremendous technological and economical potential associated with polymeric nanocomposites including not only clay but also other inorganic nanofillers, such as carbon nanotubes, SiO_2, SiC, and Si_3N_4.

At present it is difficult to predict which, if any, market sector would not be able to benefit from this technology. Thus, it may well be that polymeric nanocomposites in the mid and longer-term will pervade all aspects of life, similar to the way plastics did in the last century. Clearly a diverse range of sectors such as aerospace, automotive, packaging (particularly food but also solar cells), electrical and electronic goods, household goods etc. will profit substantially from a new range of materials which would be offered by this technology. In the short term (<5 years), the commercial impact may include inkjet markets, nanoparticles in cosmetics, and automotive applications such as body moldings, engine covers and catalytic converts, batteries and computer chips (RTO Lecture Series, 2005).

In the mid-term (10 years), memory devices, biosensors for diagnostics, and advances in lighting are all possible. The time-scale for automotive, aerospace, and bio-nanotechnology is a long-term prospect (>15 years) as these are risk-averse sectors and thereby for large-

scale production it is necessary to carry out strict testing and validation procedures (RTO Lecture Series, 2005).

2.9 Adapted Manufacturing method for the Project

Nowadays every home, every office, every vehicle, every factory, contains various types of parts which have been injection moulded. These include items such as, yoghurt cartons, electric casings, television housings, computer casings, paint brush handles, combs, syringes, gearwheels, typewriters, crash helmets, fascia panels, telephones, brief cases, reflectors, GSM handset casings, to mention just a few items made from plastic injection moulds. These products have been produced wholly or partially on Injection Moulding Machines.

2.9.1 Plastic Injection Moulding Machines

Plastic injection moulding machines are well known for producing moulded plastic articles from plastic materials wholly or partially.

There are many variations in injection moulding machines; however, the basic machines are either the screw-ram, or plunger type. The difference between these two types is the method in which the plastic material is delivered from the hopper to the nozzle of the machine. Machines of the reciprocating-screw type are used more because of the faster cycles, lower melting temperatures, and better mixing of the material. Basically the screw is capable of reciprocating as well as turning so that it can act as a plunger and as an extruder. As the melts build up at the end of the screw, the screw moves backwards. Once there is enough melt to fill the mould (measured by how far back the screw has travelled) the screw is driven forward, pushing the melt through the nozzle, along the sprue into the mould

cavity. A non-return valve is fitted at the end of the screw to prevent the melt from being pushed back along the screw.

2.9.2 History of Plastic Injection Moulding Machine

The Injection Moulding machines have undergone various stages of developments, evolving from the versions based on the pressure die casting technique for metals in late 1880s to the present highly sophisticated, complex, computerized Reciprocating Screw Injection machines versions.

In 1868, perhaps in response to a request by billiard ball maker Phelan and Collander, John Wesley Hyatt invented a way to make billiard balls by injecting celluloid into a mould. By 1872, John and his brother Isaiah Hyatt in the United States patented what was regarded as the first injection moulding machine, specifically for use with Celluloid. The machine though primitive yet it was quite suitable for its purposes. It contained a basic plunger to inject the plastic into a mould through a heated cylinder. This was an important invention but probably before its time because in the following years very few developments in moulding processes were reported. It was not until the 1920s, in Germany, that a renewed interest was taken in the process. The first German machines were very simple pieces of equipment and relied totally on manual operation. Levers were used to clamp the mould and inject the melted plastic with the result that the pressures which could be attained were not very high. Subsequent improvement led to the use of pneumatic cylinders for clamping the mould which not only lifted some of the burden off the operator, but also meant that higher pressure could be used.

The next major development in moulding which is the introduction of hydraulically operated machines did not occur until the late 1930s when a wide range of thermoplastics started to become available. However these machines still tended to be hybrids based on die casting technology (the original injection moulding machines were based on the pressure die casting technique for metals).

Revolutionizing the plastics industry in 1946, James Hendry built the first screw injection moulding machine with an auger design to replace Hyatt's plunger type injection machine of 1872. The auger is placed inside the cylinder and mixes the injection material before pushing forward and injecting the material into the mould.

Further design improvement of injection moulding machines for plastics was not taken really seriously until the 1950s when a new generation of equipment was developed. The machines catered more closely for the particular properties of polymer melts and modern machines are of the same basic design although of course the control systems are very much more sophisticated nowadays.

2.9.3 The Plastic Injection Moulding Process

The process starts with the feeding of the polymer resin (pellets) down to the auger (screw) through a large open-bottomed container (hopper). An electric (or hydraulic) motor is responsible for turning the auger inside a heated cylinder which feeds the pellets up through the grooves of the auger. A gate before the mould cavity restricts the flow of the melt into the mould and limits backflow. The pressure created by pushing the forward through the grooves up to the gate also produces heat on the inside of the cylinder which helps to melt the polymer and prepare it for injection into the mould.

As the auger moves forward it injects polymer melt into the mould at high pressure (typically 10,000 - 30,000 psi), holds it, and adds more melt to ensure the contraction due to cooling and solidification does not leave gaps in the final product. Eventually the gate solidifies and isolates the mould from the injection cylinder.

The moulds are typically air or water cooled. Sometimes small holes are bored into the mould that allow a cooling liquid (such as water) to be circulated. Injection mould cooling consumes about 85% of the cycle time for the entire process.

After solidification, the clamp holding the two halves of the mould together closed is opened allowing the part to be removed. The injection moulding process can then be repeated.

2.10.0 Design Theory

2.10.1 Design Considerations

In the manufacture of plastic resins, the final step often involves extrusion of dried granular polymer to homogenize and palletize the material. Alloys, blends, recycle materials filled compounds and colour concentrates also are made using extrusions as a final mixing step. Sheet that is later stamped or thermoformed is first extruded. Film, fibre, tubing, pipe, weather stripping and numerous other profiles are sheathed with plastic or rubber in extruders. These are examples of continuous extrusion processes. Blow moulding of containers is an example of a noncontinuous extrusion operation that uses the basic elements of screw extrusion in a modified fashion. Injection moulding is another example of a noncontinuous screw operation in which an extrusion screw melts incoming polymer and homogenizes the melt before injection into the moulds. Therefore extrusion screws are

basic mechanical elements in many polymer processes and warrant appropriate attention. The design attention is therefore, focused on a single-stage, single-screw flight (i.e. pitch equals lead) machines for continuous extrusion of thermoplastics.

The following design criteria form the basis of this work:

1. The design targets the use of high density polyethylene (HDPE) as matrix
2. The ratio between the length and diameter of screw or the L/D ratio was selected to be 24 from standard chart.
3. Screw flight angle is to be 17.7^{o} (In practice, a screw flight angle of 17.7^{o} is frequently used because it is the angle which occurs if the pitch of the screw is equal to the diameter and so it is convenient to manufacture).
4. Maximum screw speed of 50rev/min was selected.
5. Provision is made for opening of the barrel in the event of servicing or cleaning.
6. Barrel diameter of 40mm was selected.
7. Flight depth (metering zone) of 3mm was selected.
8. Maximum melt viscosity is to be 500 Ns/m^2.
9. Gearbox of ratio 89.1:1 was selected.
10. Screw length of 960 mm was selected.

2.10.2 Design of components

2.10.2.1 The Hopper

A simple gravity feed with a conical hopper having a 20-45^{o} taper is to be designed; discharge of material is by its own weight. The following assumptions have been made;

1. The bulk density of the material is constant
2. Material in the hopper is in incipient slip condition at the walls and the wall friction is fully immobilized.

Based on the factors mentioned above, a convergent conical hopper was designed. The half angle of the cone is 45^{o}.

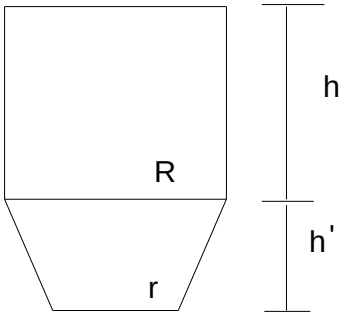


Figure 2.11: Schematic representation of convergent Hopper

From mensuration, the total volume, V, of the hopper is given by Keneth (1950)

$$V = \pi R^2 h + (1/3)\pi h^1 \left(R^2 + r^2 + Rr\right) \quad - \quad - \quad - \quad - \quad (1)$$

Where R is the bigger radius and r, the smaller radius

The pressure at the base approaches a limiting value as the height, h, increases. Hence, the maximum pressure at the feed end, which Zeher Tadmor (1979) gave as:

$$P_{\max} = \rho bD / 4\, fK \quad - \quad - \quad - \quad - \quad - \quad - \quad (2)$$

Where D is the hopper diameter, f is the static coefficient of friction on the wall, ρb is the bulk density of the material and K is the ratio of principal stresses at all points.

$$K = (1 - \sin\ \delta)/(1 + \sin\ \delta) \quad - \quad - \quad - \quad - \quad - \quad (3)$$

Where δ is the effective angle of friction

2.10.2.2 The Flow Theory

The movement of materials through the flights of a single-screw machine is composed of three distinctive types of flow, they are:

i. Drag flow, Q_D

ii. Pressure back flow, Q_P

iii. Leak flow, Q_L

The total output of the barrel, Q is given as the algebraic sum of all the flows

$$Q = Q_D - Q_P - Q_L \quad - \quad - \quad - \quad - \quad - \quad - \quad (4)$$

The geometry of a single-flighted screw pump is as shown in fig.2.12

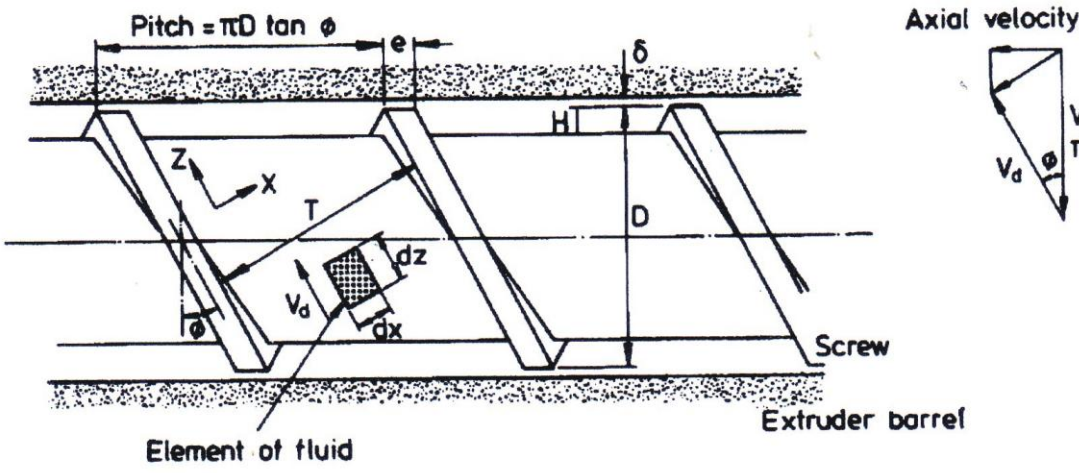


Figure 2.12: Single start Screw

Leakages: the dimension of the slit through which the leak flow is taking place are:

Height = δ, length = e Cosδ

Width = $\pi D / Cos\ \delta$

Taking account of the overall pressure drop, ΔP and factor, E to allow for eccentricity, the leakage flow becomes; (Eastop, 1993)

$$Q_L = \lambda - D^2 E \delta^3 \tan \phi \Delta P / 12 \eta e L \quad - \quad - \quad - \quad - \quad - \quad -(5)$$

The algebraic sum of the flows as stated in equation 4 becomes

$$Q = \frac{\pi^2 D^2 N h Sin\ \phi Cos\ \phi}{2} - \frac{\pi D h^3 Sin^2 \phi \Delta P}{12 \eta L} - \frac{\pi^2 D^2 E \delta^3 \tan \phi \Delta P}{12 \eta e L} \quad - \quad (6)$$

Where N is the speed of rotation (rev/min), L, the length of screw (m) and η denotes the viscosity of the material (N/m-s).

By eliminating ΔP in equation 6, and ignoring small leakage flow, an expression is obtained for Q. When Q is differentiated w.r.tϕ and h and equated to zero, ϕ is found to be 30^o after solving simultaneously. Hence, Fisher (1976) gave the volume flow rate as

$$Q = \frac{AhSin\ \phi Cos\ \phi}{1 + BL^3} \quad - - - - - - - \quad (7)$$

Where

$$A = \frac{\pi^2 D^2 N}{2} \quad - - - - - - - - \quad (8)$$

$$B = \pi D/2 \quad - - - - - - - - \quad (9)$$

And with $\phi = 30^o$, h is the flight clearance

Zeher Tadmor (1979) gave the expression for the mass flow rate, G in the solid conveying zone as

$$G = V_P \rho_b \left[\pi/4\left(D_b^2 - D_s^2\right) - eH/\sin\theta\right] \quad - - - - - \quad (10)$$

D_b is the barrel diameter, D_s, the screw diameter, ρ denotes the bulk density and θ is the mean helix angle.

Where the tangential velocity, V_p is given by

$$V_p = \frac{V_b \tan\phi \tan\theta}{\tan\phi + \tan\theta} \quad - - - - - - - \quad (11)$$

Whereas the barrel velocity V_b is expressed as

$$V_b = \pi N D_b \quad - \quad - \quad - \quad - \quad - \quad - \quad - \quad - \quad (12)$$

And $\tan \theta = L_s / \pi D$ - - - - - - - (13)

Zeher Tadmor (1979) also gave an expression for the overall pressure drop from entrance to exit as

$$P_2 - P_1 = 12 \mu L \left(\frac{V_0}{2H^2} - \frac{Q}{WH^3} \right) \quad - \quad - \quad - \quad - \quad - \quad (14)$$

Where $V_0 = \pi N D$ - - - - - - - (15)

$H, W,$ and D, denote channel depth, channel width, and inner diameter (all in metres) respectively, and Q is flow rate in m^3/s.

2.10.2.3 The Heat Flow Theory

This section deals with the heat flow/gain pattern and requirement of the barrel to attain full melt of the charge.

Most processes that involve flow heating are critically dependent on the uniformity of the temperature in the work piece. For the design, an electrical resistance heating was chosen because of its neatness, variable and high temperature range, ease of maintenance and control.

Quantity of heat gained by a material is given by Eastop (1993) as;

$$Q = mc \Delta \theta \quad - \quad - \quad - \quad - \quad - \quad - \quad - \quad (16)$$

Where m is the mass flow rate, C is the specific heat capacity and $\Delta\theta$ is the temperature rise. According to Ohm's law, electric power is given as;

$$P = IV_d \quad - - - - - - - \quad (17)$$

and the amount of energy responsible for this, $H = IV_d t$ - -(18)

Where $I, V_{d,}$, and t stand for electric current (amps), potential difference (volts) and the time (seconds) respectively.

For this work, the following assumptions were made;

1. Heat loss to the surrounding from inside the barrel is minimal

2. There exists a steady state heat conduction

3. Heat supplied is concentrated directly on the charge inside the barrel.

The total heat supplied is equal to the quantity of heat gained by the charge and the barrel.

$$H = \left(mc\,\Delta\theta\right)_{charge} + \frac{2\pi LK\left(t_1 - t_2\right)}{\ln\left(r_2 / r_1\right)} \quad - - - - \quad (19)$$

2.10.2.4 The Barrel

Barrels are classified as thin barrels or thick barrels depending on the thickness to diameter (t/d) ratio. For t /d < 0.1 $\Rightarrow$ thin barrel and t/d > 0.1 $\Rightarrow$ thick barrel (Black, 1968).

The analysis of stresses induced in a thin walled cylinder as shown in Figure 2.13 below will be made neglecting the effects of curvature of the cylinder wall and by assuming that the tensile stresses are uniformly distributed over the section of the walls.

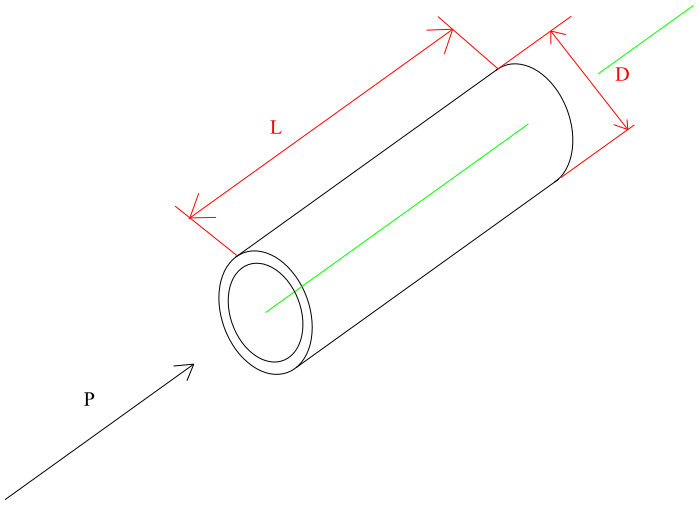


Figure 2.13: Analysis of stresses induced in a thin walled cylinder

2.10.2.5 The Circumferential (Hoop) Stress

The fluid force acting on the longitudinal section per unit length is given as P x d and for equilibrium of forces, may be equated to the resisting force = $2t\sigma_0$ hence the safe thickness, t is given as

$$t = \rho d / 2\sigma_0 \quad - \quad - \quad - \quad - \quad - \quad - \quad - \quad (20)$$

2.10.2.6 The Longitudinal Stress

The fluid acting on a ring section = $\frac{1}{4}\pi d^2 P$. The resisting force in this direction = $\pi dt\sigma_1$. Hence for equilibrium of forces in the longitudinal section, the safe thickness is given as

$$t = \rho d / 4\sigma_1 \quad - \quad - \quad - \quad - \quad - \quad - \quad (21)$$

Where σ_1, σ_o are longitudinal and hoop stresses respectively and

ρ, d are internal pressure and diameter, and t, is the wall thickness

2.10.2.7 Barrel Heat Flow

For a heat flow through a cylinder of internal radius r_1, and external radius r_2, with a temperature difference $(t_1 - t_2)$, the following equation holds. (Eastop, 1993).

$$Q = 2\pi LK \frac{(t_1 - t_2)}{\ln(r_2/r_1)} \quad - \quad - \quad - \quad - \quad - \quad - \quad (22)$$

Where;

Q = Rate of heat flow per metre length

K = Conductivity of the material (48.3 W/mk for mild steel)

2.10.2.8 The Screw

The screw is a very vital part in this machine. It plays a major role in receiving, conveying, mixing, metering, etc. The screw hence, has, on the average, three distinct zones along its length as illustrated below.

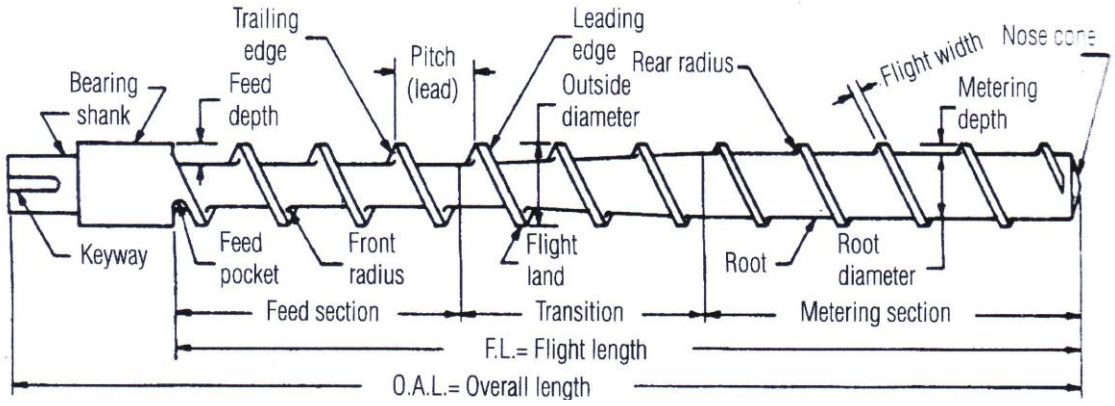


Figure 2.14: Basic elements of a single-stage extruder screw

2.10.2.9 The Feed Section

The purpose of this zone as the name implies is to pick up the cold material from the hopper and feed it to the compression zone. It is usually of parallel core diameter.

2.10.2.10 The Compression or Transition Section

This section is formed by the gradual increase of the root diameter of the screw until the diameter of the metering section is reached. It is a zone of melting, pumping and mixing. The material gradually transits from solid to liquid state.

2.10.2.11 The Metering Zone

The metering zone is the final part of the screw and acts rather as a metering pump from which the molten plastic material is delivered to the die system at constant volume and pressure. However, it must be noted that in spite of the changing core diameter or flight depths in a screw pump, the external diameter remains constant throughout the length of the screw. More so, the screw must not have a contact with the barrel surface.

2.10.2.12 Shaft Design

The fabricated screw assembly can be assumed to be a beam with reactional forces as indicated below

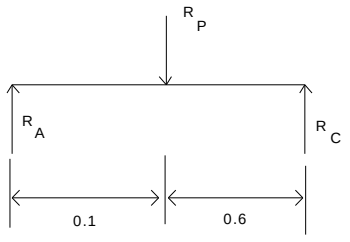


Figure 2.15: Line diagram of the shaft

The bearings are located at points A and C having reactional forces R_A and R_C.

R_p is reaction at the pulley due to its own weight and tension from belt and R is reaction due to weight of the screw. It is assumed that the shaft has no weight. The torsional moment acting on the shaft is:

$$m_t = 9550 \times kw/(rev/\min) \quad \text{(Sharma and Aggarwal, 2006)} \quad - \quad (23)$$

Kw = power, rev/min = speed (rpm)

The ASME code equation for design of transmission shafting is given as

$$d^3 = \frac{16\sqrt{\left[(K_b M_b) + 1/8\,\alpha\, Fd\left(1+k^2\right)\right]^2 + (K_t M_t)^2}}{\pi S_S\left(1-k^4\right)} \quad - \quad - \quad - \quad (24)$$

S_S is the allowable shear stress

K_t, the combined shock and endurance factor for bending

K is the rate of internal to external diameters α is the column action factor and F is axial tension or compression Black (1968).

However, for no axial load no internal diameter (i.e. form solid shaft), $K = 0,\ f = 0, \alpha = 1$.

Hence $d^3 = 16/\pi S_S \sqrt{(K_b M_b)^2 + K_t M_t)^2} \quad - \quad - \quad - \quad - \quad (25)$

K_b and K_t are given as 1.5 and 1.0 respectively for gradually applied or steady loading, M_b and M_t are bending and torsional moments respectively.

2.10.2.13 Bearing Selection

A single row rolling contact bearings was considered appropriate for this design. However, for bigger machines, thrust bearings might serve well due to its high stability.

The magnitude of equivalent load on the bearing is given as (Keneth, 1950):

$$W = \mathrm{X}.V.W_R + Y.W_A \quad - \quad - \quad - \quad - \quad - \quad - \quad (26)$$

Where, W=equivalent load (N)

X and Y are the radial and column factors respectively

V = rotation factor = 1, for bearing with rotating inner race

W_R is the radial load and W_A denotes axial load

$$W_R = \frac{power}{\omega r} \quad - \quad - \quad - \quad - \quad - \quad - \quad - \quad (27)$$

W_A = weight of shaft + total weight on shaft

The dynamic load rating for rolling contact bearings under variable loads is as follows; the approximate rating (service) life of a ball or roller bearing. (Palmgren, 1946)

$$L_R = \left(C/W\right)^k \times 10^6 \text{ revolution} \quad - \quad - \quad - \quad - \quad - \quad (28)$$

$$Or \;\; C = W\left(L_R/10^6\right)^{1/k} \quad - \quad - \quad - \quad - \quad - \quad - \quad (29)$$

L = rating life, C = basic dynamic load rating, W = equivalent dynamic load

$K = 3,$ for ball bearings

$=10/3$, for rollers bearings

$L = 60\,NL_H\,revs$ - - - - - - - (30)

N = speed, L_H = life rating in hours

2.10.2.14 Motor Selection

Torque = $F \times r$ - - - - - - (31)

F = total weight of screw plus load (pulley + material in barrel). The relation is given as

$W = P \times A$ - - -- - - - - - (32)

P = pressure in barrel

A = area of screw

The tangential force, $F = W \tan\theta$ - - - - - (33)

Where $\tan\theta = lead/\pi \times pitch = 1/\pi$ - - - - - (34)

(for single flight screw)

Maximum torque, $T = F \times r$ - - - - - - (35)

Hence, power = $2\pi NT/60$ - - - - - - (36)

2.10.2.15 The Pelletising Die

The die as desired in this work is of a pelletising type. A conical channel pressure flow has been considered most appropriate.

The expression for the volumetric flow rate has been given by Zeher (1979) as

$$Q = \frac{3\pi\Delta P}{8\mu L}\{\frac{\left[R_1^{\ 3}R_2^{\ 3}\right]}{R_1^{\ 2} + R_1R_2 + R_2^{\ 2}}\} \quad - \quad - \quad - \quad - \quad - \quad - \quad (37)$$

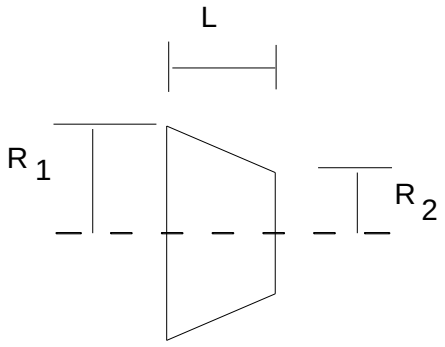


Figure 2.16: Die Section

μ is the viscosity of flow, ΔP stands for change in pressure.

More so, $Q = A_1V_1 = A_2V_2$ - - - - - - (38)

CHAPTER THREE

MATERIALS, DESIGN AND METHODS

3.1 Materials

3.1.1 Experimental materials and equipment

1) Single Walled Carbon Nanotube (SWCNT)
2) High Density Polyethylene
3) Analytical weighing balance
4) Conventional Injection Moulding Machine
5) Modified Injection Moulding Machine
6) Standard tensile bar mould
7) Nose mask and hand gloves
8) Scanning Electron Microscopy
9) Transmission Electron Microscopy
10) Atomic Force Microscopy
11) Differential Scanning Calorimeter
12) X-ray Diffractometer
13) Rheometer
14) Instron testing machine
15) Fluke electrometer.

3.1.2 Fabrication materials and equipment

1) Variable speed gear motor
2) Stainless steel shaft 30mm diameter
3) 2mm stainless steel sheet
4) Ball bearing 206
5) 5x50mm diameter mild steel barrel
6) Screw feeder
7) Hydraulic motor
8) Hydraulic pipelines
9) Hydraulic valves
10) Engineering tool box
11) Lathe machine
12) Milling machine
13) Drilling machine
14) Welding machine
15) Shaping machine
16) Polishing machine
17) Power hark saw
18) Hydraulic press
19) Grinding machine.

3.2 Machine Design

The research work was carried out using normal machine design approach with particular consideration to material cost and availability as follows:-

i. Literature review of existing work

ii. Careful study of major components and parts

iii. Listing of components to be adapted and modified

iv. Design analysis based on material availability

v. Design considerations

vi. Design drawing using AutoCAD

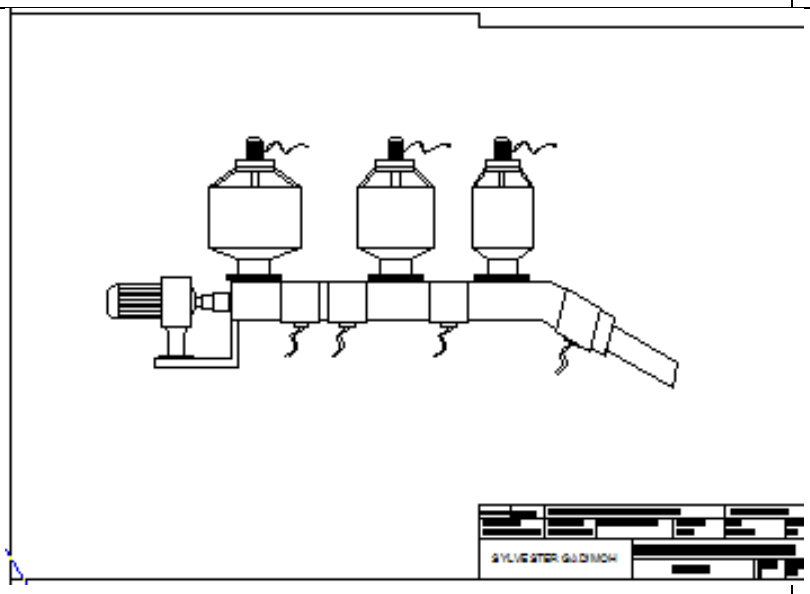
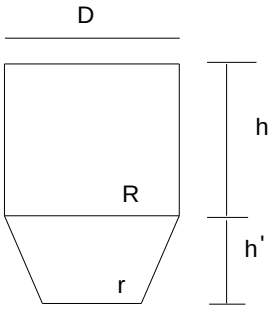
vii. Fabrication of components

viii. Assembly/coupling of components and parts

ix. Test running

x. Reports

3.2.1 Design Calculations

Initial Data	Calculations and Sketches	Result
		
	Figure 3.1: Sketch diagram of the proposed modification	
	3.2.1.1 Capacity of Hopper	
R= 0.13m r=0.025m h = 0.23m h = 0.1m		Capacity of hopper,
	Figure 3.2: Line diagram of feeder hopper.	$V=0.0144m^3$
	From equation 1, $V = \pi \times 0.13^2 \times 0.23 + 1/3 \times \pi \times 0.1$	
	$(0.13^2 + 0.0025^2 + 0.12 \times 0.025) = 0{,}01439m^3$	K = 0.1716

	3.2.1.2 Maximum Pressure at Feed	
	From equations 2 and 3 K = $\frac{1-\sin 45}{1+\sin 45} = 0.1716$	
	$P_{max} = \frac{0.5\times10^{3}\times9.81\times0.26}{4\times0.29\times0.1716}$	
$\delta = 45^{o}$	Maximum pressure = 6.407KN/m^2	$P_{max} = 6.407\ KN$
g=9.81m/52	**3.2.1.3 Volume Flow Rate**	
f = 0.290	Using equation 8	
	A = π^2 x 0.043^3 x 94/2 = 0.8577	
ρ_b = 0.5 x 10^3kg/m^3	B = π x 0.043/2 = 0.0675	
D = 0.043m	Equation. 7 gives	
N=94rev/min		A = 0.8577
ϕ =30^o	Q = $\frac{0.8577\times0.004\times\sin 30\ Cos\ 30}{1+0.00675\times0.06^{3}}$	B = 0.675
A = 0.8577	1.486 x $10^{-3}$$m^3$/s	
B=0.0675		
h=0.004m	m = 0.092 x 1.486 x 10^{-3}	
L= 0.60m	= 1.367kg/s	
ρ = 0.92	1.367 x 3600 = 4.92kg/hr	
		$Q = 1.486\times10^{-3}$

Initial Data	Calculations and Sketches	Result
V_p = 1.82m/s M = 1.367kg/s C = 1506.9J/kg^oC θ_1= 30^oC θ_2 = 120^oC π = 3.14 λ = 48.5w/mk r_1= 0.0215m r_2 = 0.024m L = 0.6m	**3.2.1.4 Heat Requirement** The heat absorbed by material according to equation 16 Q = 1.347 x 10^{-3} x 1506.9 x (120 – 30) = 182.68J/S Using equation 20 Heat absorbed by barrel material given 1^oC difference in inner and outer temperatures Q = $\frac{2\pi \times 48.5 \times 1}{in(0.024/0.0215)} = 2770.3$ J/ms For length of barrel 2770.3 x 0.6 = 1662. 18J/s Total heat required = $Q_m + Q_b$ …….. 19 = 1662.2 + 182.68 = 1844.9W Each heater supplies 1500 W No. of heaters = 1844.9	Q_m = 182.7J/s Q = 2770.3J/ms Q_b = 1662.2J/s Q = 1844.9W N ≈ 2 heaters.

Initial Data	Calculations and Sketches	Result
P= 1100W N_2 = 94 m= 4.5kg R = 0.15m T_1 = 118N T_2 = 2.689N T_C = 0.123N W_P = 44.15N	**3.2.1.5 Determination of Minimum Safe Diameter of Shaft** The greatest power transmitted by v-belt is from +35-1100 kW (Sharma, 2006). The torque transmitted by the driven pulley shaft is given as T = 1100 x 60/2π x 94 =111.75Nm Weight of pulley = 4.5 x 9.81 W_P = 44.15N The overhang of the pulley is 0.15m. the bending moment on the shaft due to the belt tension and weight of the pulley is as follows; $M_b = (T_1 + T_2 + 2T_C + W_P)R$ = [118 + 2.68 + 2 (0.123) + 44.15] 0.15 = 24.76Nm The equivalent twisting moment is the resultant of the bending moment and the transmitted torque.	T = 111.75N W_P = 44.15N

M_{eq} = 114.46Nm S_S = 55Mpa	$M_{eq} = \sqrt{\left(M_b^2 + T_2^2\right)}$ $= \sqrt{\left(24.76^2 + 111.75^2\right)}$ = 114.46Nm Moreover, $M_{eq} = (\pi/16) \times S_S D^3$ for shaft without keyways, S_S = 55Mpa $D^3 = 16 \times 114.46 / \pi \times 55M$ $D = 21.966 \times 10^{-3}$m	M_b = 24.76Nm M_{eq} = 11446Nm D = 22mm

Initial Data	Calculations and Sketches	Result
L_H = 9000hrs K= 3 for ball bearings, Sharma (2006),	**3.2.1.6 Bearing Selection** For the machine on intermittent working, life of bearing = 9000hrs. W_A = axial; load $= T_1 + T_2 + 2T_C + W_P = 165.08N$ $W_R = P/\omega r = 1100 \times 60/2\pi \times 94 \times 0.15$ $W_R = 744.98N$ For all bearings with rotating inner race, V = 1 $W_A/W_R = 165.08/744.98 = 0.222$ From the chart, (Sharma, 2006), W_A/W_R is $\leq$ e at any given $W_A/C_{o.}$ therefore, X = 1, Y = 0 Basic dynamic equivalent radial load:	$W_A = 165.08N$ $W_R = 744.98N$

	W = 1 x 1 x 744.98 + 0 = 744.98N Appling equation 43 L = 60 x 94 x 9000 = 50.76 x 10^6revs. Basic dynamic load rating (equation 44) C = 744.98 (50.76 x $10^6/10^6$)$^{1/3}$ = 2758.365 ≈ 2.76KN **3.2.1.7 Motor Selection**	
P_{max} = 6.4 x 10^3 A = 0.1756m^2	From equation 47, W = P x A we have 6.4 x 10^3 x 0.1756 = 1123.8N	W = 1123.8N
	Tangential force = W x 1/π from equation 48 = 1123.8 x 7/22 = 358N	
R = 0.3m	Maximum Torque = 358 x 0.3 = 107.3Nm	F = 358N
N_2 = 94rpm	Hence Equation 51 gives the required power for the system 2π x 94 x 107.3/60 = 1056.4W	T =107.3Nm P = 1.056 kW

3.2.2 Construction, Assembly and Operation

3.2.2.1 Material Selection

Engineering materials possess varying degree of mechanical properties and non-mechanical properties. These properties determine possible application and suitability of such materials for specific purposes. The choice of a material for any specific application is based on a number of factors such as:

i. The availability of the material

ii. The properties of the material

iii. The ease of manufacturing process

iv. The cost of the materials

3.2.2.2 Fabrication of Parts

3.2.2.3 The Hopper

The hopper was fabricated from a 1mm thick galvanized steel sheet. It comprises a cone of 45^{o} slant side and 260mm diameter. A cylinder of equal diameter was developed and formed into shape by brazing to form a frustum shaped hopper.

3.2.2.4 The Barrel

The barrel is made of 40mm schedule10 pipe (thin-walled) with a flange welded on the discharge end of the barrel to hold the die. Four 5mm tapping holes were drilled on the flange and threaded with M6x1.25 tap to hold the die plate. The feed end of the barrel was cut open to provide an opening for the hopper to be fitted. A second flange was also welded

to feed the end of the barrel. Wear and chemical corrosion resistance are the main selection criteria for the barrel. The barrel material is harder than the screw material since it is easier to replace or repair the screw than the barrel.

3.2.2.5 The Die

The die was cut out of a 15mm thick mild steel plate. Four 5mm diameter holes uniformly spaced were drilled and chamfered to minimize pressure drop and polymer hang-up.

3.2.2.6 The Frame

The frame was fabricated from a 38mm mild steel angle channel to provide support for the barrel-screw, hopper, the die, gear box and electric motor. All members forming the frame were arc welded.

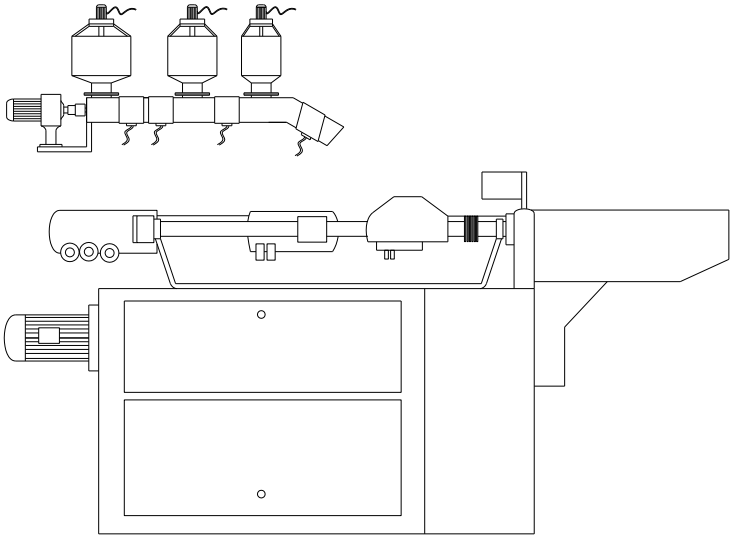
3.2.2.7 The Screw

The screw was produced from AISI 4140 steel. The screw shaft was turned down to three zones of different diameters (using lathe machine) namely: feed zone, compression and metering. A 1/4" diameter steel rod was cut into strips and welded to form screw flights. Oxyacetylene gas flame was used to soften the strips preparatory to forming them into flights. The screw flights were smoothened after they were welded on the shaft.

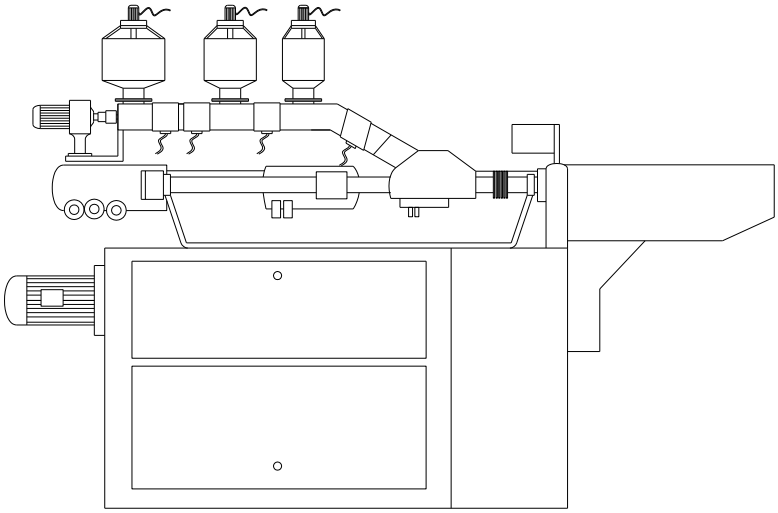
3.2.2.8 Purchased Parts

The standard components which were designed based on their availability in the market includes: bearings, pulleys, belt, electric heater bands, electric motor, gear box, flanges, temperature controllers, thermo-couples, paint and paint accessories.

3.2.2.9 Assembly and Inspection



(a)



(b)

Figure 3.3: (a) Subassembly and (b) Assembly drawing of the modified injection moulding machine

All the fabricated parts were subjected to weld joints, dimensional and visual inspections to ensure the accuracy of the dimensions, integrity and reliability of the entire frame. Welding procedure is in accordance with ANSI G 31.4, AWS D.1.1

The machine was assembled in accordance with the detailed working drawing, using both permanent (welding) and temporary joints (bolts nuts, keys, pins etc).

Assembly steps/procedures:

i. The frame assembly was aligned and welded.

ii. The electric motor was mounted on the frame with the aid of bolts and nuts.

iii. The screw was cantilevered into the barrel and supported on bearings. The screw splinned end was keyed onto driving gear. The screw and the barrel were assembled to ensure barrel to screw radial clearance was small and concentric to avoid rubbing of screw on the barrel internal surface.

vi. The drive and the driven pulleys were aligned (using ruler and a plum line), v-belt installed and correctly tensioned with the aid of adjusting slot, bolts and nuts.

vii. The electric heater bands were mounted round the barrel outer surface and firmly screwed tight with the spring washers to maintain firm contact.

viii. The die was connected to a flange at the discharge end of the barrel by bolts and nuts. The die was tightly fitted to the flange to avoid leakage of the melt.

3.2.2.10 Working Principles of the Plastic Injection Moulding Machine

The automated nano-scale feeding units have to be calibrated before the units can be put to use. The units are calibrated by running the individual feeder with the raw materials at various speeds so as to determine the quantity of the output at each set speed. These will enable the user to know the speed that corresponds to the output quantity needed.

After the calibration, the HDPE and CNTs are charged into the individual hoppers and then the automated hoppers are powered and set to the required speed. The machine is then turn on, and when the temperature has reached the required set limit, the machine operation is started.

The matrix hopper will start to feed the HDPE which becomes molten as it moves along the extruder barrel due to the heater band wound around the barrel. As the molten matrix travel under the nanofillers hoppers, the hoppers drop the nanotubes in a nano-scale manner onto the matrix which is being mixed by the shear force of the screw feeder, therefore the nanotubes and the HDPE are thoroughly mixed and passed into the injection barrel where it is further mixed.

An electric motor with hydraulic pump is responsible for turning of the screw inside the heated cylinder. A gate before the mould cavity restricts the flow of the melt into the mould and limits backflow. The pressure created by pushing the admixture forward through the grooves up to the gate also produces heat on the inside of the cylinder which helps to melt the polymer and prepare it for injection into the mould.

As the screw moves forward it injects the admixture into the mould at high pressure, holds it, and adds more melt to ensure the contraction due to cooling and solidification does not leave gaps in the final product. Eventually the gate solidifies and isolates the mould from the injection cylinder. The mould is then water cooled. After solidification, the clamp holding the two halves of the mould together closed is opened allowing the nanocomposite to be removed. The whole process is then repeated again in a cycle form.

3.2.2.11 Machine Maintenance /Safety Precaution

In order to maintain optimum machine availability and reliability, the following maintenance guidelines are recommended:

i. Ensure that there is enough hydraulic oil in the hydraulic tank.

ii. Ensure that the machine is heated up before it is operated.

iii. Ensure that the water cooling system is working properly and getting to the various points of use such as the mould, hydraulic tank, feed hoppers etc.

iv. Wear heat resistance gloves and overalls when operating the machine.

v. Avoid polymer melt spillage on the floor.

vi. Wear safety shoes

vii. Always switch off all electrical supply sources when the machine is not in use.

3.3 EXPERIMENTAL METHODS

3.3.1 Compounding Process A

The HDPE with an average molecular weight of 60,000 g/mol used in this work was obtained from Eleme Petrochemical Company Port-Harcourt, Nigeria, and the 60% singlewall carbon nanotube (SWCNT) was purchased from Carbon Solution Inc. CA, USA. All the materials were used as received. Shear mixing and injection moulding was conducted using a lab-scale Arburg injection moulding machine; with length 78 mm and diameter of 40mm, at constant temperature of 210^0C, pressure of 4 bar, and speed of 50rpm, but controlled wt% SWCNT concentration.

Control specimen (only the HDPE matrix) was first produced with the conventional injection moulding machine, and then various concentrations of 0.2, 0.4, 0.6, 0.8 and 1wt% of SWCNT were fed into the conventional injection moulding machine to produce ASTM D638 standard tensile bars which were labelled sample type A.

Ten specimens of each compounding were produced, making a total of sixty (60) specimens.

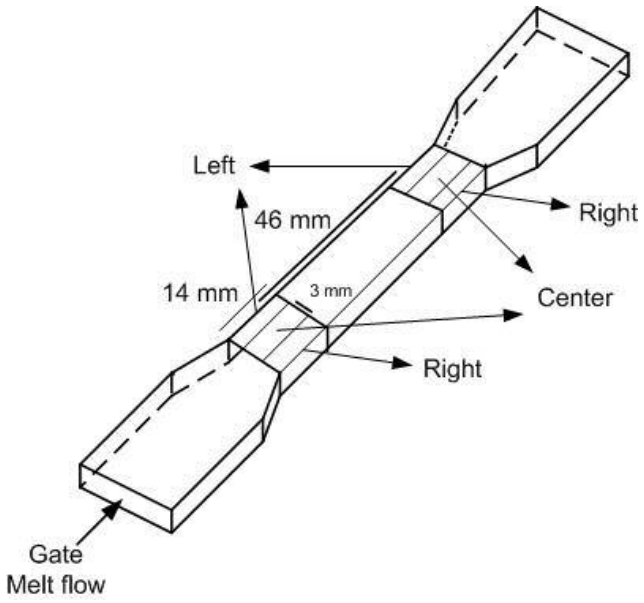


Figure 3.4: ASTM D638 Standard Tensile Bar Specimen

3.3.2 Compounding Process B

The same materials as described in compounding process A were used for compounding process B, but the new technique developed was used to produce the ASTM D639 standard tensile bars in the various wt% concentrations as in compounding process A.

Similarly, ten specimens of each compounding were produced, making a total of fifty (50) specimens.

3.4 Characterization Procedures

3.4.1 Morphological Analysis and Dispersion Evaluation of CNTs in the Samples

Three microscopy techniques were used to study and evaluate the distribution and dispersion condition of CNTs in HDPE matrix: Scanning electron microscopy (HR-SEM) TEM and AFM. A HR-SEM (Hitachi S-4700) on microtomed platinum-coated samples was used to investigate the CNTs distribution in HDPE matrix. TEM (JEOL, JEM-2100 F) was also used after HR-SEM observations to study the CNTs dispersion in HDPE matrix. Atomic force microscope (AFM, Nanoscope IIIa) was operated in the tapping mode, provided with tips of average radius of 10 nm and applying moderate forces (typically amplitude set points between 0.8 and 2 V and drive amplitudes of 50 to 500 mV). Scan rates were in the range of 0.8-1.2 Hz. The results are shown and discussed in chapter 4.

3.4.2 Crystalline Characteristics (DSC and XRD)

Differential scanning calorimetry (DSC, Q1000; TA Instruments) and X-ray diffraction (XRD, Discover, D8, Bruker) were used to study the crystalline behaviour of HDPE/CNT nanocomposites. The effect of CNT addition on crystalline structure of samples was first studied by DSC. The tests were performed in nonisothermal conditions using a heating/cooling/heating cycle with the rate of 10 ^{0}C/min. XRD technique was then used in addition to DSC to characterize the crystalline structure of the system and to evaluate the orientation in the final specimen. The results are shown and discussed in chapter 4.

3.4.3 Orientation Determination (Raman Spectroscopy)

Raman spectroscopy technique was used for CNT and HDPE orientation determination. Raman spectra were recorded on a Renishaw spectrometer equipped with an inVia Raman microscope. Orientation of SWCNTs and HDPE chains was obtained through comparing the spectra in parallel and perpendicular directions to the laser beam for Raman spectroscopy, respectively. The results are shown and discussed in chapter 4

3.4.4 Electrical Conductivity

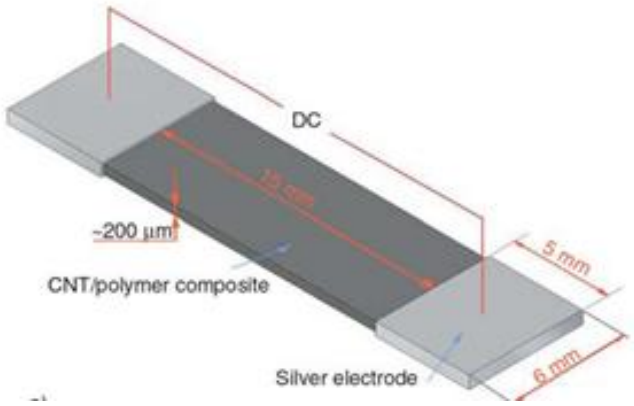


Figure 3.5: Schematic illustrations of the test specimens employed in the test

Electrical conductivity of CNT-HDPE films loaded with different weight fractions (0.2–0.1wt%) of SWCNTs was measured at room temperature using a Fluke electrometer (3Fluke 1550B MegOhmMeter, Fluke Corporation, Everett, Washington). The electrometer is capable of measuring DC electrical resistance up to 1 TΩ. DC volumetric resistance (R) was measured using two silver paint electrodes of 5 mm length painted on the film edges of 25 mm long specimens, leaving an effective span (L) of 15 mm between the silver electrodes, see Figure 3.5. Specimen width was 6 mm and film thickness ~150–200 µm. In order to reduce surface effects in the measurements, silver paint electrodes were painted

completely covering the ends of the sample. A DC voltage was applied through the length of the specimen and the conductivity (σ) was calculated using

Equation (1): $\sigma = L / AR$ …… (39)

where; A is the cross sectional area of the sample and R the measured electrical resistance. The results are shown and discussed in chapter 4.

3.4.5 Mechanical Properties Determination

The mechanical properties of the samples produced at different wt% concentrations were obtained employing a micro tester 5548 (Instron). Flexural and other properties were determined according to ASTM test methods D638, D790 and D256, respectively, using an Instron 5500R machine. The variation in mechanical properties with temperature was characterized using a Rheometric Scientific dynamic mechanical thermal analysis **(DMTA)/DMA** system. Specimens was analyzed in bending mode with a maximum strain of 5%, a frequency of 1 Hz, and a scan range of -50 to +150 ^{0}C at a heating rate of 5^{0}C/min. The results are shown and discussed in chapter 4.

3.4.6 Melt Rheology

The rheological properties of the SWCNT/HDPE nanocomposites were determined using an oscillatory rheometer (UDS-200, Paar Physica Co.). A frequency sweep experiment was performed at 210 ^{0}C in an oscillatory shear mode by using a parallel plate with a 25 mm diameter with a gap according to the disc thickness. To investigate the frequency dependence of the storage modulus (G0) and the loss modulus (G0 0) of the SWCNT/HDPE composites, a constant value of the amplitude set was used at 0.1% of

amplitude and a frequency range from 1 to 10 and 1 to 100 Hz. The results are shown and discussed in chapter 4.

3.4.7 Oxidation Temperature (TGA)

TGAs is an experimental technique in which the weight of a sample is measured as a function of sample temperature or time. The sample is typically heated at a constant heating rate. The results of a TGA measurement are usually displayed as a TGA curve in which percent weight is plotted against temperature. Different effects can cause a sample to lose, or even gain mass. These include the following:

1. Evaporation of volatile constituents; such as desorption of gases and moisture

2. Thermal decomposition in an inert atmosphere with the formation of gaseous products

3. Oxidation of constituents.

TGA are often equipped with DTA (differential thermal analysis). In addition to showing the energetic nature of weight loss events, the DTA signal can also show thermal effects that are not accompanied by a change in mass, e.g. melting, crystallization or a glass transition.

CHAPTER FOUR

RESULTS AND DISCUSSIONS

4.1 Design Results

Table 4.1: Design parameters

S/No	Description	Design parameters	Remark
1	Capacity of hopper 1	$0.0144m^3$	
2	Capacity of hopper 2	$0.010m^3$	
3	Capacity of hopper 3	$0.008m^3$	
4	Minimum power required for feeding	0.3kW	
5	Minimum power required for screw	5kW	
6	Discharge flow rate at barrel end	$1.486x10^{-5}m^3/s$	
7	Heat required by operation	2000W	This can be supplied by 4 heaters of 500W rating with good regulation
8	Hydraulic motor required to drive the screw shaft	5 Hp Hydraulic motor	
9	Minimum safe diameter of screw shaft	22mm	30mm was used to give robust allowance
10	Minimum safe diameter of feed shaft	12mm	

4.1.2 Developed Feeding and Dispersion System

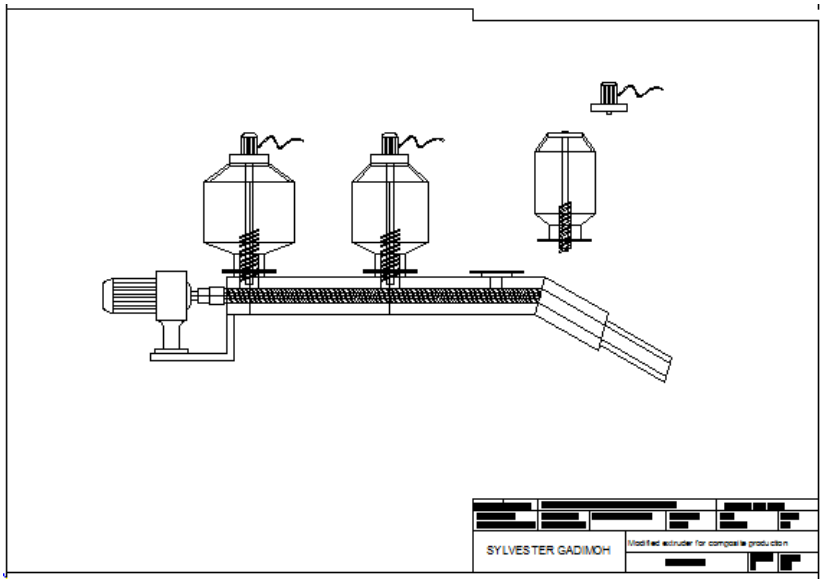


Figure 4.1: Line drawing of the developed automated feeder hoppers.

4.1.3 Production Parameters

Table 4.2: Production parameters

S/No.	Description	Parameters
1	Processing temperature	210^0C
2	Processing time	5min
3	Processing speed	50rpm
4	Processing pressure	4 bar



Plate 1: Picture of the Tensile Bar Nanocomposite produced by the machine

4.1.4 Production Challenges

When either the melt temperatures or injection speeds were too high or too low (with the other parameters held constant), the injection moulded tensile bars would show imperfections such as short shots or jetting on the surface. Therefore adequate control of all these parameters is essential to obtaining the desired results.

4.2 Results of the Comparative Analysis of Samples

It may be worthwhile to mention that each test and experiment was repeated atleast 10 times and then the average values were used.

Similarly, sample A was produced from the conventional injection moulding machine while sample B was produced with the modified injection moulding machine.

4.2.1 Morphological Analysis of samples of both compounding methods

Scanning electron microscope was used to analyse the samples to ascertain the uniformity of both methods used for the compounding of the nanocomposites. The SEM images of three randomly selected points of each specimen of the different wt% SWCNT concentrations produced are as shown below:

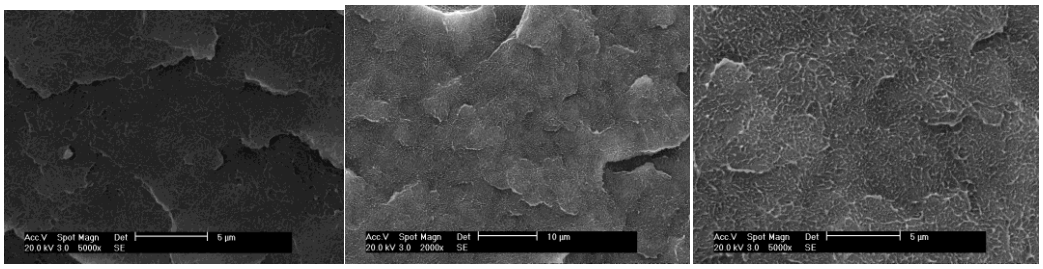


Figure 4.2: SEM images of the three specimens randomly selected from Sample A1 = 0.2 wt% SWCNT.

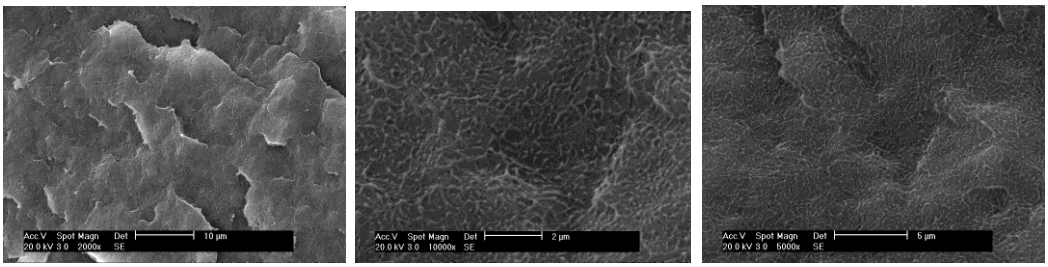


Figure 4.3: SEM images of the three specimens randomly selected from Sample A2 = 0.4 wt% SWCNT

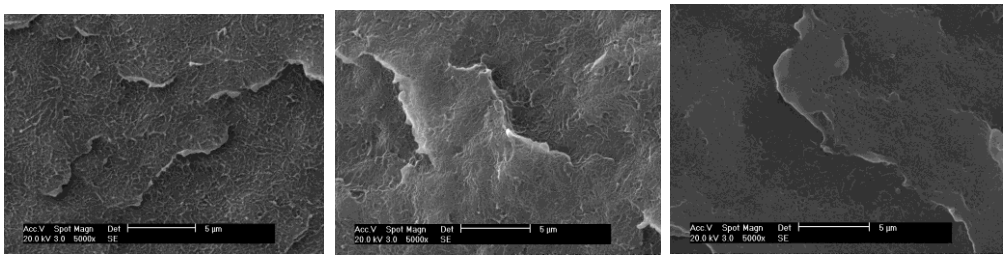


Figure 4.4: SEM images of the three specimens randomly selected from Sample A3 = 0.6 wt% SWCNT

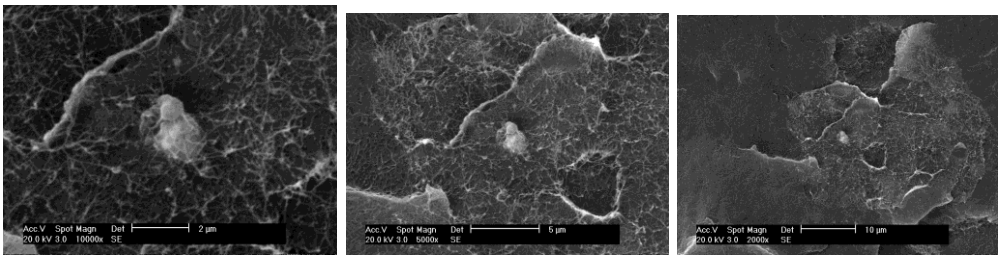


Figure 4.5: SEM images of the three specimens randomly selected from Sample A4 = 0.8 wt% SWCNT

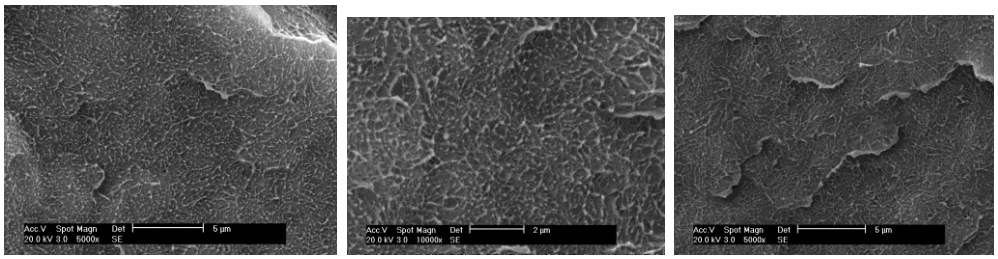


Figure 4.6: SEM images of the three specimens randomly selected from Sample A5 = 1.0 wt% SWCNT



Figure 4.7: SEM images of the three specimens randomly selected from Sample B1 = 0.2 wt% SWCNT.

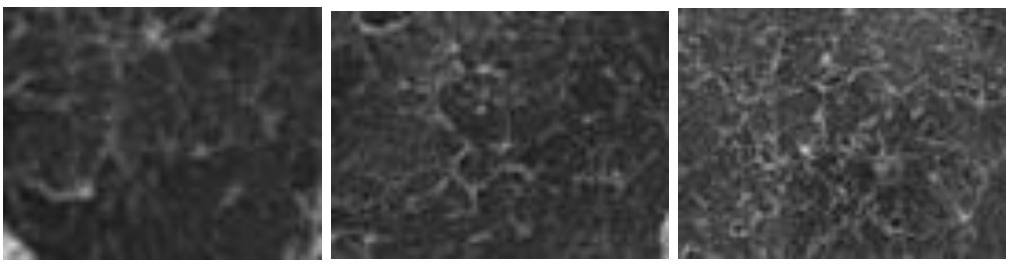


Figure 4.8: SEM images of the three specimens randomly selected from Sample B2 = 0.4 wt% SWCNT.

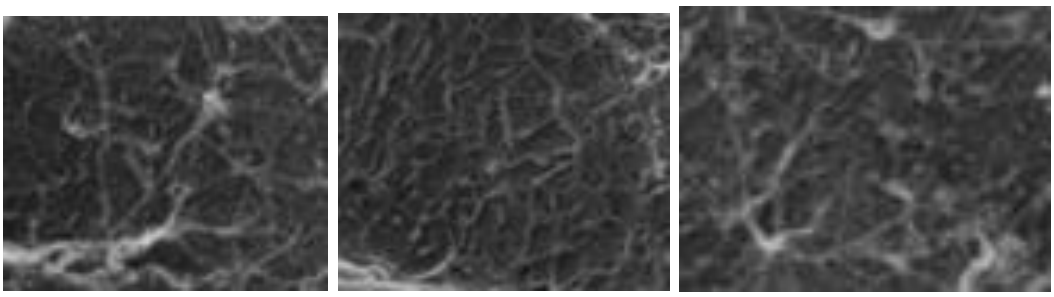


Figure 4.9: SEM images of the three specimens randomly selected from Sample B3 = 0.6 wt% SWCNT

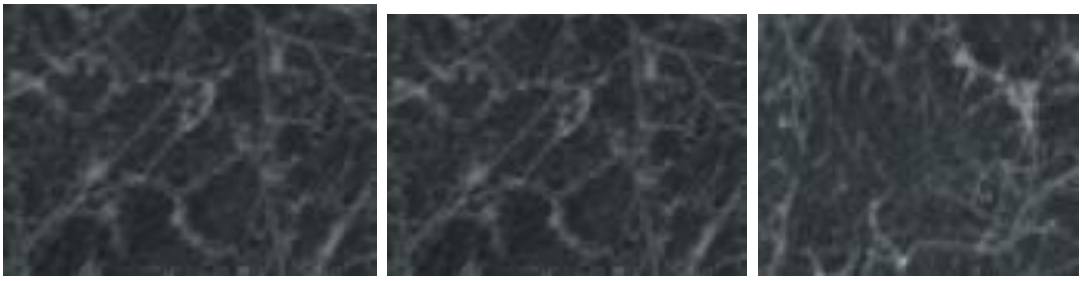


Figure 4.10: SEM images of the three specimens randomly selected from Sample B4 = 0.8 wt% SWCNT

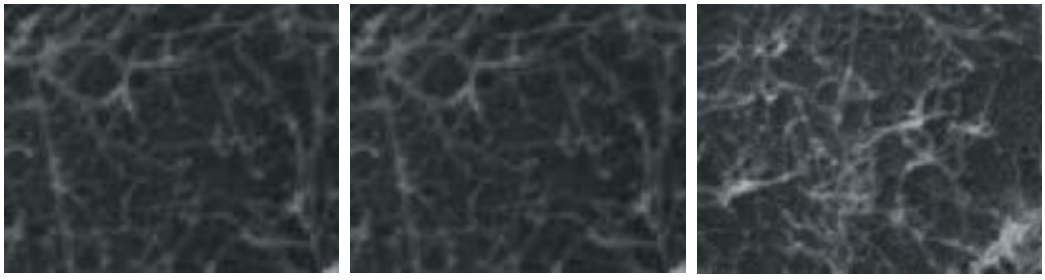


Figure 4.11: SEM images of the three specimens randomly selected from Sample B5 = 1.0 wt% SWCNT.

As can be seen from the SEM images, all samples B from the modified injection moulding machine are more uniform throughout the test as compared to all samples A from the conventional injection moulding machine. This can be attributed to the uniform feeding with non-agglomeration of the CNT by the automated feeder hoppers whereas in the conventional injection moulding machine, the feeding was not uniform as most of the

CNTs agglomerated in different sizes and positions. This implies that the modified system can be adopted for the mass production of nanocomposite products of the same properties which is difficult to achieve with present available compounding systems.

4.2.2 Dispersion Evaluation of the nanocomposite samples

The study of the dispersion of cryofractured SWCNT/HDPE nanocomposites of the various samples was carried out and the sample images are as shown below;

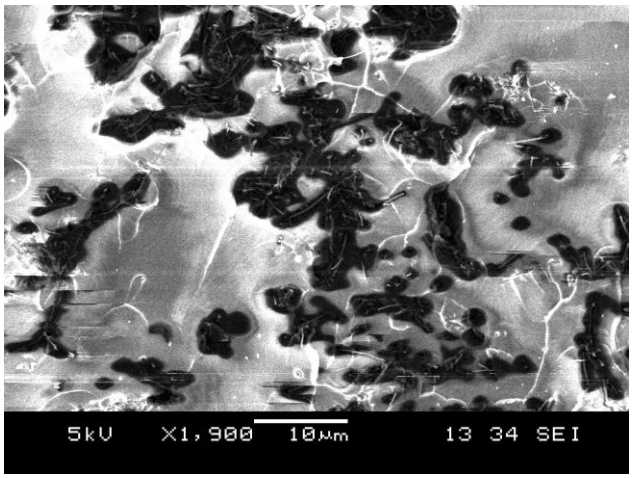


Figure 4.12: SEM image of 0.2wt% SWCNT/HDPE nanocomposite of Sample A

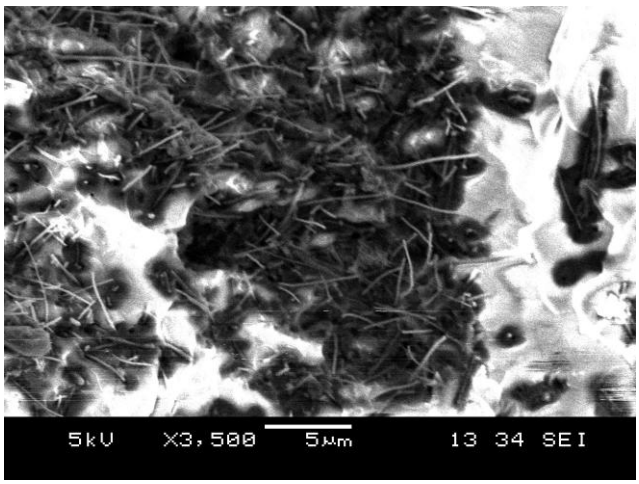


Figure 4.13: SEM image of 0.2wt% SWCNT/HDPE nanocomposite of Sample B

The SEM images above (Figure 4.12 and Figure 4.13) of the 0.2 wt% SWCNT/HDPE shows good dispersion of the nanotubes in the polymer for the sample B produced with the modified system compared to sample A produced with the conventional system. Poor dispersion was observed in the SWCNT/HDPE nanocomposites sample A, (clearly light regions with low nanotube concentration and dark regions with CNT clusters), possibly because the mechanical mixing was not adequate due to the agglomerating of the CNTs, whereas in the modified system, the CNTs were fed in a nano-scale manner by the automated hopper feeder into the extrusion barrel where initial shear mixing is done after which it is fed into the injection barrel where further shear mixing is done before it is then injected into the mould. This ensures a well dispersed CNT/HDPE nanocomposite as evident in the SEM image of Figure 4.13.

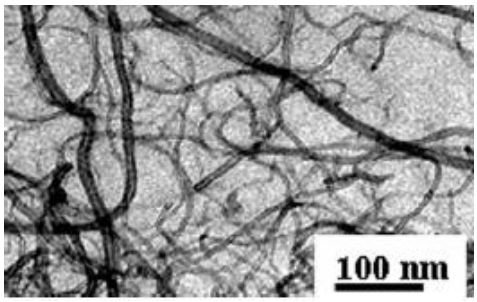


Figure 4:14: TEM image of 0.2wt% SWCNT/HDPE Nanocomposite of sample B

TEM image of the same nanocomposite sample B (Figure 4.14) shown above proves the existence of a nanotube–polymer network in the SWCNT/HDPE nanocomposites, which will certainly give rise to percolation.

Furthermore, the nanotubes alignment and distribution was also observed by AFM, as shown in Figure 4.15 below.

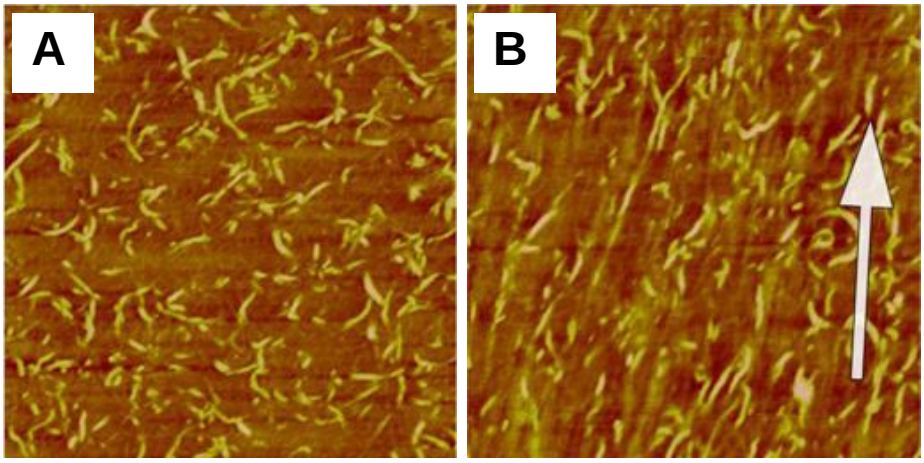


Figure 4.15: AFM image of the 0.2wt% of SWCNT/HDPE nanocomposite sample A and B respectively

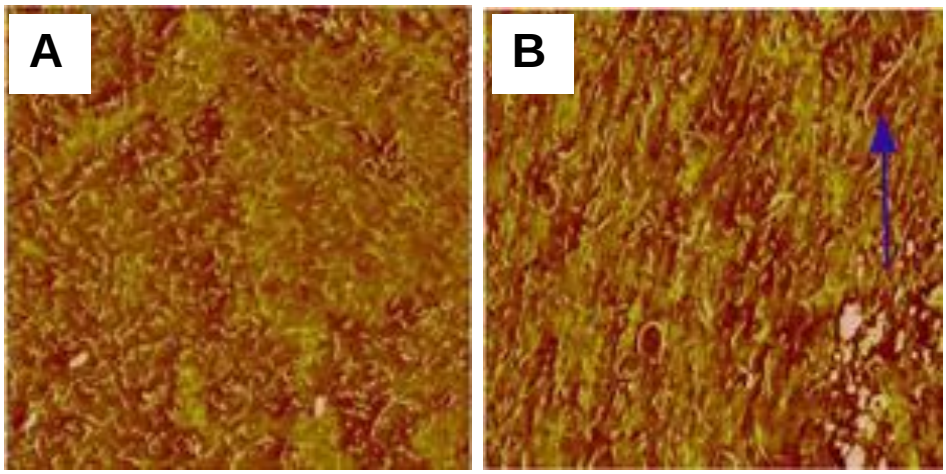


Figure 4.16: AFM image of the 0.6% SWCNT/HDPE nanocomposite sample A and B respectively.

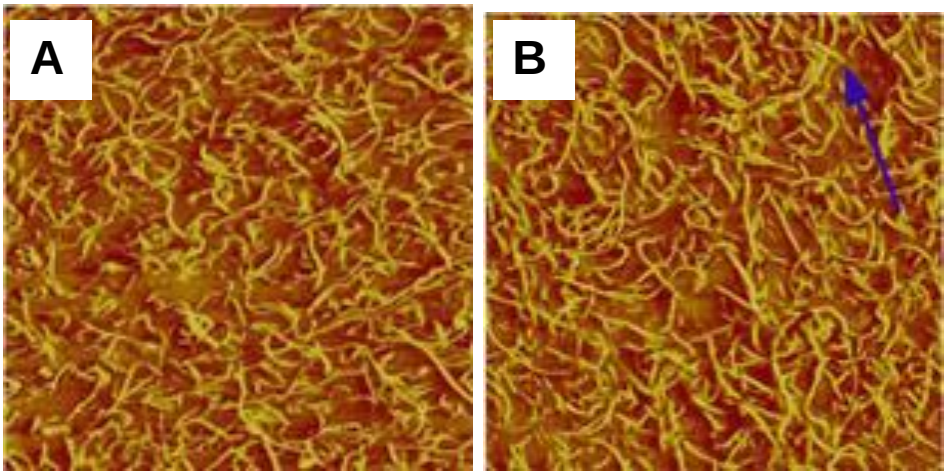


Figure 4.17: AFM image of the 1wt% SWCNT/HDPE nanocomposite sample A and B respectively

The AFM images further seem to suggest that there could be better lower percolation threshold in the sample B.

4.2.3 Crystalline Characteristics (DSC and XRD)

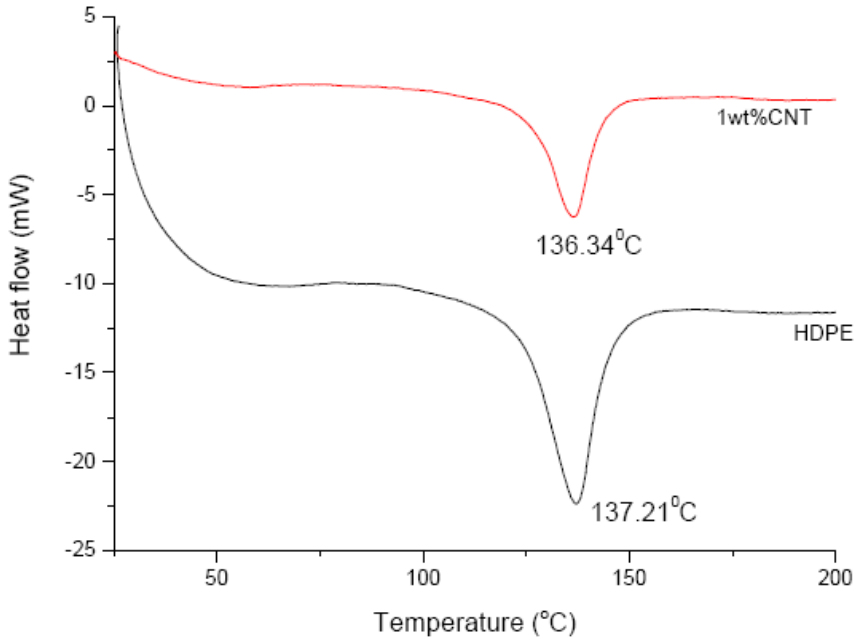


Figure 4:18. Variation of DSC heat flow vs temperature curves of 1wt% SWCNT nanocomposite

In the case of DSC curves, which are shown in Figure 4:18 above, the addition of CNT into HDPE increases the total enthalpy of crystallization. The melting point of HDPE and 1wt%CNT nanocomposite are 137.21 ^{0}C and 136.34 ^{0}C, respectively. The enthalpy of crystallization is 167.38 J/g for 1wt% of CNT composites, whereas 100% pure crystalline HDPE polymer gives an enthalpy of 293 J/g, from literature. Thus, the maximum energy is liberated during the crystallization of HDPE by adding CNT. The nucleation and growth of individual crystallites are so rapid that very large number of crystallites is formed together, thus large amount of heat liberated. It is also observed that with the addition of CNT,

crystallinity of composite increases appreciably which shows that CNT acts as a nucleation site for the crystallization of polymer.

X-ray diffraction measurements were carried out to study the nature of the crystallinity of the nanocomposite. Figure 4.19 shows the XRD patterns of pure HDPE and SWCNT/ HDPE nanocomposites from both compounding methods used. Both the pure HDPE and SWCNT/HDPEs nanocomposites display characteristic diffracting peaks which correspond to the planes of its a-phase crystallite and exhibit complete absence of the b-crystal form. While certain nucleating agents can promote b-crystal formation in HDPE, this study shows only the a-crystal formation in all the SWCNT/HDPEs nanocomposites samples.

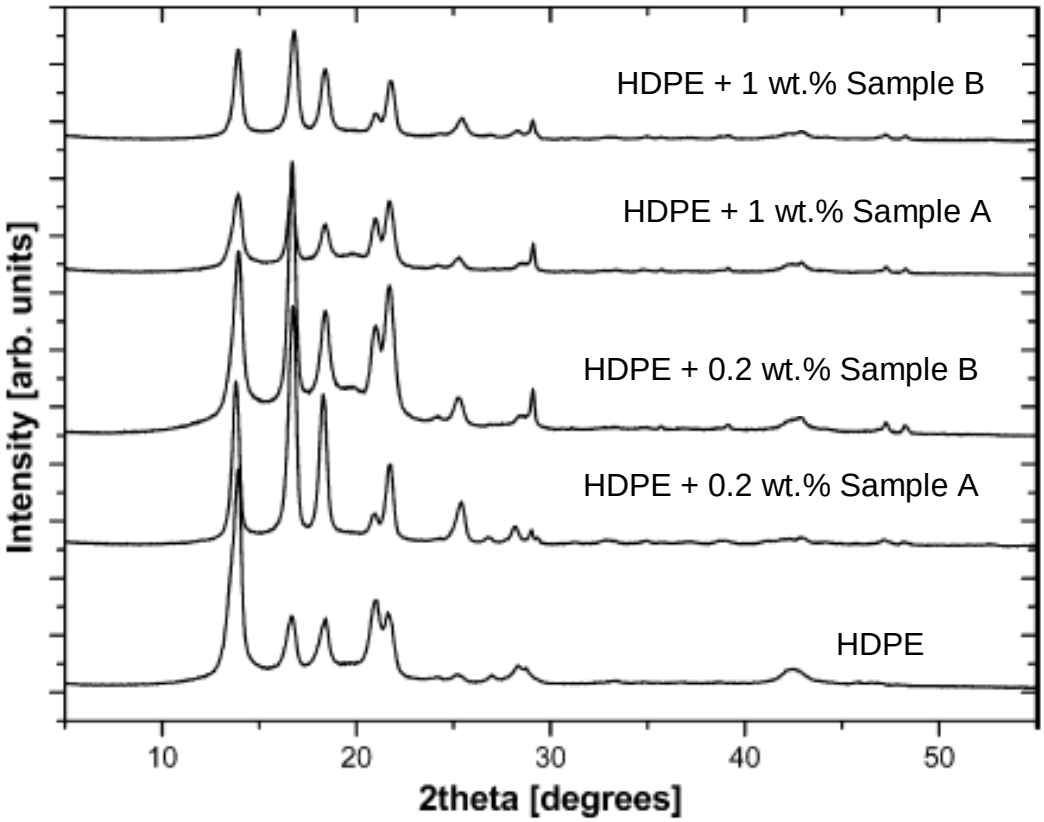


Figure 4.19: XRD patterns showing the intensities vs 2Θ for the pure HDPE and for the nanocomposites as indicated on the plot.

4.2.4 Orientation Determination (Raman Spectroscopy)

Raman spectroscopy was used to investigate the interfacial interaction between HDPE matrix and SWCNT. Raman spectra of polymer/CNT composites have attracted a lot of attention, both theoretically (Saito, 1998; Kurti, 1998) and experimentally (Kasuya, 1998; Pimenta, 1998), and has become a tool for the study and characterization of CNT nanocomposites, in order to identify carbon nanotubes (i.e. graphitization, inner diameter and density), access their dispersion in polymers, evaluate nanotube/matrix interactions and detect polymer phase transitions.

The Raman spectra of HDPE, 1wt%CNT/HDPE and pure SWCNTs were compared in Figure 4.20. The spectrum of HDPE exhibits typical Raman modes of PE. CNTs show two main Raman lines, one at 1570 cm^{-1} (G-line, due to the in-plane vibration of the C–C bonds), the other at 1342 cm^{-1} (D line, induced by defects and disorder) (Ferrari and Robertson, 2000). The overtone of the D band, 2D at about 2690 cm^{-1}, is also evident.

In the Raman spectra of CNT/HDPE the characteristic bands of CNTs are easily identified. The comparison of the Raman spectra of all the composites with those of CNT and polymer evidences a G-line and D-line shift to higher wave numbers, as reported for other nanocomposites with CNTs, (McCarthy, et. al. 2002; McNally, et. al, 2005; Valentini, et al., 2003; Piscanec, et al., 2007).

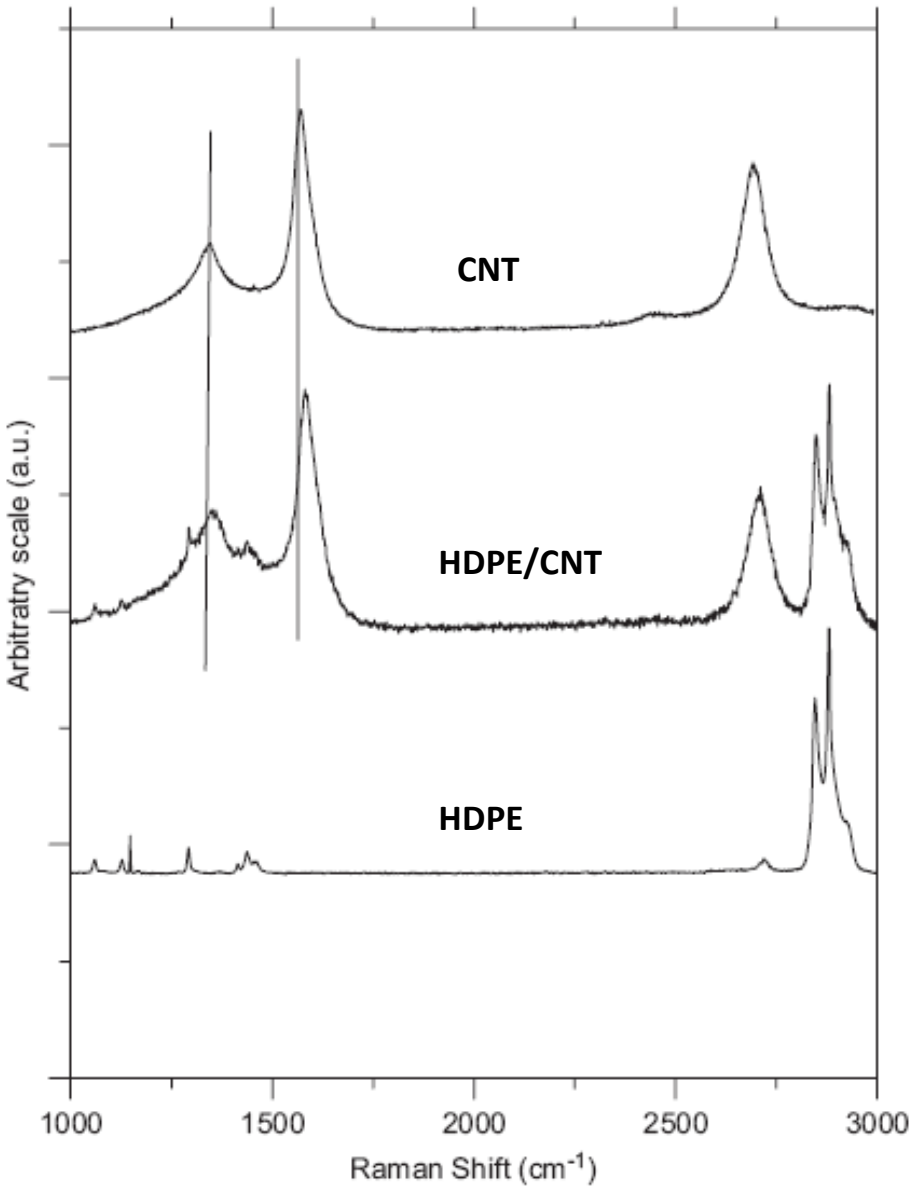


Fig. 4.20: Comparison of the Raman spectra of pure HDPE (lower trace), pure CNTs (upper trace), and 1wt% CNT/HDPE composite (middle trace).

The up-shifting of the D and G bands is also a consequence of strong compressive forces associated with PE chains on CNT, (Gorrasi,et al., 2007).

By adding the nanotube into the polymer matrix, the G band is up shifted, as shown in Figure 4.20. The shifting of the band to higher frequencies can be attributed to good

dispersion of the nanotubes in the HDPE matrix, as a consequence of polymer penetration into the nanotube bundles during melt mixing process. The latter is expected to contribute significantly to the influence of the crystallization, due to the increase of the formation of nucleant agents which favour the crystallization process, as already witnessed in section 4.2.2. Similar upshifting of the G band has been reported for SWCNT/polyethylene matrix (McNall, 2005).

4.2.5 Electrical Conductivity

Figure 4.21 shows electrical conductivity of the composite films as a function of weight loading for samples A and samples B. Overall, the conductivity of the agglomerated sample A is higher than that of the uniformly dispersed sample B at higher CNT loading. At low CNT loadings (<0.6 wt %) electrical conductivity was only observed in sample B, thus indicating the formation of a percolation network.

At higher loadings (≥0.6wt %), the conductivity of both dispersion states is again similar, since the conductive network has been well defined and no further drastic changes are expected according to percolation theory. The higher conductivity of the agglomerated sample A compared to the ‘uniformly dispersed’ sample B may be related to the increased CNT-to-CNT contact/junctions in the agglomerated sample A.

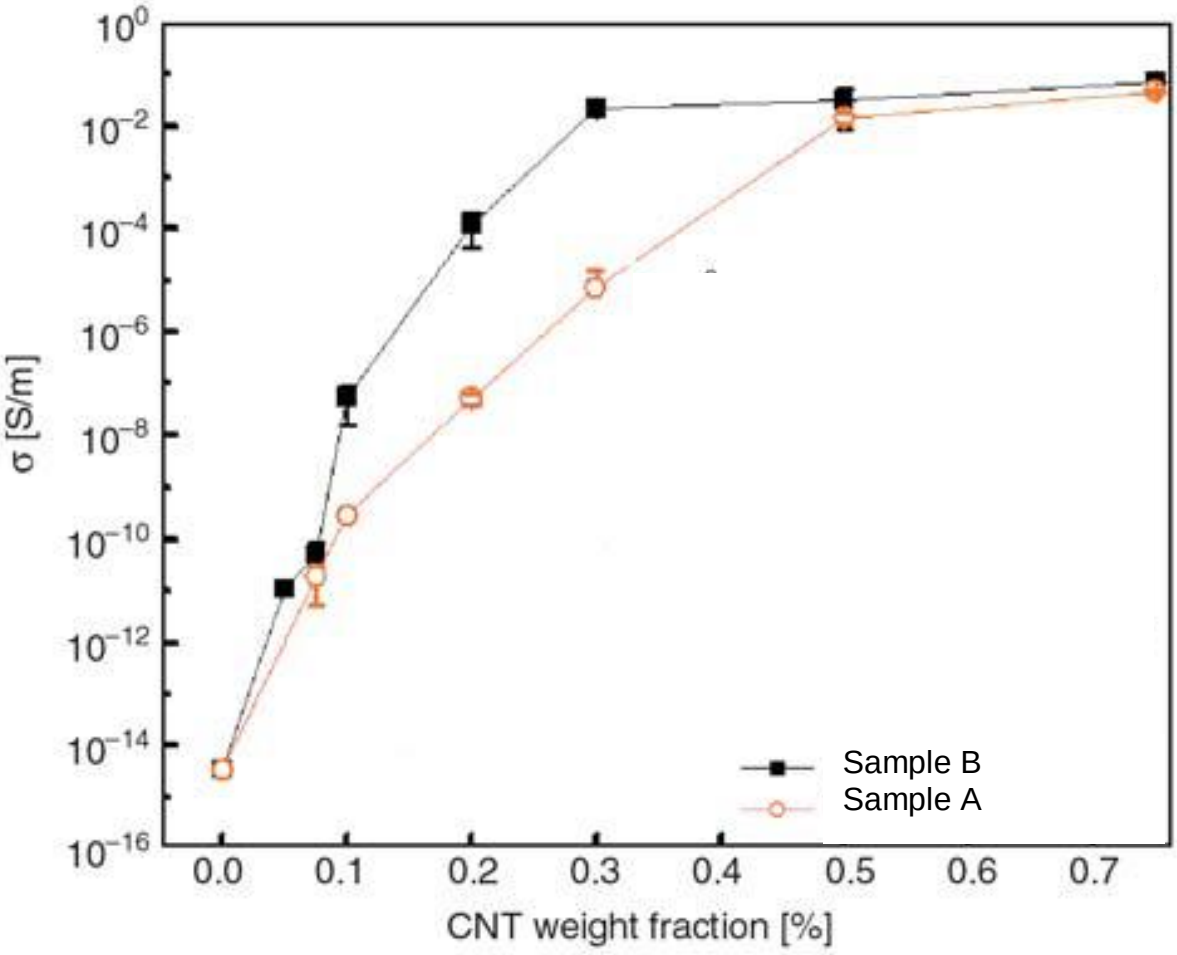


Figure 4.21: Electrical conductivity vs. CNT weight fraction (%) loading for uniformly dispersed sample B and agglomerated sample A.

4.2.6 Mechanical Properties

The mechanical properties of both samples made from the conventional injection moulding machine and the new technique developed are presented in Figure 4.22. Improvements in flexural strength and modulus were observed for sample B. The observed improvements may be attributed to the excellent dispersion of SWCNT in resin phase and the better interphase or interfacial bonding between resin and carbon nanotubes in the sample.

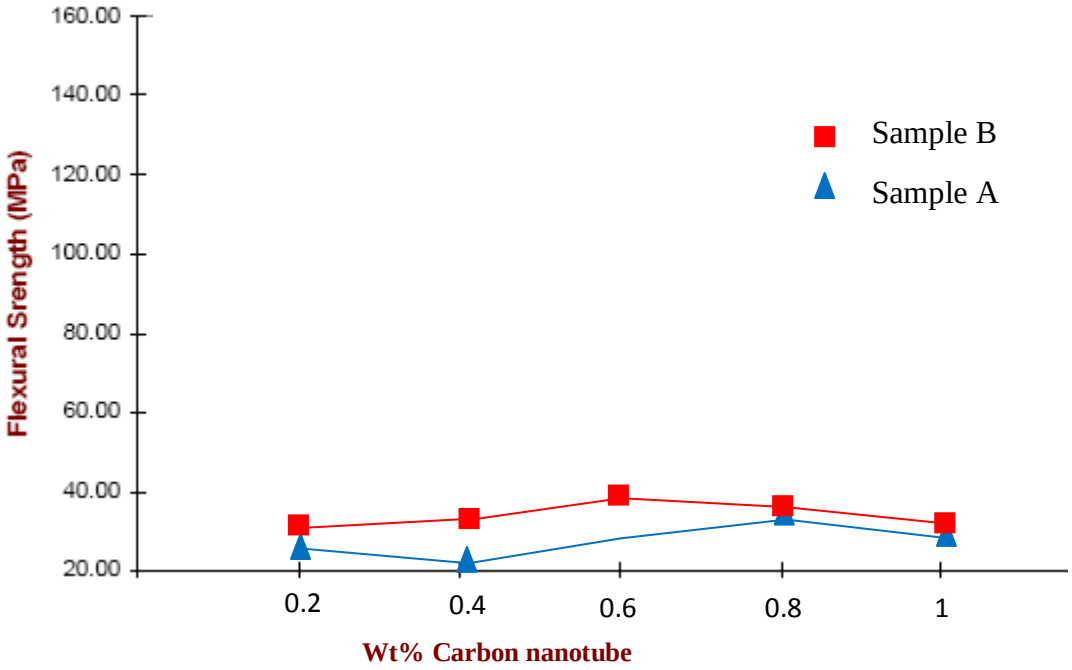


Figure 4.22: Comparison of the flexuaral strength vs CNT wt% loading of sample A and B

The mechanical behaviour of 1wt% CNT/HDPE nanocomposite of sample B was studied by using DMTA, a technique in which storage modulus and loss modulus of the sample under oscillating load are monitored against time, temperature and frequency of oscillation. The storage modulus is indicative of the elastic modulus of the nanocomposite and the loss modulus is indicative of the energy lost due to the friction of polymer chain movement and the damping factor is very sensitive to the structural transformation.

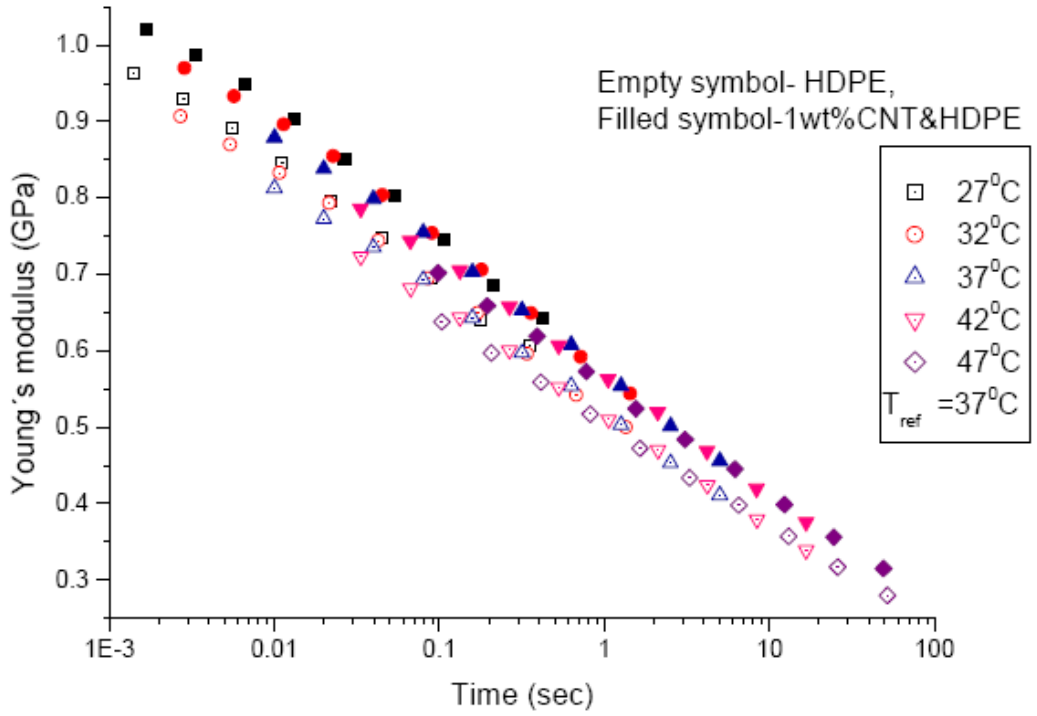


Figure 4.23: Young's modulus vs time for HDPE and 1wt% CNT Composite of sample B

Figure 4.23, shows that the Young's modulus at different temperatures varies from 27^0C to 47^0C at an interval of 5^0C at different time intervals. It is further observed that Young's modulus increases with an addition of CNT to HDPE. The incorporation of CNTs stiffens the matrix. Thus, the elastic modulus of the nanocomposite is significantly increased by the presence of CNTs. It is increased by 5.3% by adding 1wt% of CNT-HDPE composite at 27^0C at 0.73msec and this increment started to decrease with time at higher temperature. The experiments were conducted at the reference temperature of 37^0C.

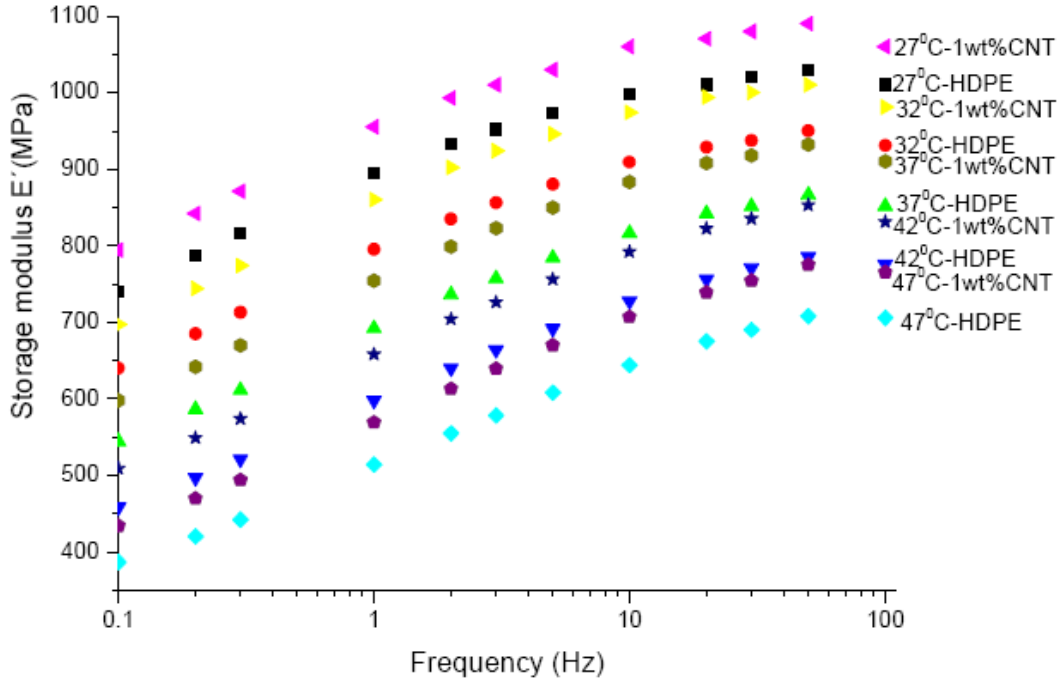


Figure 4.24: Storage modulus vs frequency for HDPE and 1wt% CNT Composite of sample B

Figure 4.24, shows the variation of storage modulus (E') at different frequencies which varies from 0.1Hz to 100Hz with the temperature range of 27^0C to 47^0C. It is observed from the experimental results that E' increases with frequency of oscillation up to 50Hz and then started to decrease. The increment of E' by adding 1wt% CNT in HDPE are 7.3%, 8.9%, 9.9%, 10.9% and 12.1% at 0.1Hz in the temperature of 27^0C, 32^0C, 37^0C, 42^0C and 47^0C, respectively. Hence, it can be concluded that good interfacial adhesion between HDPE and CNT exists in the nanocomposite which could be the main reason for the observed improvement in the storage modulus. The E´ is increased by the stiffening effect of the nanotubes which is particularly high at higher temperatures. The presence of CNT enables the matrix to sustain a high modulus value to higher temperature. However, E' decreases with an increase in temperature irrespective of the presence of CNT at all the frequency range because the molecular motion with polymer changes with temperature.

The percentage increase of E' varies with temperature and also with frequency of oscillation.

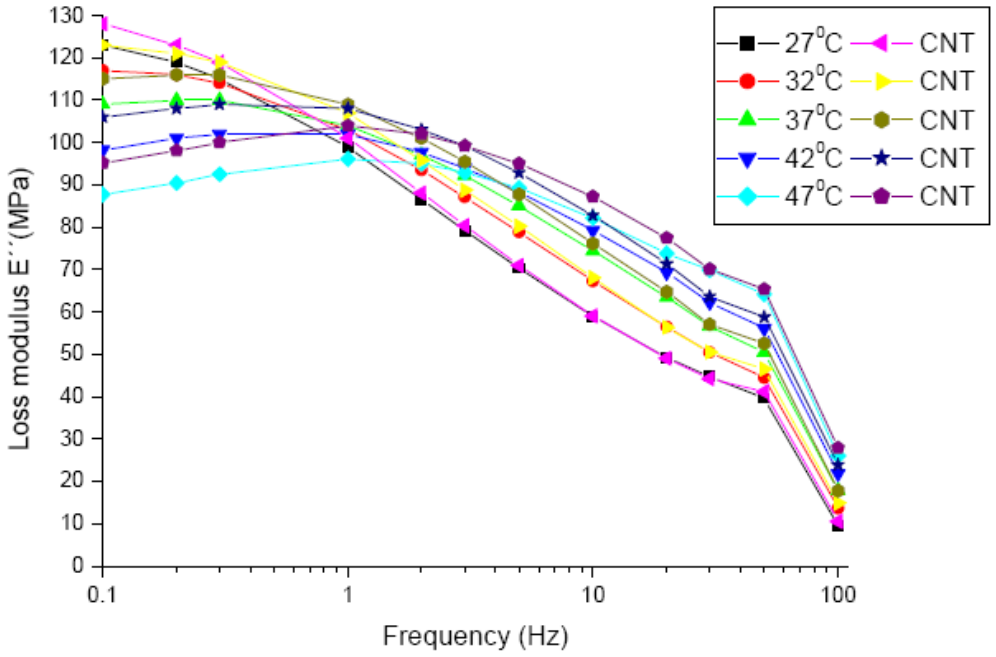


Figure 4.25: Loss modulus vs frequency for HDPE and 1wt% CNT Composite of sample B

Figure 4.25, shows the effect of frequency of oscillation and temperature on the loss modulus (E''). It is observed that up to 1Hz there is an appreciable difference in E'' between pure polymer and CNT composite and this difference increases with an increase in temperature. However, it vanishes beyond 1Hz irrespective of the presence of CNT. E'' increases with an increase in temperature in all range of frequency beyond 1Hz but opposite trend was observed at below 1Hz. At 1Hz, the difference of E'' between pure polymer and the nanocomposite vanishes irrespective of temperature and merges to a very small range of values and no difference was found at above 1Hz till 100Hz. E'' also increases with an

addition of CNT at below 1Hz and the enhancement of E'' increases with an increase of temperature.

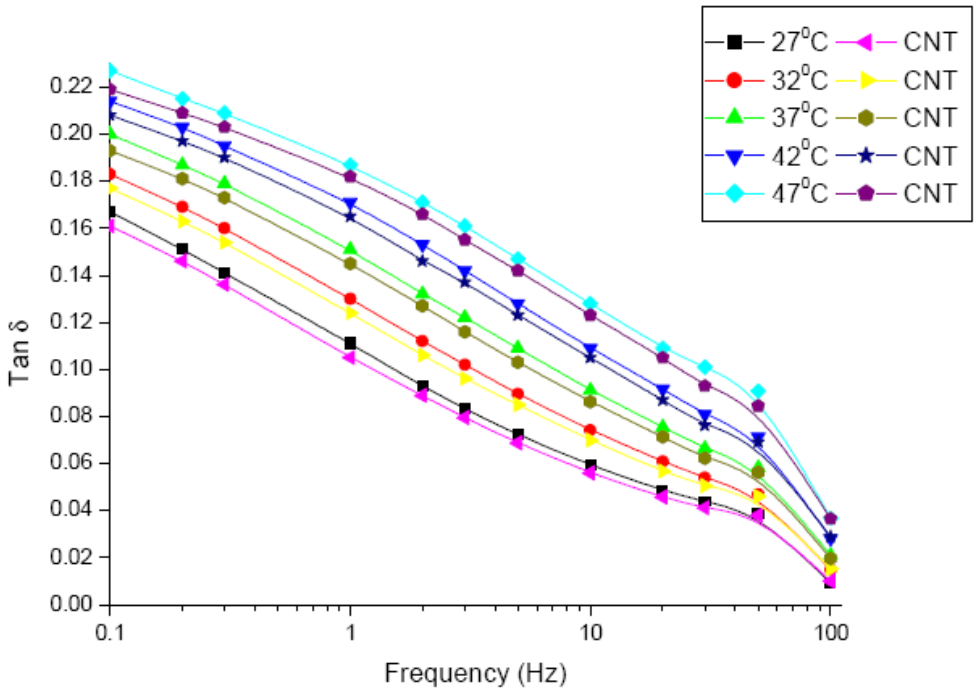
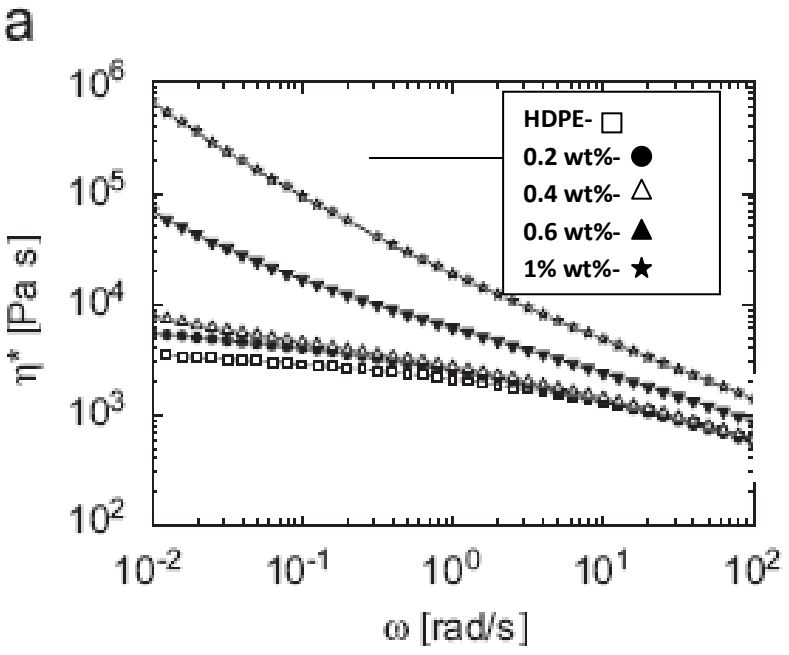


Figure 4.26: Damping factor (Tan δ vs frequency) of HDPE and 1wt% CNT Composite of sample B

The variation of damping factor is shown in Fig.4.26, It is observed that damping factor decreases linearly with increase in frequency from 0.1Hz to 50Hz. But beyond 50Hz, damping factor reduces drastically. There is an appreciable difference in tan δ between pure polymer and CNT nanocomposite at below 50Hz which is due to increase of storage modulus with an addition of CNT and good interfacial adhesion between polymer and CNTs. This difference vanishes irrespective of the presence of CNT at 50Hz and above. At same frequency, difference between pure polymer and CNT composite of tan δ remains the same at different temperatures of the sample. The damping factor increases with increase in temperature, which is due to the reducing storage modulus of the composite.

4.2.7 Melt Rheology

The results of the frequency sweep experiments for the SWCNT/HDPE composites are shown in Figure 4.27. At low frequencies, as the CNT amount increases, the viscoelastic properties of the nanocomposites clearly deviate from the liquid-like behaviour of the neat HDPE matrix. As suggested by Potschke et al. (2002), we can assume that the addition of nanotubes to the polymer matrix generates interconnected structures of CNT–polymer, which influence the rheological response of the sample. As the content of nanotubes increases such interactions begin to dominate and eventually lead to percolation, i.e. to the formation of a CNT–polymer network, corresponding to a liquid-like to solid-like transition. In particular, at nanotube content of 0.2 wt% marked alterations in the viscoelastic behaviour are observed for the sample B, especially at low frequencies: the complex viscosity shows a non-Newtonian behaviour (Fig. 4.27a) and the storage modulus a plateau (Fig. 4.27b), indicating the liquid-like to solid-like transition, and confirming that which was established by the SEM and AFM images.



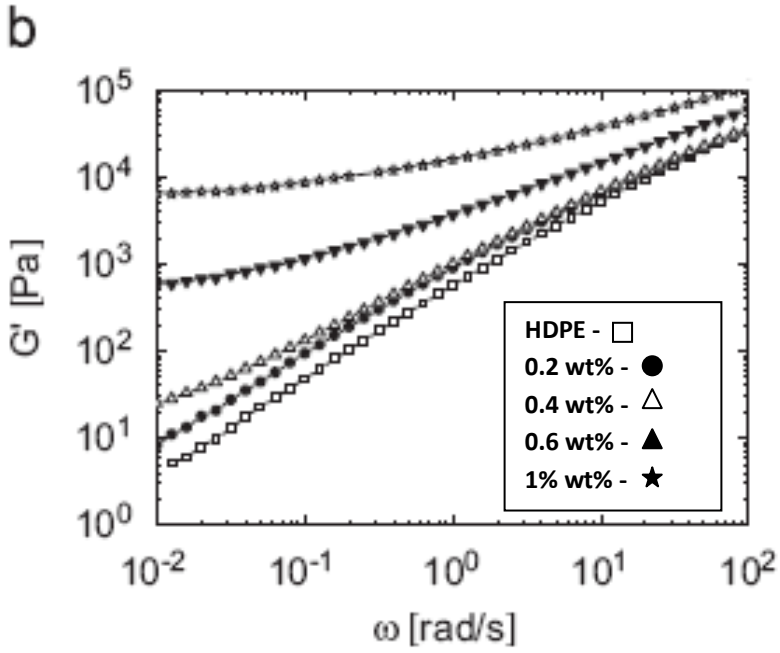


Figure 4.27: (a) Complex viscosity (Z_) vs. frequency (ω) and (b) storage modulus (G0) vs. frequency (ω) for the SWCNT/HDPE nanocomposites and the pure HDPE (T ¼ 200 ^{0}C).

4.2.8 Oxidation Temperature (TGA)

In this work, the oxidation temperature of the nanocomposites was found by differentiating the percentage of weight loss curve with temperature which is shown in Figures 4.28-4.30. The temperatures at which the maximum rate of oxidation took place are 455^{0}C, 465^{0}C and 483^{0}C for HDPE, sample A5, and sample B5 respectively. This curve also shows the maximum area under the curve for pure polymer and it is drastically reduced for both samples of CNT nanocomposite though there is a little difference between them in case of oxidation temperature.

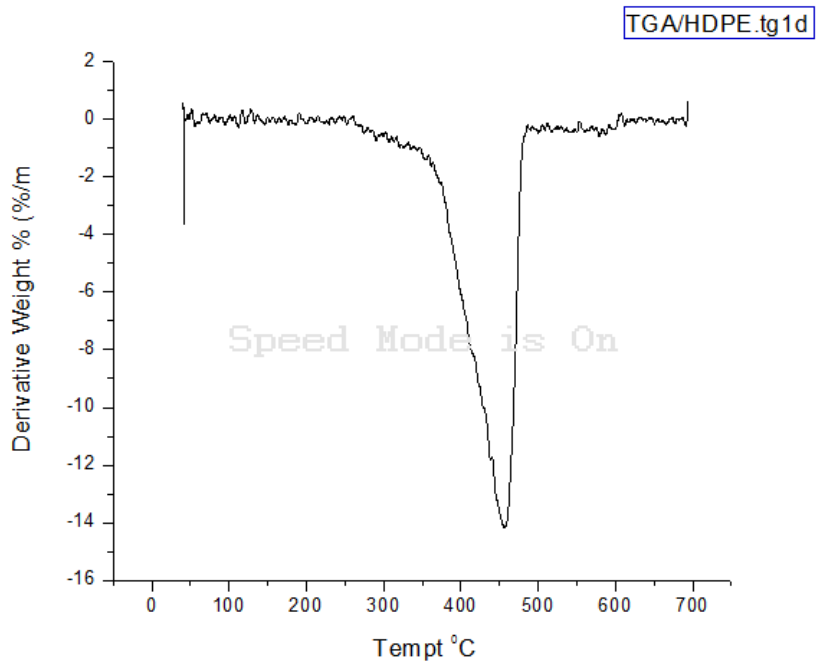


Figure 4.28: Variation of d(weight loss)/dT of HDPE

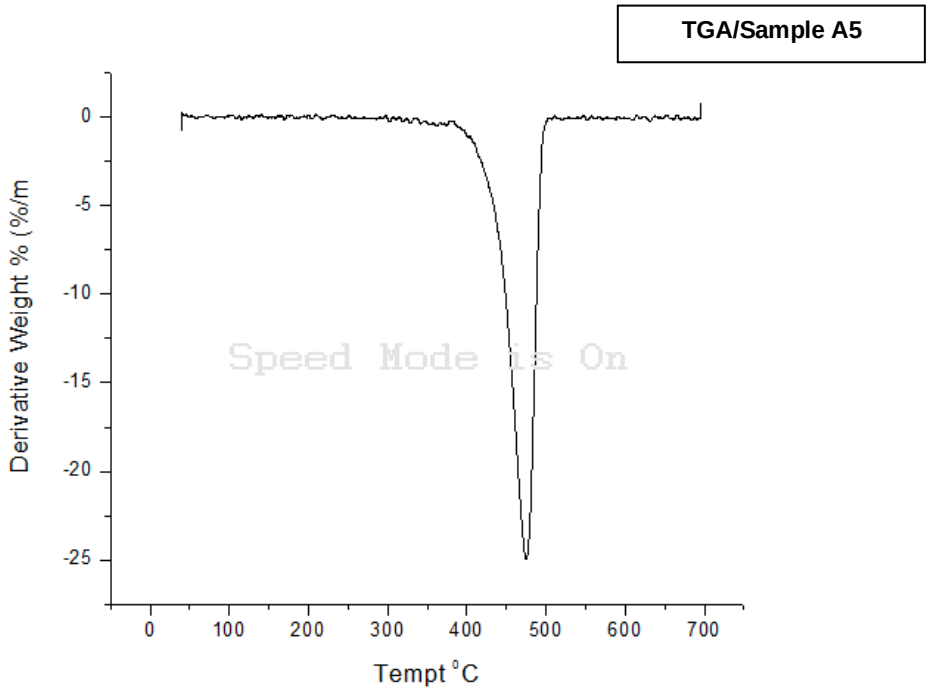


Figure 4.29: Variation of d(weight loss)/dT of 1wt% Sample A5

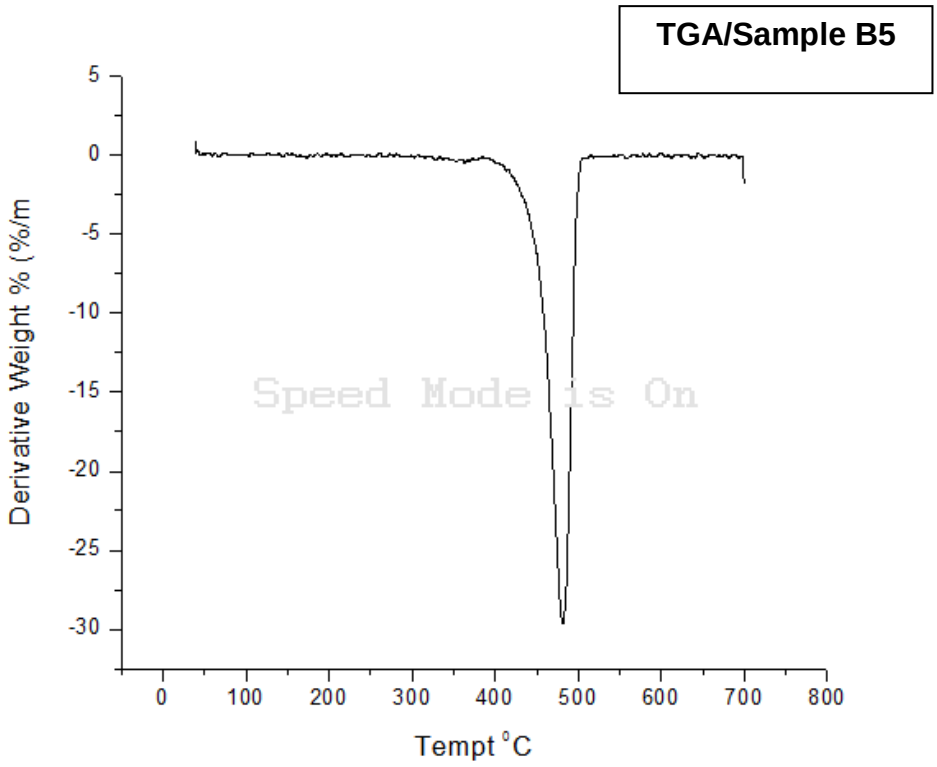


Figure 4.30: Variation of d(weight loss)/dT of 1wt% Sample B5

This implies that sample B is more disperse than sample A and the HDPE since it required higher temperature to get heat up to the oxidation temperature due to the better formed percolation compare to sample A and the HDPE.

CHAPTER FIVE

5.0 SUMMARY, CONCLUSIONS AND RECOMMENDATION

5.1 SUMMARY

An injection moulding machine has been modified for the direct compounding of nanocomposite. The technique involves incorporating automated hopper feeders which automatically feed CNT into a molten stream of matrix piece wisely so that it is thoroughly dispersed by the action of the shear mixing of the extruder screw directly attached to the feeder, the material is then passed into the injection barrel where it is further mixed and dispersed before injecting into the mould. A series of single-walled carbon nanotube /high density polyethylene (SWCNT/HDPE) nanocomposites with varying concentrations (0.2, 0.4, 0.6, 0.8, 1 wt %) were then compounded using both conventional and the modified injection moulding machine for the purpose of comparative analysis of both compounding systems. A good dispersion of the CNT in the matrix and a good CNT–polymer interfacial adhesion were verified by scanning electron microscopy (SEM), TEM and atomic force microscopy (AFM) for sample B compare to sample A. The Raman measurements shows that the characteristic bands of the nanocomposite shifted to slightly higher wavenumbers when increasing the CNT content in the nanocomposite, indicating an effective interaction between SWCNTs and HDPE matrix.

Melt rheological investigations in dynamic mode indicate the dispersion degree and the percolation state of the CNTs within the polymer matrix. The rheological percolation threshold of the nanocomposites is between 0.2 and 1 wt% for the nanocomposite from the modified system while 0.8 and 1 wt % was obtained for nanocomposite from the CIM

system. For both systems, we found a six orders of magnitude increase in electrical conductivity from 0.2 to 1 wt% for the modified system and 0.8 to 1wt % for the CIM, which is the consistence with the percolation threshold obtained in rheology test.

As Figure 4.21 demonstrates, there is a large difference in the electrical properties of the SWCNT/HDPE nanocomposite specimens based on the fabrication method utilized. It was determined that, by using the modified system, a very low percolation threshold was obtained (~0.20-0.25%). In contrast, a higher percolation threshold was obtained for the nanocomposite produced with the CIM (~0.8-1wt %).

From the mechanical property analysis, it is concluded that storage modulus increases with an addition of CNT and this increment increases with temperature but E' decreases with an increase in temperature and beyond 1Hz, the presence of CNT is not playing any role in case of loss modulus.

On the overall, there is a good interfacial bond between CNT and HDPE which is observed from appreciable increment of storage modulus and decreasing tendency of loss modulus.

It can be concluded that Young's modulus of the nanocomposite is increased by the presence of CNTs due to crystallinity of the nanocomposite.

5.2 Conclusions

A new injection moulding technique for compounding of nanocomposites has been developed through the modification of the conventional injection moulding machine. The modified machine was used for the production of well dispersed and low percolation threshold nanocomposite. A comparative analysis was carried out with the convention injection moulding machine shows that the new technique developed has been able to

overcome the difficulty being experienced using existing/traditional compounding techniques due to the strong tendency of the nanotubes to agglomerate without the need to functionalize the nanotube.

This work has recorded the following achievement and contribution to knowledge;

1) Educate the public on the challenges in the production of carbon nanotube nanocomposite.
2) Developed a new technique for achieving good dispersion in the production of carbon nanotube polymer nanocomposite which hitherto had been a great technical problem.
3) Show that good dispersion give rise to low percolation threshold.
4) Demonstrate the possibility of using HDPE to produce conducting panels and other applications.

5.3 Recommendation

From the results shown, it is recommended that this new method be employed to produce solar panel for further analysis and confirmation especially in the area of efficiency of the solar panel. This might resolve that present drawback of the low efficiency of polymer based solar panel.

REFERENCES

Ajayan, P.M., Schadler, L.S., Braun, P.V. (2003): Nanocomposite Science and Technology. WILEY-VCH Verlag GmbH & Co. KGaA, Weinheim ISBN: 3-527-30359-6

Ajayan P.M., Stephan, O., Colliex, C. and Trauth, D. (1994). Aligned Carbon Nanotube Arrays Formed by Cutting a Polymer Resin Nanotube Composite, Science, 265(5176): 1212–1214.

Alexandre, M. and Dubois, P. (2000). Polymer-layered Silicate Nanocomposites: Preparation, Properties and Uses of a New Class of Materials, Mater. Sci. Eng. Rep., 28: 1–63.

Allaoui, A., Bai, S., Cheng, H.M. and Bai, J.B. (2002). Mechanical and Electrical Properties of a MWNT/Epoxy Composite, Composites Science and Technology, 62(15): 1993–1998.

Andrews R., Jacques D, Minot N.I. and Rantell T. (2002), Fabrication of carbon multiwall nanotube/polymer composites by shear mixing. Micromol Mater Eng 2002.287 (6) :395-403.

Andrews, R. and Weisenberger, M.C. (2004). Carbon Nanotube Polymer Composites, Current Opinion In Solid State & Materials Science, 8(1): 31–37.

Antonucci F., Faiella G., Giordano M., Nicolais L., and Pepe G. (2007). Electrical properties of single walled carbon nanotube reinforced polystyrene composites. Macromolecular Symposia, 247, 172–181. DOI: 10.1002/masy.200750120

Assouline, E., Lustiger, A., Barber, A.H., Cooper, C.A., Klein, E., Wachtel, E. And Wagner, H.D. (2003). Nucleation Ability of Multiwall Carbon Nanotubes in Polypropylene Composites, J. Polym. Sci., Part B: Polym. Phys., 41(5): 520–527.

Bauhofer W., and Kovacs J. S.: A review and analysis of electrical percolation in carbon nanotube polymer composites. Composites Science and Technology, 69, 1486–1498. DOI: 10.1016/j.compscitech.2008.06.018

Benedict, L.X., Crespi, V.H., Louie, S.G. and Cohen, M.L. (1995). Static Conductivity and Superconductivity of Carbon Nanotubes – Relations Between Tubes and Sheets, Physical Review B, 52(20): 14935–14940.

Berber, S., Kwon, Y.K. and Tomanek, D. (2000). Unusually High Thermal Conductivity of Carbon Nanotubes, Physical Review Letters, 84(20): 4613–4616.

Bethune, D.S., Klang, C.H., de Vries, M.S., Gorman, G., Savoy, R., Vazquez, J. and Beyers, R. (1993). Cobalt-catalysed Growth of Carbon Nanotubes with Single-Atomic-Layer Walls, Nature, 363: 605–607.

Bhattacharyya, A.R., Sreekumar, T.V., Liu, T., Kumar, S., Ericson, L.M., Hauge, R.H. and Smalley, R.E. (2003). Crystallization and Orientation Studies in Polypropylene/Single Wall Carbon Nanotube Composite, POLYMER, 44(8): 2373–2377.

Bin, Y.Z., Kitanaka, M., Zhu, D. and Matsuo, M. (2003). Development of Highly Oriented Polyethylene Filled with Aligned Carbon Nanotubes by Gelation/Crystallization from Solutions, MACROMOLECULES, 36(16): 6213–6219.

Black P.H. and Eugene A. (1968). Machine Design, 2nd Ed. McGraw Hill Books New York.

Bower, C., Rosen, R., Jin, L., Han, J., and Zhou, O. (1999). Deformation of Carbon Nanotubes in Nanotube-polymer Composites, Applied Physics Letters, 74(22): 3317–3319.

Bubert, H., Haiber, S., Brandl, W., Marginean, G., Heintze, M. and Bru¨ ser, V. (2003). Characterization of the Uppermost Layer of Plasma-treated Carbon Nanotubes, Diamond and Related Materials, 12(3–7): 811–815.

Chen, G.Z., Shaffer, M.S.P., Coleby, D., Dixon, G., Zhou, W., Fray, D.J. and Windle, A.H. (2000). Carbon Nanotube and Polypyrrole Composites: Coating and Doping, Adv. Mater., 12(7): 522–526.

Chen, J. and Tanguay, M. (2004). Autoclave Processing in the Aerospace Manufacturing Technology Center (AMTC), In: Internal Technical Paper for, AMTC, NRC (under reviewing).

Chen, J., Hamon, M.A., Hu, H., Chen, Y., Rao, A.M., Eklund, P.C. and Haddon, R.C. (1998). Solution Properties of Single-walled Carbon Nanotubes, Science, 282: 95–98.

Chen, T.K., Tien, Y.I. and Wei, K.H. (1999). Synthesis and Characterization of Novel Segmented Polyurethane/Clay Nanocomposites via Poly (caprolactone)/Clay, J. Polym. Sci., Part A: Poly. Chem., 37(13): 2225–2233.

Choi, E.S., Brooks, J.S., Eaton, D.L., Al-Haik, M.S., Hussaini, M.Y., Garmestani, H., Li, D. and Dahmen, K. (2003). Enhancement of Thermal and Electrical Properties of Carbon Nanotube Polymer Composites by Magnetic Field Processing, Journal of Applied Physics, 94(9): 6034–6039.

Chowdhury S R, Chen Y, Wang Y, and Mitra S. (2009). Microwave-induced rapid nanocomposite synthesis using dispersed single-wall carbon nanotubes as the nuclei. J Mater Sci.,; 44:1245–1250

Christopher, O.O. and Lerner, M. (2001). Nanocomposites and Intercalation Compound, Encyclopedia of Physical Science and Technology, Vol. 10, 3rd edn. (Reproduced in part with permission from Elsevier _ 2006.)

Colbert, D. T., and Smalley, R. E., (2001). Past, Present, and Future of Fullerene Nanotubes. Buckytubes, Proc. Int. Fullerenes Workshop, Tokyo Japan, February 20–21, 2001, Kluwer, Dordrecht, Netherlands.

Coleman, J.N., Cadek, M., Blake, R., Nicolosi, V., Ryan, K.P., Belton, C.,..Blau, W.J. (2004). High-performance Nanotube-reinforced Plastics: Understanding the Mechanism of Strength Increase, Advanced Functional Materials, 14(8): 791–798.

Crawford, R. J (1998). Plastic Engineering. Elsevier India Private Ltd, New Delhi, India.

Deng, J., Ding, X., Zhang, W., Peng, Y., Wang, J., Long, X.,…Chan, A.S.C. (2002). Carbon Nanotube-polyaniline Hybrid Materials, Eur. Polym. J, 38: 2497–2501.

Dondero, W.E. and Gorga, R.E. (2006). Morphological and Mechanical Properties of Carbon Nanotube/Polymer Composites via Melt Compounding, J. Polym. Sci., Part B: Polym. Phys., 44(5): 864–878.

Dray R.F. (2005). Extrusion Screw Design. www.rdray.com/scrdsgn.htm 1(20/07/05)

Dresselhaus, M.S., Dresselhaus, G. and Eklund P.C. (ed.). (1996). Science of Fullerences and Carbon Nanotubes, Academic Press: London.

Dresselhaus, M.S., (2004). Electronic, Thermal and Mechanical Properties of Carbon Nanotubes, Philosophy Transactions of the Royal Society of London A, 362(1098): 2065–2098.

Dror, Y., Salalha, W., Khalfin, R.L., Cohen, Y., Yarin, A.L. and Zussman, E. (2003). Carbon Nanotubes Embedded in Oriented Polymer Nanofibres by Electrospinning, Langmuir, 19(17): 7012–7020.

Eastop T.D and A. McConkay (1993). Applied Thermodynamics for Engineering Technologists. 5th Ed. ELBS and Longman, London

Ebbesen, T.W., Lezec, H.J., Hiura, H., Bennett, J.W., Ghaemi, H.F. and Thio, T. (1996). Electrical Conductivity of Individual Carbon Nanotube, Nature, 382(6586): 54–56.

Eitan, A., Jiang, K., Dukes, D., Andrews, R. and Schadler, L.S. (2003). Surface Modification of Multiwalled Carbon Nanotubes: Toward the Tailoring of the Interface in Polymer Composites, Chemistry of Materials, 15(16): 3198–3201.

Ericson, L.M., Fan, H., Peng, H.Q., Davis, V.A., Zhou, W., Sulpizio, J., … Smalley, R.E. (2004). Macroscopic, Neat, Single-walled Carbon Nanotube Fibre, Science, 305(5689): 1447–1450.

Ericson, L. M. (2000). Strength Characterization of Suspended Single-Wall Carbon Nanotube Ropes, Masters Thesis, Rice University, USA.

Fan, Z. and Advani, S. (2005). Characterization of Orientation State of Carbon Nanotubes in Shear Flow, Polymer, 46: 5232–5240.

Fielding, J.C., Chen, C. and Borges, J. (2004). Vacuum Infusion Process for Nanomodified Aerospace Epoxy Resins, In: SAMPE Symposium & Exhibition, Long beach, CA.

Fisher E.G. (1976). Extrusion of plastics. 3rd edition, Newness Butterworth London.

Friedrich K, Fakirov S and Zhang Z. (2005). Polymer Composite From Nano- to Macro-Scale 2005 Springer

Gabbott P. (2008): Principles and Applications of Thermal Analysis, Blackwell Publishing, London.

Giannelis, E.P. (1996). Polymer Layered Silicates Nanocomposites, Adv. Mater., 8: 29–35.

Gitin M. M. (2002). Handbook of Gear Design. 2nd Edition, Tata McGrew-Hill Publishing Company, New Delhi

Gojny F.H, Nastalczyk J., Roslaniec Z. and Schuilte K. (2003). Surface modified multi-walled carbon nanotubes in CNT/epoxy oomposites. Chem Phys Lett 2003:370:820—4.

Gong, X., Liu, J. and Baskaran, S. (2000). Surfactant Assisted Processing of Carbon Nanotube/Polymer Composites, Chem of Materials, 12(4): 1049–1052.

Gong, X., Liu, J., Baskaran, S., Voise, R.D. and Young, S. (2000). Surfactant-assisted Processing of Carbon Nanotube/Polymer Composites, Chem. Mater., 12: 1049–1052.

Gorga, R.E. and Cohen, R.E. (2004). Toughness Enhancements in Poly(methyl methacrylate) by Addition of Oriented Multiwall Carbon Nanotube, J. Polym. Sci., Part B: Polym. Phys., 42(14): 2690–2702.

Gorga, R.E. and Tsabba, Y. (2006). Mechanical Properties of Single-wall and Multi-wall Carbon Nanotube Composites, Textile Research Journal (submitted).

Gou, J., Liang, Z., Zhang, C. and Kramer, L. (October, 2002). Nanotube Bucky Paper-epoxy Composites: Modeling, Fabrication and Characterization, In: 10th Foresight Conference on Molecular Nanotechnology, MD, USA.

Ha M. L. P., Grady B. P., Lolli G., Resasco D. E., and Ford T. W. (2007). Composites of single-walled carbon nanotubes and styrene-isoprene copolymer latices. Macromolecular Chemistry and Physics, 205, 446–456 (2007). DOI: 10.1002/macp.200600521

Haggenmueller, R., Gommans, H.H., Rinzler, A.G., Fischer, J.E. and Winey, K.I. (2000). Aligned Single-wall Carbon Nanotubes in Composites by Melt Processing Methods, Chemical Physics Letters, 330(3–4): 219–225.

Hall A.S. (1961). Schaum's Outlines Machine Design. McGraw Hill Publishers, New York

Harold Belofsky (1995). Plastics: Product Design and Process Engineering. Hanser Publishers, New York.

Harris, P.J.F. (1999). Carbon Nanotubes and Related Structures, Cambridge University Press: Cambridge, UK.

Hone, J., Whitney, M., Piskoti, C. and Zettl, A. (1999). Thermal Conductivity of Single-walled Carbon Nanotubes, Physical Review B, 59(4): R2514–R2516.

Hsiao, K.T., Alms, J. and Advani, S. (2003). Use of Epoxy/Multiwalled Carbon Nanotubes as Adhesives to Join Graphite Fibre Reinforced Polymer Composites, Nanotechnology, 14(7): 791–793.

Hussain F., Derrick, D., Haque, A. and Shamsuzzoha, A.M. (2005). S2 Glass/Vinyl Ester Polymer Nanocomposites: Manufacturing, Structures, Thermal and Mechanical Properties, Journal of Advanced Materials, 37(1): 16–27.

Iijima, S. (1991). Helical Microtubules of Graphitic Carbon, Nature, London, United Kingdom, 354(6348): 56.

Iijima, S. and Ichihashi, T. (1993). Single-shell Carbon Nanotubes of 1-nm Diameter, Nature, London, United Kingdom, 363(6430): 603–605.

Jana, S.C. and Jain, S. (2001). Dispersion of Nanofillers in High Performance Polymers using Reactive Solvents as Processing Aids, Polymer, 42: 6897–6905.

Jang, J., Bae, J. and Yoon, S.H. (2003). A Study on the Effect of Surface Treatment of Carbon Nanotubes for Liquid Crystalline Epoxide-carbon Nanotube Composites, Journal of Materials Chemistry, 13(4): 676–681.

Jia Z, Wang Z, Xu C, Liang J., Wei B, Wu D, and Zhu S (1999). Study on poly (methyl methacry1ate /carbon nanotube composites. Mater Sd Eng A 1999:271:395—400.

Jin Z, Pramoda K.P, Goh S.H. and Xu G. (2002). Poly(vinylidene fluoride)-assisted melt-blending of multi-walled carbon nanotube /poly (methyl methacrylate) composites. Mater Res. Bull:37(2):271-8.

Jin L. and Bower C. (1998). Alignment of Carbon Nanotubes in a Polymer Matrix by Mechanical Stretching, Applied Physics Letters, 73(9): 1197–1199.

Jin, Z., Pramoda, K.P., Xu, G. and Goh, S.H. (2001). Dynamic Mechanical Behavior of Melt processed Multi-walled Carbon Nanotube/Poly (Methyl Methacrylate) Composites, Chemical Physics Letters, 337(1–3): 43–47.

Johnson, B., Santare, M.H. and Advani, S. (2004). Manufacturing and Performance of Carbon Nanotube/High Density Polyethylene Composites, In: International Conference on Flow Processes in Composite Materials, July, 2004.

Kasuya A, Sugano M, Maeda T, Saito Y, Tohji K, and Takakashi H, (1998). Resonant Raman scattering and the zone-folded electronic structure in single-wall nanotubes. Phys Rev B 1998; 57:4999–5001.

Kearns, J.C. and Shambaugh, R.L. (2002). Polypropylene Fibres Reinforced with Carbon Nanotubes, Journal of Applied Polymer Science, 86(8): 2079–2084.

Keneth J. S. (1950). Kent's Mechanical Engineering Handbook. 12th Edition. John Wiley and Sons Inc. New York.

Khurmi R.S and J.K Cuipta, (1979). A Textbook of Machine Design. S. Chand and Co. Ltd India.

Kim S, and Marand E (2008). High permeability nano-composite membranes based on mesoporous MCM-41 nanoparticles in a polysulfone matrix Microporous and Mesoporous, Materials;114: 129–136

Kimura, T. and Ago, H. (2002). Polymer Composites of Carbon Nanotubes Aligned by a Magnetic Field, Adv. Mater., 14(19): 1380–1383.

Kothurkar N.K. (2004). Solid state, transparent, cadmium sulfide-polymer nanocomposite, University of Florida.

Krishnan, A., Dujardin, E., Ebbesen, T.W., Yianilos, P.N. and Treacy, M.M.J. (1998). Young's Modulus of Single-walled Nanotubes, Physical Review B, 58(20): 14013–14019.

Kurti J., Kresse G., and Kuzmany H. (1998). First-principles calculations of the radial breathing mode of single-wall carbon nanotubes. Phys Rev B; 58:R8869–72.

Kutz M. (2002). Materials Selection, John Wiley & Sons, New York.

Laachachi A, Leroy E, Cochez M, Ferriol M, Lopez and Cuesta J.M., (2005). Use of oxide nanoparticles and organoclays to improve thermal stability and fire retardancy of poly(methyl methacrylate). Polym Degrad Stab.;89: 344-352

Lau, K.T. and Hui, D. (2002). The Revolutionary Creation of New Advanced Materials carbon Nanotube Composites, Composites Part B, 33: 263. (Reproduced in part with permission from Elsevier _ 2006.)

Lau, K.T., Lu, M., Lam, C.K., Cheung, H.Y., Sheng, F.L. and Li, H.L. (2005). Thermal and Mechanical Properties of Single-walled Carbon Nanotube Bundle-reinforced Epoxy Nanocomposites: the Role of Solvent for Nanotube Dispersion, Composites Science and Technology, 65(5): 719–725.

Lau, K.T., Sankar, J., and Hui, D. (2006). Enhancement of the Mechanical Strength of Polymerbased Composites Using Carbon Nanotubes, in Nanoengineering of Structural, Functional, and Smart Materials, Schulz, M.J., Kelker, A.D. and Sunderasen, M.J. (ed.) 1st edn., CRC Taylor & Francis, USA, ISBN 0-8-8493-1653-7, Chapter 14. (Reproduced in part with permission from Taylor & Francis _ 2006.)

Li J., Ma P. C., Chow W. S., To C. K., Tang B. Z., and Kim J.K. (2007): Correlations between percolation threshold, dispersion state, and aspect ratio of carbon nanotubes. Advanced Functional Materials, 17, 3207–3215. DOI: 10.1002/adfm.200700065

Li, F., Cheng, H.M., Bai, S. and Su, G. (2000). Tensile Strength of Single-walled Carbon Nanotubes Directly Measured from their Macroscopic Ropes, Applied Physics Letters, 77(20): 3161–3163.

Li, H.J., Guan, L., Shi, Z. and Gu, Z. (2004). Direct Synthesis of High Purity Single-walled Carbon Nanotube Fibres by Arc Discharge, Journal of Physical Chemistry B, 108(15): 4573–4575.

Li, Y.L., Kinloch, I.A. and Windle, A.H. (2004). Direct Spinning of Carbon Nanotube Fibres from Chemical Vapor Deposition Synthesis, Science, 304(5668): 276–278.

Liang, Z., Shankar, K.R., Barefield, K., Zhang, C., Wang, B. and Kramer, L. (2003). Investigation of Magnetically Aligned Carbon Nanotube Bucky Paper/Epoxy Composites, In: Conference Proceedings at SAMPE, CA.

Liu, J., Fan, S. and Dai, H. (2004). Recent Advances in Methods of Forming Carbon Nanotubes, MRS Bulletin, April 2004: 244–250.

Lourie, O., Cox, D.M. and Wagner, H.D. (1998). Buckling and Collapse of Embedded Carbon Nanotubes, Physical Review Letters, 81(8): 1638–1641.

Lu, J.P. (1997). Elastic Properties of Single and Multilayered Nanotubes, Journal of Physics and Chemistry of Solids, 58(11): 1649–1652.

Luo, J.J. and Daniel, I.M. (2003). Characterization and Modeling of Mechanical Behavior of Polymer/Clay Nanocomposites, Compos. Sci. Technol., 63(11): 1607–1616. (Reproduced in part with permission from Elsevier _ 2006.)

Mahfuz, H., Baseer, M.A. and Zeelani, S. (2005). Fabrication, Characterization and Mechanical Properties of Nano Phased Carbon Prepag Laminates, In: SAMPE Journal, 41(2).

Martin, C.A., Sandler, J.K.W., Shaffer, M.S.P., Schwarz, M.K., Bauhofer, W. Schulte, K. and Windle, A.H. (2004). Formation of Percolating Networks in Multi-wall Carbon-nanotube epoxy Composites, Composites Science and Technology, 64(15): 2309–2316.

Mazumder, S.K. (ed.). (2002). Composites Manufacturing, Materials, Product and Process Engineering, CRC Taylor & Francis, USA.

McCullen, S.D., Kinlaw, A. and Gorga, R.E. (2006). Effect of Multi-wall Nanotube Diameter on Dispersion and Mechanical Properties in Polypropylene Matrix Composites, Journal of Applied Polymer Science (in preparation).

McGill Researchers Develop New Carbon Nanotube Production Method (2004). Journal of Thermal Spray, 13(4): 489–490.

McMorrow, B., Chartoff, R. and Klosterman, D., (2003). Processing and Characterization of a Carbon Nanofibre/Vinylster Resin Composite, SAMPE 2003 Proceedings, Long Beach, CA, USA.

McNally T, Potschke P, Halley P, Murphy M, Martin D, and Bell S. (2005). Polyethylene multiwalled carbon nanotube composites. Polymer, 46:8222–32.

Meyyappan, M. (ed.). (2004). Carbon Nanotubes, Science and Application, CRC Taylor & Francis, USA.

Mitchell, C.A., Bahr, J.L., Arepalli, S., Tour, J.M. and Krishnamoorti, R. (2002). Dispersion of Functionalized Carbon Nanotubes in Polystyrene, Macromolecules, 35: 8825–8830.

Moore, E.M., Ortiz, D.L., Marla, V.T., Shambaugh, R.L. and Grady, B.P. (2004). Enhancing the Strength of Polypropylene Fibres with Carbon Nanotubes, Journal of Applied Polymer Science, 93(6): 2926–2933.

Morgan A B., and Wilkie C A. (2007). Flame Retardant Polymer nanocomposite Wiley Publishing/CRC Press USA.

Nagpal G.R. (2002). Machine Design. Khanna Publishers, Delhi.

O'Donnell, S.E. and Sprong, K.R. (2004). AIAA 4th Aviation Technology, Integration and Operations Forum, Chicago.

Octeau, M.A., Yousefpour, A. and Hojjati, M. (2004). Procedure Manual for using Resin Transfer Molding (RTM) Manufacturing Set-up, August 2004, LM-AMTC-0025.

Organization for Economic Cooperation and Development (1984). "Working of Plastics" OECD, USA.

Oriakhi, C.O. (1998). Nano Sandwiches, Chem. Br., 34: 59–62.

Ou, R., Gupta, S., Parker, C., and Gerhardt, R. J. of Phys. Chem. 2006, 22365-22373.

Palmgren, A. (1946). Ball and Roller Bearing Engineering, 2nd Edition. Burbank and co. London

Pan, Z.W., Xie, S.S., Lu, L., Chang, B.H., Sun, L.F., Zhou, W.Y., Wang, G. and Zhang, D.L. (1999). Tensile Tests of Ropes of very Long Aligned Multiwall Carbon Nanotube, Applied Physics Letters, 74(21): 3152–3154.

Park C., Ounaies Z., Watson K.A., Crooks RE., Smith JJ, Lowther SE,…Clair TLS. (2002). Dispersion of single wall carbon nanotubes by in situ polymerization under sonication. Chem Phys Lett. 2002:364:303-8.

Park, C., Park, O., Lim, J. and Kim, H. (2001). The Fabrication of Syndiotactic Polystyrene/Organophilic Clay Nanocomposites and Their Properties, Polymer, 42: 7465–7475.

Park, J.H. and Jana, S. (2003). Mechanism of Exfoliation of Nanoclay Particles in Epoxy-Clay Nanocomposites, Macromolecules, 36: 2758–2768. (Reproduced in part with permission from American Chemical Society _ 2006.)

Peter R. N. C. (1998). Mechanical Design, Arnold, London 1998.

Pimenta MA, Marucci A, Empedocles SA, Bawendi MG, Hanlon EB, and Rao AM (1998). Raman modes of metallic carbon nanotubes. Phys Rev B; 58:R16016–9.

Pitalskya Z.S, Tasisb D, Papagelisb K, and Galiotis C. (2010). Carbon nanotube–polymer composites: Chemistry, processing, mechanical and electrical properties. Progress in Polymer Science. 35: 357–401

Potschke, P., Fornes, T.D. and Paul, D.R. (2002). Rheological Behaviors of Multiwalled Carbon Nanotube/Polycarbonate Composites, Polymer, 43: 3247–3255.

Qian, D., Dickey, E.C., Andrews, R. and Rantell, T. (2000). Load Transfer and Deformation Mechanisms in Carbon Nanotube-polystyrene Composites, Appl. Phys. Lett., 76(20): 2868–2870.

Quin Adler, (2011). Carbon Nanotube-Polymer Composites for Solar Cell Applications Santa Clara University, SURF 2011 Participant.

Ratna D. (2005). Epoxy Composites: Impact Resistance and Flame Retardancy Rapra Review Reports Volume 16, Number 5.

Reichert, P., Kressler, J., Thomann, R., Mulhaupt R. and Stoppelmann, G. (1998). Nanocomposites Based on a Synthetic Layer Silicate and Polyamide-12, Acta Polymer, 49(2–3): 116–123.

Ren, Y., Li, F., Cheng, H.M. and Liao, K. (2003). Advanced Composites, Letters, 12(1).

Roy, S., Hussain, F., Lu, H. and Narasimhan, K. (2005). Characterization and Modeling of Strength Enhancement Mechanism in Polymer Clay Nanocomposites, In: AIAA Conference Proceedings, Texas.

RTO Lecture Series, EN-AVT-129, May 2005.

Sabba, I. and Thomas, E.L. (2004). High-concentration Dispersion of Single-wall Carbon Nanotubes, MACROMOLECULES, 37(13): 4815–4820.

Safadi, B., Andrews, R. and Grulke, E.A. (2002). Multiwalled Carbon Nanotube Polymer Composites: Synthesis and Characterization of Thin Films, Journal of Applied Polymer Science, 84(14): 2660–2669.

Saito R, Takeya T, Kimura T, Dresselhaus G, and Dresselhaus M.S. (1998). Raman intensity of single-wall carbon nanotubes. Phys Rev B 1998;57:4145–53.

Salavati-Niasari , Davar F, and Fereshteh Z. (2009). Synthesis and characterization of ZnO nanocrystals from thermolysis of new precursor, Chemical Engineering Journal 2009;146: 498–502

Salavati-Niasari M, and Bazarganipour M. (2007). Effect of single-wall carbon nanotubes on direct epoxidation of cyclohexene catalyzed by new derivatives of cisdioxomolybdenum(VI) complexes with bis-bidentate Schiff-base containing aromatic nitrogen–nitrogen linkers, J. Molecular Catalysis A: Chemical 278 2007;278: 173–180

Salavati-Niasari M, Ghanbari D, and Davar F. (2010). Shape selective hydrothermal synthesis of tin sulfide nanoflowers based on nanosheets in the presence of thioglycolic acid. J. Alloy. Compd. 2010; 492:570–575

Salavati-Niasari M, Ghanbari D, and Davar F. (2009). Synthesis of different morphologies of bismuth sulfide nanostructures via hydrothermal process in the presence of thioglycolic acid J. Alloy. Compd. 2009; 488: 442–447

Salvetat, J.P., Andrew, G., Briggs, D., Bonard, J.M., Bacsa, R.R., Kulik, A.J.,…Forro´ , L. (1999). Elastic and Shear Moduli of Single-walled Carbon Nanotube Ropes, Physical Review Letters, 82(5): 944–947.

Sandler, J., Broza, G., Nolte, M., Schulte, K., Lam, Y.M., and Shaffer, M.S.P. (2003). Crystallization of Carbon Nanotube and Nanofibre Polypropylene Composite, Journal of Macromolecular Science-Physics, B42(3–4): 479–488.

Sandler, J., Shaffer, M.S.P., Prasse, T., Bauhofer, W., Schulte, K. and Windle, A.H. (1999). Development of a Dispersion Process for Carbon Nanotubes in an Epoxy Matrix and the Resulting Electrical Properties, Polymer, 40(21): 5967–5971.

Schadler, L.S., Giannaris, S.C. and Ajayan, P.M. (1998). Load Transfer in Carbon Nanotube Epoxy Composites, Applied Physics Letters, 73(26): 3842–3844.

Schlittler, R.R., Seo, J.W., Gimzewski, J.K., Durkan, C., Saifullah, M.S.M. and Welland, M.E. (2001). Single Crystals of Single-walled Carbon Nanotubes formed by Self-assembly, Science, 292(5519): 1136–1139.

Schmidt, D., Shah, D. and Giannelis, E.P. (2002). New Advances in Polymer/Layered Silicate Nanocomposites, Current Opinion in Solid State and Materials Science, 6(3): 205–212.

Seidel G. D., and Lagoudas D. C. (2009). A micromechanics model for the electrical conductivity of nanotube polymer nanocomposites. Journal of Composite Materials, 43, 917–941 (2009). DOI: 10.1177/0021998308105124

Sennett, M., Welsh, E., Wright, J.B., Li, W.Z., Wen, J.G. and Ren, J.F. (2003). Dispersion and Alignment of Carbon Nanotubes in Polycarbonate, Applied Physics A: Materials Science & Processing, 76(1): 111–113.

Shaffer, M.S.P. and Windle, A.H. (1999). Analogies between Polymer Solutions and Carbon Nanotube Dispersions, Macromolecules, 32: 6864–6866.

Shaffer, M.S.P., Fan, X. and Windle, A.H. (1998). Load Transfer in Carbon Nanotube Epoxy Composites, Carbon, 36: 1603–1612.

Sharma, P.C and Aggarwal D.K (2006). Machine Design, S.K. Kataria and sons, Nai Sarak Delhi.

Shirley J.E and Mischke C.R. (2006). Mechanical Engineering Design, 6th Edition,Tata McGrew-Hill Publishing Company, New Delhi

Smalley, R.E. (1999). Elastic Strain of Freely Suspended Single-wall carbon Nanotube Ropes, Applied Physics Letters, 74(25): 3803–3805.

Star, A., Stoddart, J.F., Steuerman, D., Diehl, M., Boukai, A., Wong, E.W.,…Heath, J.R. (2001). Preparation and Properties of Polymer-wrapped Single-walled Carbon Nanotubes, Angew Chem Int Ed, 40: 1721–1725.

Tang, W.Z., Santare, M.H. and Advani, S.G. (2003). Melt Processing and Mechanical Property Characterization of Multi-walled Carbon Nanotube/High Density Polyethylene (MWNT/HDPE) Composite Films, Carbon, 41(14): 2779–2785.

Thostenson, E., Li, C. and Chou, T. (2005). Review Nanocomposites in Context, Journal of Composites Science & Technology, 65: 491–516. (Reproduced in part with permission from Elsevier _ 2006.)

Thostenson, E.T., Ren, Z. and Chou, T.W. (2001). Advances in the Science and Technology of Carbon Nanotubes and their Composites: a Review, Composites Science and Technology, 61(13): 1899–1912.

Treacy, M.M.J., Ebbesen, T.W. and Gibson, J.M. (1996). Exceptionally High Young's Modulus Observed for Individual Carbon Nanotubes, Nature, 381(6584): 678–680.

Usuki, A., Kawasumi, M., Kojima, Y., Okada, A., Kurauchi, T. and Kamigaito, O.J. (1993). Swelling Behavior of Montmorillonite Cation Exchanged for V-amino Acids by E-caprolactam, Mater. Res., 8(5): 1174.

Valentini, L., Puglia, D., Frulloni, E., Armentano, I., Kenny, J.M. and Santucci, S. (2004). Dielectric Behavior of Epoxy Matrix/Single-walled Carbon Nanotube Composites, Composites Science and Technology, 64(1): 23–33.

Walters, D.A., Casavant M.J., Qiin, X.C., Huffman, C.B., Boul, P.J., Erickson, L.M. and Smith, K. (2001). In Plane Aligned Membranes of Carbon Nanotube, Chem. Physics. Lett., 338: 14–20.

Wang S, Hua Y, Zonga R, Tanga Y, Chenb Z, and Fana W. (2004). Preparation and characterization of flame retardant ABS/montmorillonite nanocomposite. Applied Clay Science 2004; 25: 49–55

Wenzhong T., Michael H. S., and Suresh G. A., (2003). Melt processing and mechanical property characterization of multi-walled carbon nanotube/ high density polyethylene (MWNT/HDPE) composite films, Carbon 41 (2003) 2779–2785

Wilbrink, M.W.L., Argon, A.S., Cohen, R.E. and Weinberg, M. (2001). Toughen Ability of Nylon-6 with CaCO3 Filler Particles: New Findings and General Principles, Polymer, 42(26): 10155–10180.

Wilkins, R., (2005). Material Res. Soc. Symp. Proceedings, 851(NN6.5).

Williams H.L (1975). Polymer Engineering., Elsevier Scientific Publishing Co., London.

www.dow.com/sal/process/ext/equip.htm: "Extruding Polystyrene resins" Styron Asian Ltd.

www.itdg.com , Recycling of plastics, Intermediated Technology Development Group

www.plastcs.ca/epic (2005): Environmental and plastic Industry Council,

Xia, H.S., Xia, H., Wang, Q., Li, K. and Hu, G.H. (2004). Preparation of Polypropylene/Carbon Nanotube Composite Powder with a Solid-state

Mechanochemical Pulverization Process, Journal of Applied Polymer Science, 93(1): 378–386.

Xiao G., Tao Y., Lu J., and Zhang Z. (2010). Highly conductive and transparent carbon nanotube composite thin films deposited on polyethylene terephthalate solution dipping. Thin Solid Films, 518, 2822–2824 (2010). DOI: 10.1016/j.tsf.2009.11.021

Xiao, K.Q. and Zhang, L.C. (2004). The Stress Transfer Efficiency of a Single-walled Carbon Nanotube in Epoxy Matrix, Journal of Materials Science, 39(14): 4481–4486.

Yakobson, B.I., Brabec, C.J. and Bernholc, J. (1996). Nanomechanics of Carbon Tubes: Instabilities Beyond Linear Response, Physical Review Letters, 76(14): 2511–2514.

Yano, K. and Usuki, A. (1993). Synthesis and Properties of Polyimide-Clay Hybrid, J. Polym. Sci., Part A: Polym. Chem., 31: 2493–2498.

Yano, K., Usuki, A., Okada, A. and Kurauchi, T. (1991). Synthesis and Properties of Polyimide-Clay Hybrid, Polymer Prep. (Jpn), 32(1): 65.

Zeher T and Costas G. G. (1979). Principle of Polymer Processing, John Wiley and sons, Inc. New york.

Zeng, J., Saltysiak, B., Johnson, W.S., Schiraldi, D.A. and Kumar, S. (2004). Processing and Properties of Poly (Methyl Methacrylate)/Carbon Nano Fibre Composites, Composites Part B-Engineering, 35(2): 173–178.

Zhang, B., Xie, C., Hu, J., Wang, H. and Gui, Y.H. (2006). Novel 1–3 Metal Nanoparticle/Polymer Composites Induced by Hybrid External Fields, Composites Science and Technology, 66: 1558–1563.

Zhang, M., Atkinson, K.R. and Baughman, R.H. (2004). Multifunctional Carbon Nanotube Yarns by Downsizing an Ancient Technology, Science, 306(5700): 1358–1361.

Zhou, W., Vavro, J., Guthy, C., Winey, K.I., Fischer, J.E., Ericson, L.M.,…Smalley, R.E. (2004). Single Wall Carbon Nanotube Fibres Extruded from Super-acid Suspensions: Preferred Orientation, Electrical, and Thermal Transport, Journal of Applied Physics, 95(2): 649–655.

APPENDICES

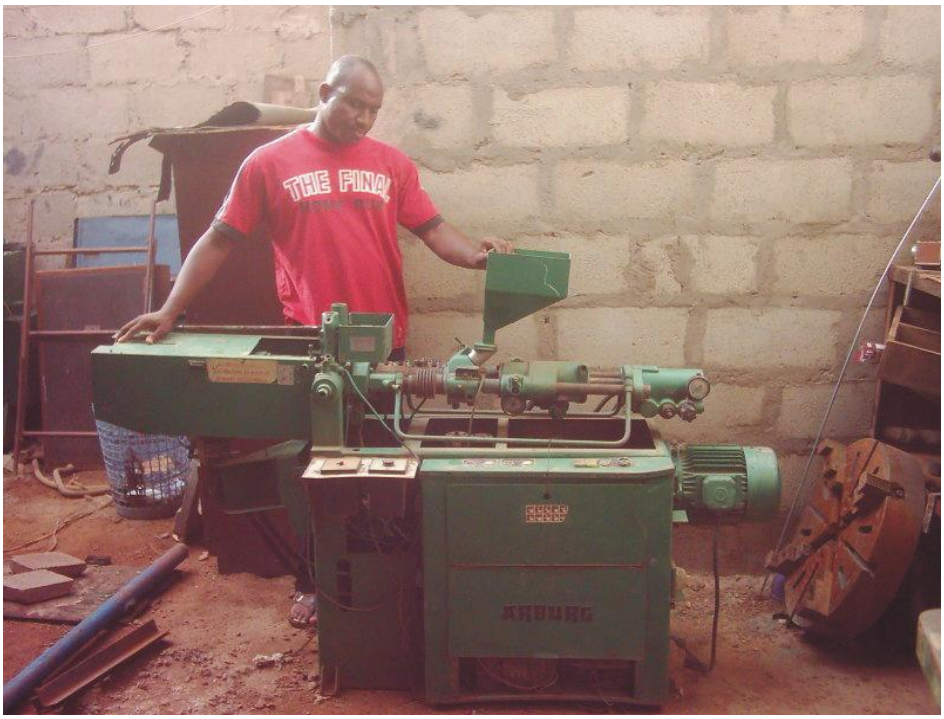


Plate 2: Small Scale Conventional Injection Moulding Machine



Plate 3: Fabrication work on the Modification of the Injection Moulding Machine



Plate 4: Assembly of the Modified Injection Moulding machine



Plate 5: Assembled machine



Plate 6: XRD Test in progress Zhejing University, China



Plate 7: SEM Test in progress at Zhejing University, China



Plate 8: Professor Cheng Jing of Chinese Medical University